DRAG REDUCTION BY ADDITIVES IN MULTIPHASE FLOW IN PIPES

BY

IHAB HISHAM ALSURAKJI

A Dissertation Presented to the

DEANSHIP OF GRADUATE STUDIES

KING FAHD UNIVERSITY OF PETROLEUM & MINERALS

DHAHRAN, SAUDI ARABIA

In Partial Fulfillment of the
Requirements for the Degree of

DOCTOR OF PHILOSOPHY

In

MECHANICAL ENGINEERING

November, 2016

In the name of Allah, the Most Gracious and the Most Merciful

KING FAHD UNIVERSITY OF PETROLEUM & MINERALS

DHAHRAN- 31261, SAUDI ARABIA

DEANSHIP OF GRADUATE STUDIES

This thesis, written by Ihab H. Alsurakji under the direction his thesis advisor and approved by his thesis committee, has been presented and accepted by the Dean of Graduate Studies, in partial fulfillment of the requirements for the degree of **DOCTOR OF PHILOSOPHY IN MECHANICAL ENGINEERING.**

Dr. Abdelsalam Al Sarkhi
(Advisor)

Dr. Zuhair Mattoug Gasem
Department Chairman

Dr. Hassan M. Badr
(Member)

Dr. Salam A. Zummo
Dean of Graduate Studies

Dr. Mohamed A. Habib
(Member)

26/12/16
Date

Dr. Luai M. Alhems
(Member)

Dr. Muhammad Atiqullah
(Member)

Dedicated

to

My Beloved Parents, Sister, Brothers,

My Beloved Wife and My Little

Daughter

ACKNOWLEDGMENTS

All praise and thanks are due to Almighty Allah, Most Gracious and Most Merciful, for his immense beneficence and blessings. He bestowed upon me health, knowledge and patience to complete this work. May peace and blessings be upon prophet Muhammad (PBUH), his family and his companions.

Thereafter, acknowledgement is due to KFUPM for the support extended towards my research through its remarkable facilities and for granting me the opportunity to pursue graduate studies.

I acknowledge, with deep gratitude and appreciation, the inspiration, encouragement, valuable time and continuous guidance given to me by my thesis advisor, Dr. Abdelsalam Al Sarkhi. I am highly grateful to my Committee member Dr. Hassan M. Badr, Dr. Mohamed A. Habib, Dr. Luai Al Hadhrami, and Dr. Mohammad Atiqullah for their valuable guidance, suggestions, motivation, and support.

I am deeply indebted and grateful to KACST for their help and support during research.

You who I carry your name with pride, who I miss from an early age, who my heart trembles when I remember you, who you leave me for God's mercy, I gift you this thesis …*my Father*

To my angel in my life, to the meaning of love and the meaning of compassion, dedication and to the source of patience, optimism and hope...*my Mother*.

To my brothers and my sister, who I see certain optimism and happiness in their smile. To the flame of intelligence and thinking.

To the joy of my life who shared me every moment throughout my studying. To her support, encouragement, quiet patience, unwavering love, unyielding devotion...*my*

Wife. I appreciate my baby, *my little girl Hanin* for abiding my ignorance during my thesis writing. Words would never say how grateful I am to both of you.

Special thanks are due to my senior colleagues at the university, for their help, prayers and who provided wonderful company and good memories that will last a life time.

Finally yet importantly, to a person who had great influence on me are already passed away. I am very grateful to my master's advisor Dr. Meamer El Nakla, who was a great teacher, I am very proud of him. May Allah forgive him.

TABLE OF CONTENTS

LIST OF TABLES

LIST OF FIGURES

LIST OF ABBREVIATIONS

Nomenclature

%DR	:	Percentage drag reduction
C	:	Concentration [ppm]
D	:	Pipe diameter [m]
DRA	:	Drag reducing Agent
DRP	:	Drag reducing polymer
Δh_L	:	Head loss [m]
ΔP	:	Pressure drop [Pa]
dP/dL	:	Pressure gradient [$Pa.m^{-1}$]
f	:	Fanning friction factor
g	:	Gravitational acceleration [$m.s^{-2}$]
L	:	Pipe length [m]
r	**:**	Pipe radius [mm]
R	**:**	Maximum pipe radius [mm]

Q	:	Volumetric flow rate [$m^3.s^{-1}$] or [$m^3.min^{-1}$]
Re	:	Reynolds number
Re$_s$	:	Reynolds number based on fluid superficial velocity
TI	:	Turbulence intensity
$\acute{u}$	:	Standard deviation of the velocity fluctuation at x-direction over a specified time
$\bar{U}$	:	Average velocity [$m.s^{-1}$]
U	:	Turbulent velocity in x-direction [$m.s^{-1}$]
$\acute{v}$	:	Standard deviation of the velocity fluctuation at y-direction over a specified time
V	:	Velocity in y-direction [$m.s^{-1}$]
$\bar{V}$	:	Velocity Vector
V$_s$	:	Superficial velocity [$m.s^{-1}$]
W	:	Velocity in z-direction [$m.s^{-1}$]
W	:	Energy consumption [$W.m^{-1}$]

Subscripts

1	:	Without DRP
2	:	With DRP
ave	:	Average
DRP	:	Drag reducing polymer
z	:	The direction aligned with the z-axis of a Cartesian coordinate system
u	:	x-direction
v	:	y-direction
SL	:	Superficial liquid
SG	:	Superficial gas
Pol.	:	Polymer
L	:	Liquid
G	:	Gas (air)
W	:	Water
O	:	Oil
m	:	Mixture

PS	:	Power saving

Greek symbols

$\bar{\boldsymbol{\omega}}$	:	Vorticity vector
$\boldsymbol{\sigma}$	:	Variance
$\boldsymbol{\mu}$	:	Dynamic Viscosity [N.sec.m^{-2}]
$\bar{\boldsymbol{\mu}}$	:	Mean velocity
$\boldsymbol{\nabla}$	:	Gradient Operator
i, j, k	:	Standard unit vectors
$\boldsymbol{\gamma}$	:	Specific Weight [N.m^{-3}]

ABSTRACT

Full Name : [Ihab Hisham Hefzi Alsurakji]

Thesis Title : [Drag Reduction by Additives in Multiphase Flow in Pipes]

Major Field : [Mechanical Engineering]

Date of Degree : [November, 2016]

An experimental investigation of multiphase gas-oil-water flow was performed for studying the influence of water-soluble and oil-soluble DRPs in single-phase, two-phase, and three-phase flows. These experiments have been presented for oil, air, and water flowing in a 22.5 mm I.D., 8.33 m long PVC horizontal pipe. The effect of gas flow rate, water flow rate, oil flow rate, DRPs types, and DRPs concentrations on pressure gradient and flow patterns were investigated. Stratified-wavy, slug, and annular flow regimes were studied. The results showed a large reduction in pressure gradient due to DRPs at high liquid mixture superficial velocity, which was accompanied by significant effect of DRPs on the flow patterns transition boundaries. For gas-water-oil flow, the maximum drag reduction was achieved when water-soluble DRP was used. Moreover, under similar conditions, using oil-soluble or water-soluble may not results in same drag reduction. It has been concluded from the comparisons in case of single-phase, two-phase, and three-phase, the water-soluble DRP ZETAG® 8165, because of structural difference, can dampen the turbulent eddies, decrease the interfaces roughness, and resist wall stresses much better than the oil-soluble DRP PIB.

Furthermore, this thesis presents experimental investigations conducted to understand the influence of water-soluble DRP in single and two-phase (stratified-wavy) flows by using Particle Image Velocimetry (PIV) technique. The effects of liquid flow rates and DRP concentrations on streamlines, and the instantaneous velocity were also investigated. A verification of PIV results have been performed by comparing it with the computational results obtained by FLUENT software. It has been reported that, the PIV is a powerful technique in understanding the mechanism of DRP in single-phase and two-phase flow, especially at the regions near the pipe wall and near to the phases interface.

As for the use of DRPs, the results of energy analysis in terms of head loss reductions and the percentage savings in the energy consumptions in single and multiphase flow systems before and after adding DRPs are incredible. The results showed that there were drastic reductions in the head losses, and a huge savings in the energy consumptions which leads to an increase in the throughput. Also, it was shown that the ability of water-soluble DRP is higher than the oil-soluble DRP in decreasing the head loss and increasing the percentage saving in energy consumption for the range of experimental setup studied. In addition, the effect of pipe diameters on the head loss and percentage energy saving were investigated as well. The results demonstrated the effect of larger pipe diameter was more significant than the smaller one.

ملخص الرسالة

الاسم الكامل: ايهاب هشام حفظي السركجي

عنوان الرسالة: المضافات الكيميائية المقللة للضغط في الجريان متعدد الطور في الانابيب

التخصص: الهندسة الميكانيكية

تاريخ الدرجة العلمية: صفر 1438

تم عمل تحقيق مختبري للجريان متعدد الحالات غاز-زيت-ماء وذلك بهدف تحديد تأثير المبلمرات المذابة بالماء والمبلمرات المذابة بالزيت على الجريان احادي الحالة، وعلى الجريان ثنائي الحالة، وعلى الجريان ثلاثي الحالة. تمت هذه التجارب باستخدام الزيت النفطي، والهواء، والماء من خلال تدفقهم في انبوب بلاستيكي افقي قطره الداخلي يعادل 22.5 ملم وطوله يعادل 8.33 م. تمت دراسة تأثير معدل تدفق الغاز، ومعدل تدفق الماء، ومعدل تدفق الزيت النفطي، وأنواع مختلفة من المبلمرات، وتركيزات مختلفة للمبلمرات على الضغط وأنماط التدفق. كما تمت دراسة التدفق الطبقي-المتموج، والتدفق النبضي، والتدفق الحلقي. أظهرت النتائج انخفاض كبير في الضغط الاحتكاكي بسبب المبلمرات في حالة الجريان ذو السرعة السطحية العالية، والذي كان يرافقه تأثير كبير من المبلمرات على الانتقال بين أنماط التدفق. في حالة تدفق الغاز والماء والزيت النفطي، تبين ان الحد الأقصى للحد من السحب حدث عند استخدام المبلمرات المذابة في الماء. وعلاوة على ذلك، وفي ظل ظروف مماثلة، فان استخدام المبلمرات المذابة في الزيت النفطي أو المبلمرات المذابة في الماء لن تنتج نفس المقدار في الحد من السحب. وقد تم الاستنتاج من المقارنات في حالات الجريان احادي الحالة، وثنائي الحالة، وثلاثي الحالة، ان المبلمرات المذابة في الماء، بسبب اختلاف بنيتها الهيكلية، قادرة على اخماد الدوامات المضطربة، و تقليل خشونة الاسطح المتلاصقة، ومقاومة اجهاد الجدران اكثر بكثير من المبلمرات المذابة بالزيت.

من ناحية اخرى، تقدم هذه الأطروحة التحقيقات التجريبية التي أجريت لفهم كيفية عمل المبلمرات المذابة في الماء في حالة الجريان احادي الحالة والجريان ثنائي الحالة (الطبقي-المتموج) باستخدام تقنية حساب سرعة الجسيمات بواسطة الصور (بي اي في). كما تم دراسة اثر معدلات تدفق السائل وتركيز المبلمرات على الخطوط الانسيابية، والسرعة اللحظية. وقد أجري التحقق من نتائج تقنية حساب سرعة الجسيمات بواسطة الصور عن طريق مقارنتها مع النتائج الحسابية التي تم الحصول عليها بواسطة برنامج الفلونت. وقد أفيد من هذه المقارنة، أن حساب سرعة الجسيمات بواسطة

الصور هي تقنية مفيدة جدا في فهم آلية عمل المبلمرات في حالة الجريان احادي الحالة وفي حالة الجريان ثنائي الحالة، ولا سميا في المناطق القريبة من جدار الأنبوب وفي مناطق التقاء الاطوار.

أما بالنسبة لاستخدام المبلمرات، فان نتائج تحليل الطاقة من حيث خفض فقدان الارتفاع ونسبة التقليل في استهلاك الطاقة في أنظمة التدفق احادي الحالة والتدفق متعدد الاطوار قبل وبعد إضافة المبلمرات كانت مذهلة. حيث اظهرت النتائج ان هناك لنخفاض كبير في خسائر الضغط، و توفير كبير في استهلاك الطاقة والذي من شأنه ان يزيد في الانتاجية. ايضا تبين ان قدرة المبلمرات المذابة في الماء اعلا من المبلمرات المذابة في الزيت من حيث التقليل في خسائر الضغط و الزيادة في نسبة توفير استهلاك الطاقة وذلك وفقا للتحقيقات التجريبية التي شملتها الدراسة. وبالإضافة إلى ذلك، تمت ايضا دراسة تأثير أقطار الأنابيب على فقدان الارتفاع ونسبة التقليل في الطاقة. وأظهرت النتائج أن تأثير قطر الانبوب الاكبر أكثر أهمية من الانبوب ذو القطر الاصغر.

CHAPTER 1

INTRODUCTION

1.1 Background

Multiphase flow is a phenomenon that is experienced naturally or artificially in fluid conduits e.g. bubbly, stratified and slug flow in pipes. Literally, it means a flow consisting of a phase made up of different properties such as oil-water mixture or more than a phase such as air-water mixture. The most observed multiphase flow is two-phase flow, which can be in liquid-liquid, liquid-gas, gas-solid, and liquid-gas-solid. Gas-oil-water and oil-water flows are common in the production and transportation of petroleum fluids. Understanding of single-phase or multiphase pipe flow behaviors is crucial to many applications including design, operation, and production of flow lines and wells.

Consequently, there is a numerous interest to lower the pumping and operating cost especially for long distance pipes network oil transportation, and this can be achieved by making these pipes carry a given flow with a smaller frictional pressure drop (drag). Recent studies on drag reduction in single and multiphase flows show that drag reducing polymers (DRPs) can decrease pressure drop as well as change the spatial distribution of fluids in the pipeline [Al-Sarkhi 2010 and Abubakar et al. 2014].

The phenomenon of Drag Reduction (RD) is defined as the ability of low concentrations of certain additives to reduce the frictional resistant in turbulent single or multiphase flow along a pipeline. Drag reducing additives can be classified into five categories: polymers, surfactants, fibres, micro-bubbles and compliant coating [Abubakar et al. 2014]. Whereas, this thesis presents only the effect of using two types of drag reducing polymers (DRPs), which are water-soluble DRP and oil-soluble DRP, in turbulent single and multiphase flows.

Drag reducing polymers (DRPs) are long chains of high molecular weight polymers that can be water-soluble or oil-soluble. DRPs are used as thickening agents and they are highly adsorbent due to the cavities between them and hydrogen bonding (e.g. between the polymer and water) which make them like gel. For example, water is brought into the network (chain connection) through the process of osmosis and quickly journeys into the central part of the polymer network, where it is reserved. Figure 1.1 shows the process of absorbing water by polymer.

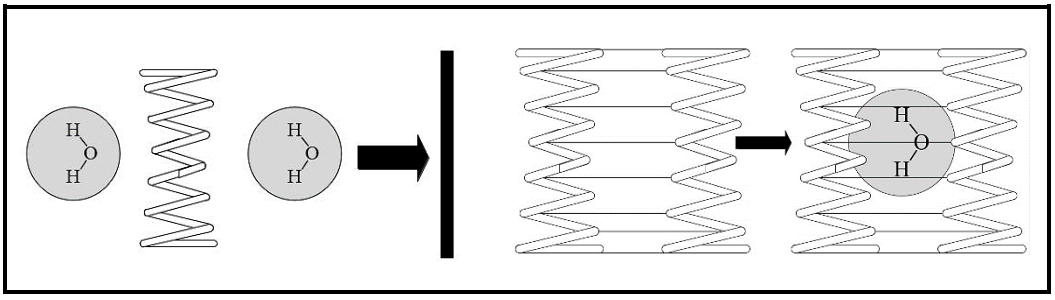

Figure 1.1 Sketch of how the polymer absorbed the water.

It has been shown that the DRPs work in turbulent flow regimes only [Toms 1948]. A DRP, introduced into the liquid flowing in a pipeline in parts per million (ppm) levels,

changes the flow pattern by suppressing the formation of turbulent bursts and the propagation of the turbulent eddies. Consequently, it increases the laminar sub-layer near the pipe wall. In other words, a DRP streamlines turbulent flows and reduces the wall Reynolds stresses. As a result, DRPs can increase the throughput capacity, save energy, and as a result reduce operational costs. As pressure gradient in the pipeline decreases, the amount of energy required to pump the fluid along the pipeline decrease.

According to Choi and Jhon [1996], the most effective drag-reducing polymers compile a flexible structure and high molecular weight. The phenomenon of drag reduction in a turbulent flow due to certain additives, such as polymers possess high molecular weight has been the subject of intensive research during the last sixteen years.

According to Flory [1953], the general chemical formula for the DRP is shown in Figure 1.2. In this figure, R denotes to carbon chains of various lengths and N represents the repetition of the unit in parenthesis. N may have a value of around 1000 in quality drag reducing polymers resulting in molecular weights of millions.

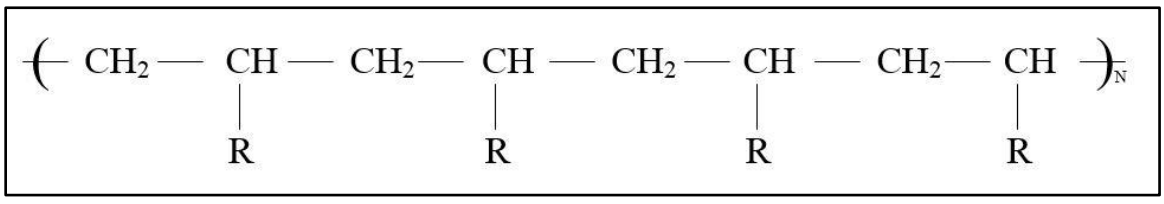

Figure 1.2 The general chemical formula for the polymer [Flory P. J. 1953].

Different ways adopted by researchers to inject the DRPs inside the pipeline. Specific details about the mechanism adopted in this study of inserting DRPs will be explained later. For a single-phase flow, as soon as DRP enters the pipeline, it dissolves into the pipeline fluid and DRP molecules begin to uncoil and outspread throughout the pipeline flow. DRP damps the turbulent activities near the pipe wall, which results in reduction in Reynolds stresses as shown in Figure 1.3.

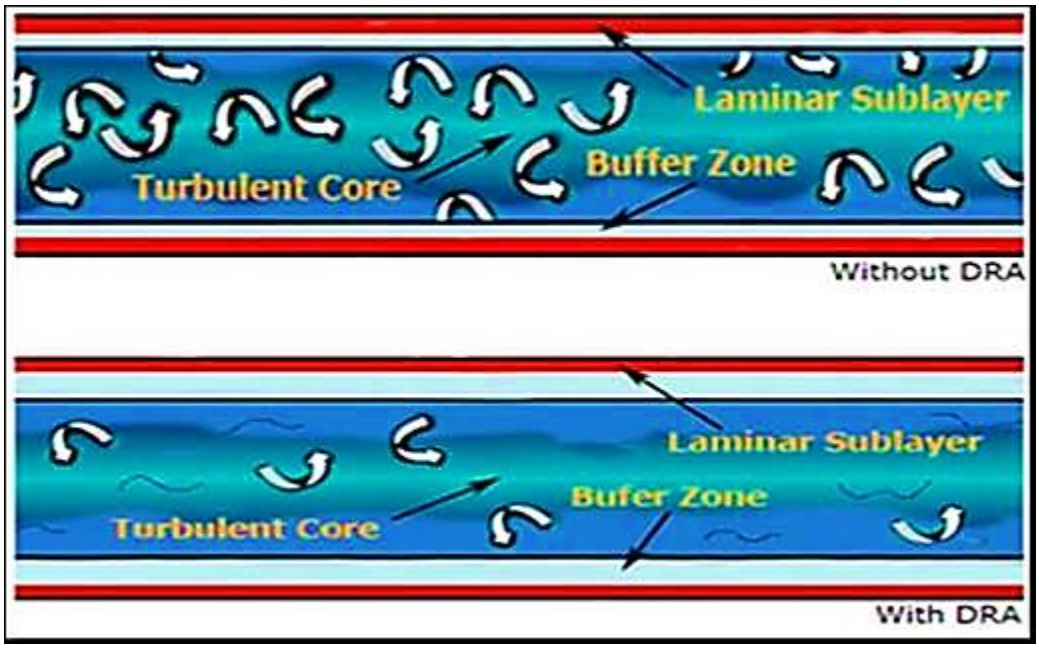

Figure 1.3 Effect of using DRA on the turbulent flow [Available: http://flo-quest.com/activeingr.php].

1.2 Dissertation Objectives

This study aims to provide insight into the effect of injecting water- and oil-soluble DRPs, which is injected at the beginning of the test section, on the pressure gradient, percentage drag reduction, and flow patterns in stratified-wavy, slug, and annular flow regimes, in the presence of air, using a 22.5 mm I.D. horizontal pipeline. Likewise, the obtained data have been utilized using PIV technique to come up with a clear explanation of the DRP mechanism. The following objectives will be achieved in this thesis;

- Using the Particle Image Velocimetry (PIV) technique to study the DRPs mechanism and the increase in the flow rate for single-phase and two-phase flow.
- Verifying the PIV results by running FLUENT for single-phase turbulent flow and comparing the velocity profile with the Particle Image Velocimetry (PIV) experimental results.
- Set of experimental results with and without DRPs for single-phase, two-phase and three-phase horizontal pipe.
- A survey of all models and theory about the mechanisms of drag reduction by DRPs in single and multiphase flow.
- Influence of the water cut and oil soluble vs. water soluble DRP on multiphase flow behavior (pressure drop, holdup, and flow patterns).

1.3 Dissertation Structure

This thesis is divided into ten chapters. Chapter-1, the current one, is the introduction. The descriptions of the following nine chapters are as follows:

Chapter-2 presents a literature review on the flow patterns in single, two, and three-phase flow. It includes a review of drag reduction by additives in single and multiphase flow in pipes; especially the effect of polymers on the pressure gradient, holdup, and flow patterns. Also, a review of the developed models and theory about the mechanism of drag reduction by DRPs in single and multiphase flow.

Chapter-3 provides a detailed description of the experimental setup, the instrumentation used, DRPs injection procedure, and calibration flow meters.

Two groups of uncertainty analysis applied to check the experimental data quality is reported in chapter-4.

Chapter-5 is presenting the effect of the water-soluble DRP on the single-phase water flow and oil-soluble DRP on the single-phase oil flow in horizontal pipe.

Moreover, effect of water-soluble DRP and oil-soluble DRP on two-phase air-water and air-oil flow in horizontal pipe have been investigated, respectively. Also, a comparisons in term of drag reduction between air-water and air-oil flow are given in chapter-6.

In addition, chapter-7 presents effect of DRPs on three-phase air-oil-water horizontal flow and provides comparisons with air-oil and air-water flow in terms of drag reduction. Chapter-8 is presenting a new technique used to analyze the effect of DRPs on the flow field. This new technique is called Particle Image Velocimetry (PIV). Also, it provides a comparison with numerical results.

Last but not least, based on the experimental findings, conclusions and some recommendations for future work are presented in chapter-9.

Each chapter of the main five chapters (5-8) is designed to stand for itself. Therefore, each chapter begins with a brief introduction giving background about one specific objective. After that, the results obtained by conducting the experiments are discussed in the second section and compared with the previous related work done. Finally, in the last section of each chapter the summary is highlighted the main conclusions.

In addition, Appendix-C presents detailed energy analysis of the two-phase air-water flow in terms of head loss and saving in energy consumptions.

CHAPTER 2

LITERATURE REVIEW

2.1 Overview

This chapter aims to highlight the important works published by the researchers in the field of drag reduction (DR), types of drag reducing additives (DRAs), influence of DRAs on the frictional pressure drop, holdup, and flow patterns of horizontal pipe flow, flow through pipes for single, two and three-phase flow, mechanisms of drag reduction by DRAs, relevant to this study. Furthermore, it provides theoretical background of single, two and three-phase flow along with their flow patterns characteristics in horizontal pipeline.

Therefore, the literature review is divided into three sections in order to shed the light into the research area that has not been investigated or need more clarifications. The three divisions are:

- Flow patterns.
- Drag reduction in multiphase flow.
- Techniques used to study the mechanisms of drag reduction by DRAs.

2.2 Flow Patterns

When more than one components e.g. immiscible liquids flow together in a pipe, a particular type of geometric distribution or topology of the components is called a flow pattern or flow regimes. A variety configuration of flow patterns results from the deformable interface between two fluids flow in a pipe. Every flow patterns possesses unique hydrodynamic features. Therefore, numerous studies have been carried out to clarify the hydrodynamic aspects of two-phase gas-liquid/liquid-liquid flow in horizontal flow. Even though, there still exist some uncertainties that need more elucidation. For the three-phase gas-liquid-liquid flow in horizontal pipe remains as a less explored area and gained more interest in recent years.

Many parameters affects the formation of each flow patterns and it's transition. Such parameters can be classified into the following categories;

- Fluid characteristics such as; viscosity, and density of each phase.
- Pipe characteristics such as; wetting properties, surface tension, and its geometrical variable).
- Operating conditions such as; the input fluid ratio, the mixture velocity, and the fluid flow rates.

Consequently, understanding the liquid-liquid and the gas-liquid flow characteristics or flow patterns are essential for many applications and even for designing pipelines. Furthermore, these types of two-phase flow have significant differences. For example, the

differences in density and viscosity in case of oil and water are smaller than the case of gas-liquid flow, and it has complex interfacial chemistry compared to gas-liquid systems. Therefore, information gathered for each flow can be used as a basis to deduce the more sophisticated case of three-phase air-oil-water flow.

Several techniques were developed and applied for examining the two-phase gas-liquid/liquid-liquid flow in order to reveal the flow patterns. Identifications of flow patterns can be attained by one of the following methods; visual observation, conductivity probes, gamma ray densitometry … etc. Among these techniques, the most popular method used to identify the flow pattern in multiphase flow is the visual observation with assist of a high-speed photography oriented towards transparent portion of the pipe. However, the scopes of this work will focus on the effect of the flow rates and the effect of pipe diameter on the flow patterns using visual observation techniques.

2.2.1 Gas-Liquid Flow Patterns

The majority of studies conducting for multiphase flow are considering gas-liquid flow system, and this part focuses mainly on gas-liquid fully developed flow phenomena in horizontal pipes.

The pioneering work in this field done by Lockhart and Martinelli [1949]. Since then, gas-liquid experiments performed in order to determine flow patterns over a wide range of flow conditions. Baker [1953], Hubbard and Dukler [1966], Beggs and Brill [1973] and Mandhane et al. [1974] used the visual observation technique to obtain the flow patterns, and demonstrating their results on 2D map based on superficial velocities of liquid and gas as shown in Figure 2.1. However, the development in the visual observation technique reflected on the criteria for identifying the flow regimes, which depends strongly on the pipe orientation, superficial velocities ranges, fluid types and properties of each phase.

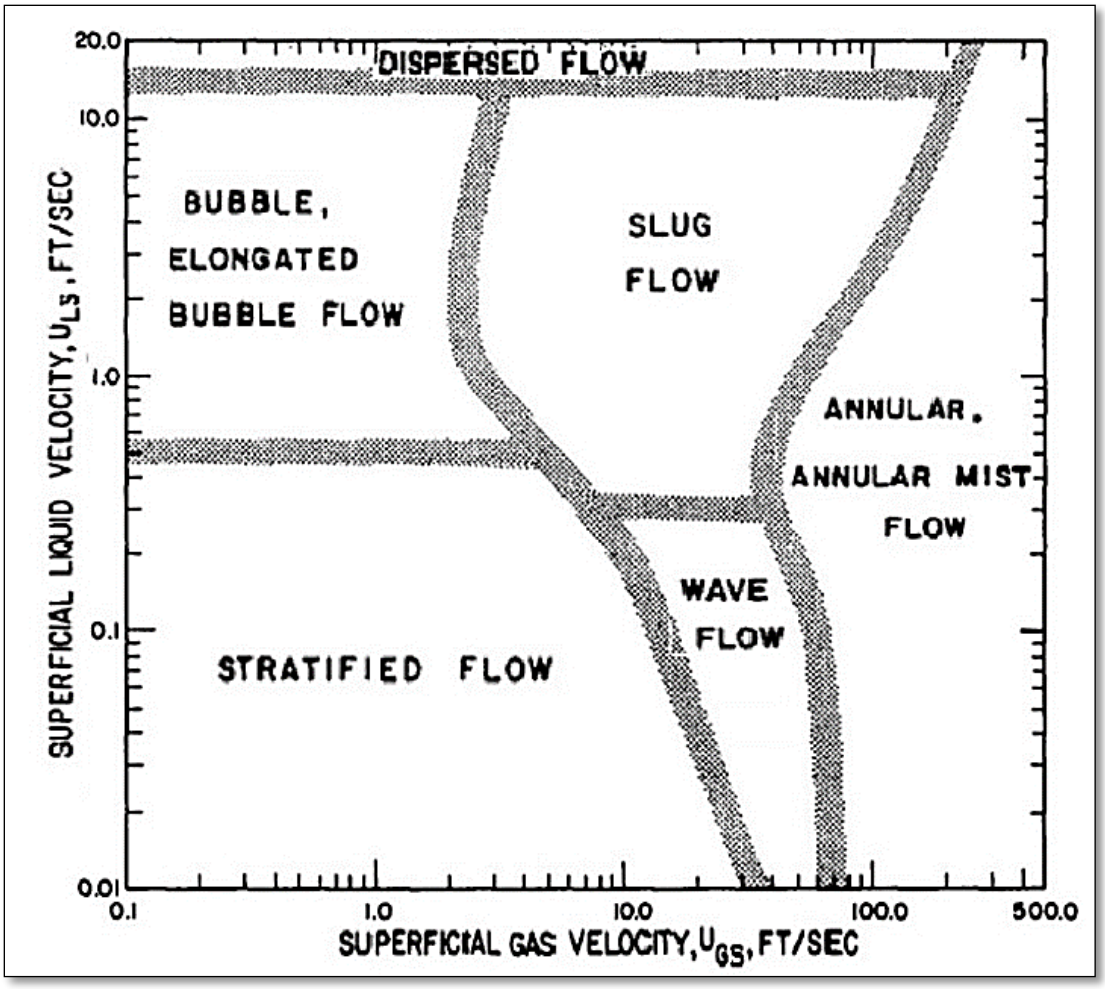

Figure 2.1 Horizontal two-phase gas-liquid flow pattern map based on superficial velocities [Mandhane et al. 1974].

Hewitt [1998] conducting experiment for two-phase gas-liquid flow in horizontal pipe. The observed flow patterns encountered in horizontal two-phase flow were classified as follows; stratified flow including the stratified-smooth and stratified-wavy, intermittent flow which include the slug flow and elongated-bubble flow, Annular flow and dispersed-bubble flow. More details are presented in Figure 2.2.

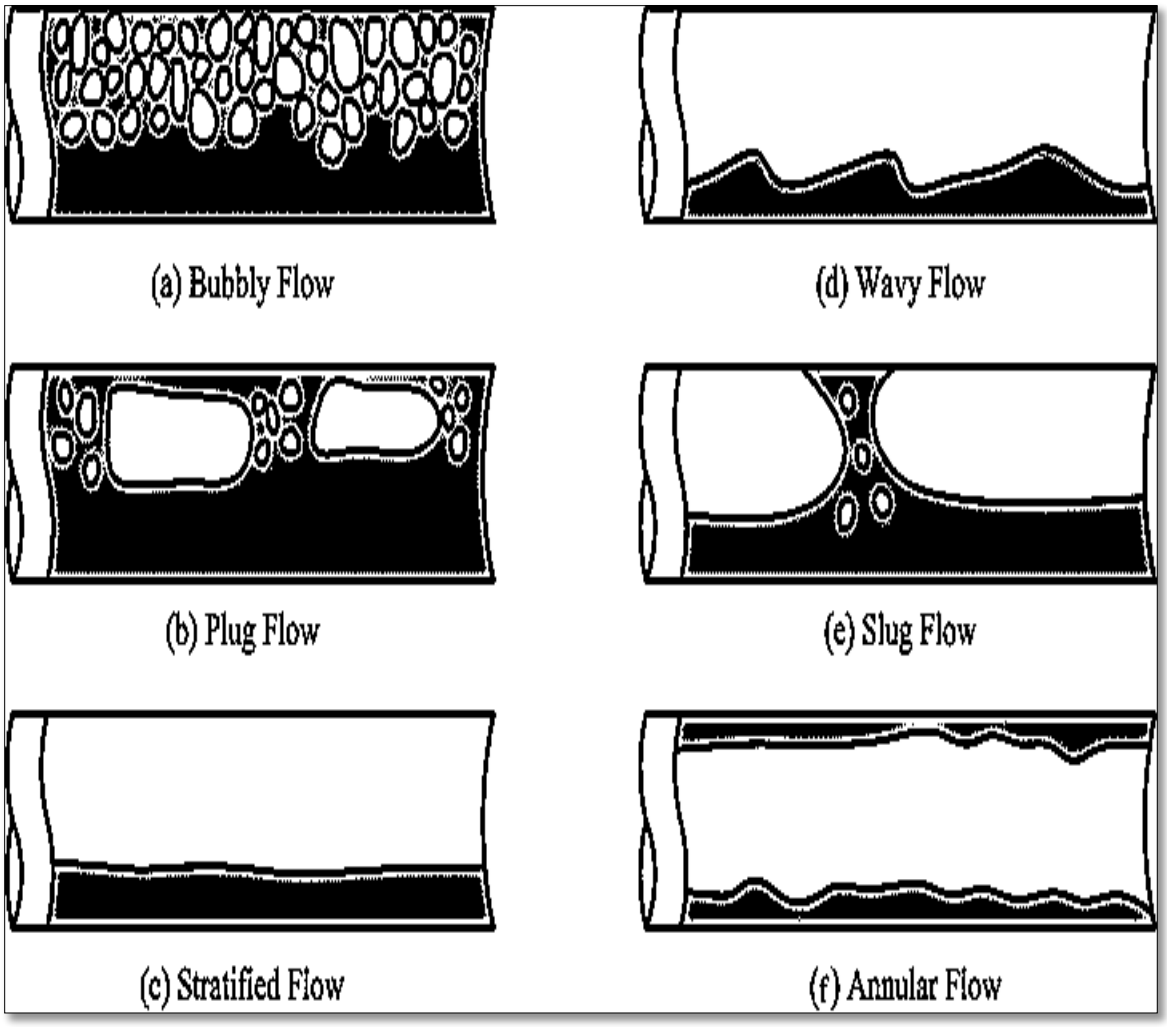

Figure 2. 2 Flow patterns in horizontal two-phase gas-liquid flow (Black = Liquid, White = gas) [Hewitt G. 1998].

2.2.2 Liquid-Liquid Flow Patterns

Two-phase liquid-liquid pipe flow is defined as the simultaneous flow of two immiscible liquids in pipes i.e. oil-water flow. This type of flow most frequently happens in the petroleum industry especially during transportation and production. Moreover, two-phase liquid-liquid flow is commonly seen in petrochemical industries. Although the accurate prediction of oil-water flow is essential, liquid-liquid flow system gained less attention compared to the gas-liquid flow system. Moreover, the liquid-liquid flow characteristics in horizontal pipe are very close to those of gas-liquid. Furthermore, the flow pattern transition concepts and models adopted for gas-liquid flow system were used for liquid-liquid flow system. This section concentrates mainly on oil-water fully developed flow phenomena in horizontal pipe.

A number of flow patterns have been observed during the simultaneous flow of oil and water. According to Lovick J. and Angeli P. [2004], the flow patterns reported ranged from fully separated to fully dispersed ones. Stratified flow, which has low phase velocities and well defined interface, received more attention during the past years. Recently, Gao Zhong-Ke et al. [2015] conducted an experiment for two-phase oil-water flow in a horizontal 20 mm I.D. pipe. They came up with a new approach aimed to unveil the flow structures based on multi-frequency complex network. Five flow structures had been articulated as shown in Figure 2.3. Many other researchers tried to identify the flow structures as demonstrated in Table 2.1.

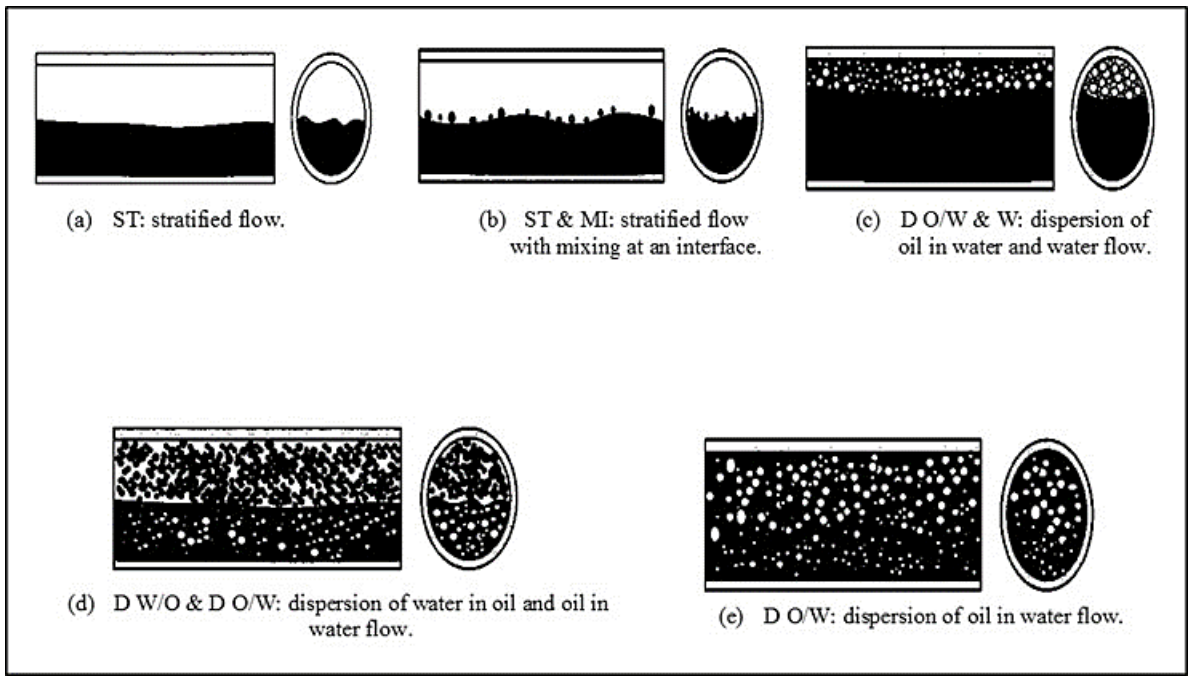

Figure 2.3 Flow patterns in horizontal two-phase gas-liquid flow (Black = water, White = oil).

Table 2.1 Summery of the literature review for the two-phase liquid-liquid flow

Publisher Name(s)	Fluids Type	Pipe Material / Dimensions	Flow Pattern Observed	Notice
Russel et al. [1959]	Oil-water	I.D.=25.4 mm L=8.0 m	Stratified flow. Mixed flow. Bubbly flow.	The fluid properties have been used as follows; - Tap water. - Clear mineral oil: density = 835 $kg.m^{-3}$, viscosity=18 cP.
Charles et al. [1961]	Oil-water	I.D.=25.4 mm L=8.78 m	Dispersion of water in oil. Concentric annular flow of oil in water. Oil-slug in water. Oil droplet in water. Water droplet in oil.	The fluid properties have been used as follows; - White mineral oil: density= 988 $kg.m^{-3}$, viscosity= (6.29; 16.8; 65) cP.
Hasson et al. [1970]	Kerosene -water	Glass Pipe I.D.=12.6 mm	Dispersed flow of one phase in the other. Slug flow. Stratified flow. Annular flow. Elongated bubbles of one phase in the other.	The fluid properties have been used as follows; - Distilled water. - Kerosene-Perchloroethylene PCE: viscosity= (0.8; 1.0) cP.
Oglesby et al. [1979]	Oil-water	--	Stratified and semi-stratified flow Semi-mixed flow Annular flow of one phase in the other. Dispersed flow of one phase in the other. Semi-dispersed flow. Dispersed mixture flow.	The fluid properties have been used as follows; - Oil: density= (857; 861; 868) $kg.m^{-3}$, viscosity= (32; 61; 167) cP.
Arirachakaran	Oil-water	I.D.= (25.4; 38.1)	Stratified flow.	The fluid properties have been

et al. [1989]		mm	Mixed flow. Bubbly flow. Intermittent flow. Dispersed flow	used as follows; - Oil: viscosity= (4.7; 58; 84; 115; 237; 2116) cP.
Valle and Kvandal [1995]	Oil-water	--	Stratified smooth flow. Stratified wavy flow. Stratified wavy-entrained flow. Stratified wavy with dispersed water and oil	--
Beretta et al. [1997]	Oil-water	I.D.=3.0 mm L=1.0 m	Slug flow. Plug flow. Annular flow. Bubbly flow. Dispersed flow.	The fluid properties have been used as follows; - Oil: viscosity= (9.8; 51; 71.17) cP.
Angeli and Hewitt [2000]	Oil-water	Stainless steel and Acrylic pipes I.D.=25.4 mm	Mixed flow. Stratified wavy with drops flow. Stratified mixed with water layer.	The fluid properties have been used as follows; - Oil: density= 801 $kg.m^{-3}$, viscosity= 1.6 cP.
Soleimani et al. [2000]	Kerosene (Exxol D80)-tap water	I.D.=25.4 mm	Oil encapsulation by water flow. Dispersed with droplets flow.	--
Bannwart et al. [2004]	Crude oil-water	Glass pipe. I.D.=25.4 mm	Annular flow.	The fluid properties have been used as follows; - Oil: density= 925.5 $kg.m^{-3}$, viscosity= 488 cP.
Rodriguez and Oliemans	Oil-water	Steel pipe.	Stratified wavy flow.	The fluid properties have been used as follows;

[2006]		I.D.=82.8 mm L=15 m		- Water: density= 1060 $kg.m^{-3}$, viscosity= 0.8 cP. - Oil: density= 830 $kg.m^{-3}$, viscosity=7.5 cP.

2.2.3 Gas-Liquid-liquid Flow Patterns

Currently, the gas-oil-water flow, which is more complicated flow than the two-phase flow, is receiving more attention from the industry and consequently from researchers. Understanding gas-oil-water flow requires knowledge on oil-water, air-oil and air-water flows since some of the flow characteristics of gas-oil-water flow are quite similar to the oil-water, air-oil, and air-water flows.

Açikgöz et al. [1992] Conducted a complex array of tests to obtain three-phase flow patterns for an air-water-oil system in a 19 mm I.D. Plexiglas pipe with a length of 2 m. Superficial velocities ranged from 0.15 to 50 $m.s^{-1}$ for the gas phase and from 0.004 to 0.66 $m.s^{-1}$ for the water phase. The superficial velocity for oil was kept constant at three values, 0.043, 0.09 and 0.24 $m.s^{-1}$. The authors constructed a flow pattern map including 10 different flow patterns for horizontal flow. The main flow patterns observed are plug, slug, stratified-wavy, and annular flow.

Hall [1992] performed a study on horizontal air-oil-water flow in a 40-m long steel pipeline with 79.9 mm I.D. Pressure gradient and phase fractions data were acquired. The phase fractions were measured with a 6.78 m long (L/D = 87) quick-closing valve section. However, only 95% of the trapped liquids could be blown out. The pressure gradient data were compared with six two-phase flow pressure gradient correlations. It was concluded that for stratified flows, the selected two-phase flow models gave good

predictions of water holdups, except the predicted holdups were always less than the measured values. Furthermore, predictions of oil holdups were not very accurate.

Taitel et al. [1995] considered three-phase stratified flow in pipes and presented a theoretical approach to solve the three-layer stratified flow equations. The gas-oil-water holdups of stratified three-phase flow at a given set of flow rates were calculated. The transition from stratified flow to slug or annular flow was modeled. However, the comparison with the experimental data, it was concluded that the criterion used in Taitel et al. [1976] for transition from stratified to non-stratified flows was valid for three-phase flow at low gas flow rate

Pan [1996] suggested a similar approach as Açikgöz et al. [1992] to define the three-phase flow patterns. The author suggested defining three-phase flow patterns as a three-part or two-part definition, depending on the shape of the flow. Configuration between oil and water phases, continuity of oil and water phases and the overall shape of the flow in general were considered to define the three-phase flow pattern. Based on experimental observations, flow patterns were classified into eight three-phase flow categories. In addition, he developed an equation for the liquid mixture effective viscosity for better prediction of holdups.

Khor [1998] studied stratified gas-oil-water flow and developed a one-dimensional three-fluid model for stratified three-phase flow. The author broke down three-phase stratified

flow into nine categories. A methodology was developed to solve the momentum equations and estimate pressure gradient and liquid holdups.

Chen et al. [1999] Investigated three-phase air-oil-water in two helically coiled tubes with 39 mm I.D. and coil diameter of 265 and 522.5 mm. Low oil fraction was used with air-water. They found that the flow pattern in helically coiled is completely different than straight pipe. The authors mentioned that further investigation is needed in this field.

Utvik et al. [2001] reported experimental comparison between two and three-phase flow. The two-phase consists of light hydrocarbon and water. And the other one made up of model oil system in three-phase pipe flow. The purpose of the comparison was to compare pressure drop and flow patterns for horizontal flow for similar fluid properties such as; oil-water interfacial tension, viscosity, and density. The results showed significant divergence with respect to pressure drop and flow patterns from two-phase to three-phase flow. The author suggested that the results explained the inconsistency often found between models and measurements on multiphase flow lines in the petroleum industry.

Mathematical simulation model of stratified and slug three-phase flow have been made by Bonizzi et al. [2003]. They were modeling the three-phase flow system as one-

dimensional transient two-phase. The two phases consisted of gas and a mixture of the two liquids. By using this model, they came up with the following results;

- The ability to predict locally the flow patterns of the two liquids, which were dispersion and stratified flow.
- The ability to predict the slug flow pattern.
- The ability to reproduce trends of the major slug properties observed while doing the experiment, such as liquid holdup, pressure gradient, and slug frequency.

Oddie et al. [2003] conducted 444 steady-state and transient experiments for oil-water and oil-water-gas multiphase flows through a transparent 11 m long, 150 mm diameter, inclinable pipe using kerosene, tap water and nitrogen. The pipe inclination varied from 0° to 90° and the flow rates of each phase varied over wide ranges. Holdups as a function of flow rates, flow pattern and pipe inclination were investigated. Various techniques for measuring holdup were compared and discussed. The flow pattern and shut-in holdup were also compared with the predictions of a mechanistic model. The comparison results showed close agreement between the observed and predicted flow patterns and reasonable agreement in holdup.

Zhang et al. [2003, 2006] came up with a unified model for prediction of gas-oil-water flow characteristics in pipelines and wellbores. Two cases were assumed. If the two liquids are completely mixed, then the three-phase flow considered as two-phase gas-liquid flow. In the other case, the three-phase flow treated as a three stratified layers flow

at low flow rates in horizontal or partially inclined pipes. Also, they proposed a closure relationships to describe the distribution between the two liquid phases. The proposed model was evaluated using experimental data for gas-oil-water.

Wegmann et al. [2007] conducted an experiment on a three-phase liquid–liquid–gas air-paraffin-water flow in a horizontal glass pipe of 5.6 mm and 7.0 mm I.D. The flow patterns observed are: Stratified-intermittent flow, Annular-intermittent flow, Intermittent-dispersed flow, Intermittent- intermittent flow, Dispersed-intermittent flow and Dispersed-annular flow. Furthermore, homogenous model has been chosen to manipulate the density and viscosity of the liquid mixture. They found that a decreasing pipe diameter changes the flow pattern maps and also the behavior of the transition boundaries. Flow pattern observed is reported in Figure 2.4

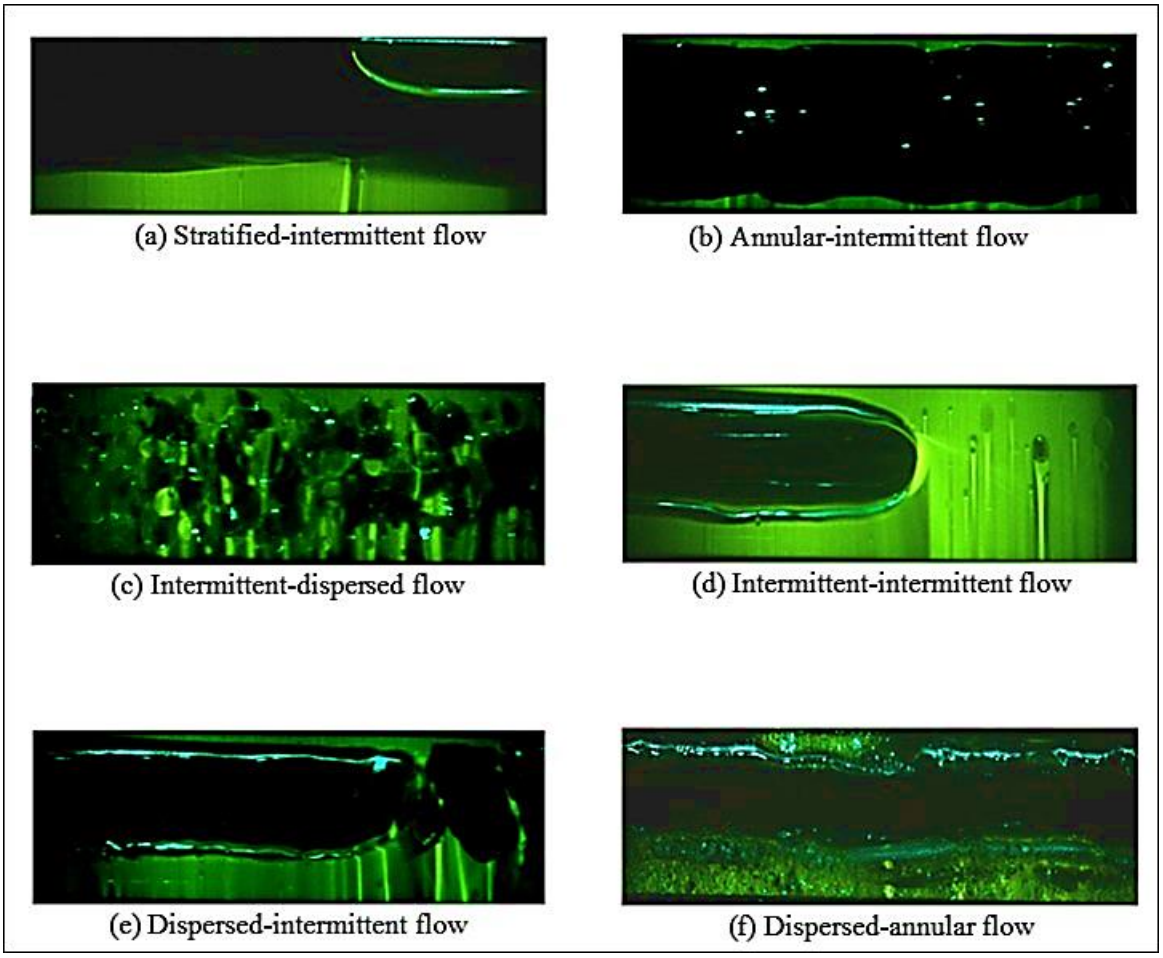

Figure 2.4 Flow patterns for three-phase gas-liquid-liquid flow (Green = water, Black = paraffin, Shiny White = air) in 7.0 mm and 5.6 mm ID horizontal pipes.

2.3 Drag reduction in multiphase flow

It has been long known that the addition of a small amount of linear, flexible, high molecular-weight, and long-chain polymer molecules in organic or in water solvents can dramatically change the flow structure in turbulent flow which results in reduction in the drag on a solid surface [Toms 1948]. The effects of adding DRPs to single-phase flows have been thoroughly studied and the mechanisms have been well understood to be related to reduction in stresses, and dampening of turbulent bursts [Al-Sarkhi and Hanratty 2001a, Manfield et al. 1999].

Predicting the nature of both gas-liquid and liquid-liquid interfaces and their combination is difficult. Therefore, three-phase flow studies are relatively few. Detailed analyses on the published work done earlier on the effect of using drag reducing agents (DRAs) with two and three-phase are reported in Table 2.2.

Table 2.2 Summery of the literature review for the effect of using DRA in a Multi-Phase flow

Fluids	Reference	DRP used	Type of Flow Pattern	Findings
Two-Phase **(Gas-Liquid flow)**	Oliver et al. [1968]	1.3% polyethylene oxide (PEO) aqueous solution and air.	-Annular-Wavy Flow. - Slug Flow.	As a result of using polymer; the annular flow disturbance and high amplitude waves become smoother flow film. While in slug flow pattern, the flow showed less circulation.
	Greskovich et al. [1971]	50 ppm of Polyox (Polyethylene oxide coagulant)	Slug Flow	A 50% drag reduction was achieved in a slug air-water flow.
	Burger et al. [1982]	DRP (CDR of 10.3 wt%) 10 ppm oil-soluble polymers	--	Studdied the effect of adding DRP (with concentration of 10.3 wt%) to a commerical application, located in the trans-Alaska pipeline system, used crude oil flowing in TAPS pipeline which has diameter of about 1220 mm and 356 mm. They found that the drag reduction increased with increasing velocity, decreasing diameter, and decreasing viscosity. Other finding was reported in their paper.
	Wilkens et al. [2007]	400 ppm of SDRA	Slug Flow	Performed an experiment using two-phase (air-water) in horizontal pipe of 52 mm ID. They found that the addition of 400 ppm of SDRA to the air-water mixture reduced the pressure drop by 25–40%. In addition to that, the addition of SDRA eliminated the occurrence of the slug flow.
	Scott [1972]	polyacrylamide polymer (Polyhall 295)	Slug Flow	They used DRP in a co-current air-water slug flow in 2.5 cm I.D. The velocity of liquid phase was fixed at constant Re_L=13,000 while varying Re_G from 1500 to 6100. They found the following; 1- At same liquid velocity, DR in two-phase flow exceeds that of single-phase flow. 2- For single-phase case, the DR was around 29 to 33 % for Re of 7000 up to 30,000. 3- DR_{Max}= 33% happens at polymer concentration of 68 ppm. 4- For slug flow pattern, the pressure gradient due to acceleration was

				greater than the frictional pressure.
	Rosehart et al. [1972]	68 ppm Polyhall 295 (Polyacrylamide)	Slug Flow	They studied the frictional pressure drop in two cases; single phase and slug flow using drag-reducing polymer. The results showed higher drag reduction in a slug flow than in a single phase. A 33% drag reduction was achieved in a slug flow.
	Sylvester et al. [1976]	100 ppm of polyethylene oxide.	Annular Flow	They studied the effect of drag-reducing polymers on an annular air-water flowing in horizontal pipe of 1.27 cm pipe diameter and a length of 6.1 m at superficial gas velocities of 86 and 111 $m.s^{-1}$. The change in pressure gradient was up to 37 %. The authors did not provide explanation for these changes.
	Sylvester et al. [1980]	200 ppm Dowell APE (aluminum salt of an alkyl phosphate ester)	Annular-mist	Drag reduction in two-phase cocurrent natural gas-hexane flow in a 25.4 mm I.D. and 30.48 m long horizontal pipe was performed experimentally. The results show that at a given liquid flow rate, as gas flow rate decrease the DR increase. On another hand, the DR decrease as friction velocity increase or as gas-liquid ratio decrease. Maximum drag reduction obtained is 34 %.
	Manfield [1999]	--	--	He conducted deep literature survey on the effect of drag reducing polymers on multiphase flow. He found that this type of research needs deep understanding of the fundamental behind it.
	Al-Sarkhi et al. [2001a]	polyacrylamide and sodium-acrylate (Percol 727)	Annular Flow	They conducted an experiment on an annular air-water flow in a 95.3 mm I.D. and 23 m horizontal length to study the effect of adding DRP. They found the following; 1- 10-15 ppm of the polymer solution produced drag reduction of 48%. 2- At higher DR, annular flow regime is changed to a stratified flow. 3- Comparing large diameter with smaller one, they found that the

				smaller diameter need large DRP concentration in order to obtain maximum DR.
	Al-Sarkhi et al. [2001b]	polyacrylamide and sodium-acrylate (Percol 727)	Annular Flow	Same experiment was repeated to study the effect of varying pipe diameter on the drag-reducing polymers from 95.3 to 25.4 mm. They found that the percentage of drag reductions for D = 25.4 mm was increased up to 63%.
	Soleimani et al. [2002]	100 ppm of polyacrylamide and sodium acrylate solution	Stratified Flow	An experiment was performed to study the effect of adding 100 ppm of DRP on stratified air-water flow in 25.4 mm horizontal pipe diameter. The following was observed; 1- As DRP added, the waves were decreased and liquid hold up increased. 2- As gas velocity was increased the interfacial drag decreased. 3- At high liquid flow, a transition from stratified to slug flow was observed.
	Baik et al. [2003]	50 ppm Polyacrylamide (Magnafloc 1011).	Stratified Flow	They tested the influence of 50 ppm on a stratified air-water flow in 0.0953 m pipe diameter and 23 m horizontal pipe length. The following was observed; 1- At low superficial gas velocity and at superficial liquid velocity of 0.15 $m.s^{-1}$, the wave amplitude decreased when adding 50 ppm of DRP. 2- Delaying the transition from stratified to slug flow. 3- DR_{Max}= 42%
	Al-Sarkhi et al. [2004]	50 ppm Polyacrylamide and sodium acrylate (Percol 727 or Magnafloc 101l).	Annular, Slug, and Pseudo-Slug Flow	An air-water flow in 25.4 mm pipe diameter and 17.0 m horizontal length was tested by inserting 50 ppm of DRP to the flow. The following was observed; 1- Adding DRP, causing flow pattern change (from annular, slug, or pseudo-slug to stratified flow) and reduction in pressure drop. 2- The effect of DRP on slug flow was

				low. A reduction on the amount of slug frequency was reported.
	Fernandes et al. [2004]	Poly-alpha-olefin polymers (of high molecular weight)	Annular Flow	They conducted an experiment in a horizontal pipe of 19 mm I.D. containing annular flow of methan (CH_4)-decane($C_{10}H_{22}$) at P=10 bar. The following was noticed; 1- While adding DRP, a reduction in frictional pressure happens due to change in flow pattern. 2- For annular flow and at fixed superficial gas velocity, as superficial liquid velocity increased the DR increased. 3- For annular flow and at fixed superficial liquid velocity, as superficial gas velocity increased the DR decreased.
	Al-Sarkhi [2005]	40 ppm polyacrylamide (Magnafloc 101l)	Annular Flow	A DRP was injected into an annular flow of air-water flow in a 0.0127 m I.D. and 7.0 m horizontal pipe length. The following was found; 1- DR was 47% at DRP concentration of 40 ppm. This percentage is sensitive to the gas and liquid flow rates. 2- At large DR, the annular flow transferred to stratified flow pattern.
	Mowla et al. [2006]	Polyalpha olefin (Polyisobutylene)	Slug Flow	A drag reduction test was performed by injecting DRP to slug two-phase flow of Air-crude oil in co-current horizontal pipes. The pipes have different specifications as follow; 1- Smooth pipe of polycarbonate with length of 10.3 m long and I.D. of 0.0254 m. 2- Rough pipe of galvanized iron with length of 8.8 m and I.D. of 0.0254 m. 3- Rough pipe of galvanized iron with length of 8.8 m and I.D. of 0.0127 m. The following results were obtained; 1- Adding DRP to the flow is reducing the pressure drop up to certain concentration after that the pressure drop remains constant. 2- DRP in rough pipe is much better than in smooth pipe. 3- DRP in small pipe diameter is effective more than in larger one.

	Jubran et al. [2005]	--	--	They performed literature survey on drag reduction in single-phase and multi-phase flow. They suggested that more work is needed in the areas of shear degradation, wax content, water cut, and pipe inclination on the performance of drag reduction.
	Daas et al. [2006]	--	Slug Flow	A slug oil-carbon dioxide flow in horizontal pipe of 100 mm ID was tested with existing DRP. Two types of oil with different viscosities 0.0025 and 0.05 Pa.s were used. DRP was found to be more effective in reducing the total pressure drop at oil viscosity equal to 0.0025 Pa.s, but DR was higher in the 0.05 Pa.s oil.
	Al-Sarkhi et al. [2006]	--	Annular Flow	Upward inclined pipe of a 0.0127 m I.D. containing annular air-water was investigated at presence 100 ppm of PDR. The following was found; 1- At DRP concentration of 100 ppm, the DR in the pipe was 71%. 2- At high concentration value, the annular flow was transferred to stratified or annular-stratified flow pattern. 3- At inclination angle of 1.28°, low superficial gas velocity, and high superficial liquid velocity maximum drag reduction was obtained.
	Fernandes et al. [2009]	75 ppm Polyacrylamide/ sodium acrylate (Magnaflox)	Annular-Entrained Flow	A vertical annular entrained two-phase flow in 25.4 mm ID and 22.12 m long was investigated under the presence of DRP. They found the following; 1- A reduction of 82% of the frictional pressure. 2- An increase in the liquid holdup by 27%.
	Al-Sarkhi et al. [2011]		All flow pattern	Developed a correlation to predict the friction factor for DRP added to annular air-liquid flow and for all flow pattern of oil-water flow for any pipe diameter. The results showed that the friction factor, which is a function of mixture Reynolds number and the ratio of the gas to liquid superficial velocities, increases with increasing $\mathrm{Re}_M \sqrt{U_{SG}/U_{SL}}$ for annular gas-liquid flow and decreases with increasing $\mathrm{Re}_M \sqrt{U_{SW}/U_{SO}}$ for oil-water flows.

Two-Phase (Liquid - Liquid flow)	Sifferman and Greenkorn [1981]	Three types of DRP were used; -Carboxymethyl cellulose (CMC) -Polyethylene oxide (POLYOX^{TM}) -Guar gum (Jaguar^{TM})	--	They examined the drag reduction by adding 0.001 to 0.3 wt% of DRP to three different fluid flow in three pipe diameters (27, 38, and 53 mm); 1- Single-phase dilute polymer-water solutions. 2- Two-phase liquid–solid. 3- Three-phase immiscible liquid–liquid–solid solutions. The following results were obtain at Reynolds numbers exceeding 105; 1- 80% of drag reduction was achieved for the dilute polymer system at concentrations of 0.3 wt%. 2- 95-98 % of DR was achieved for the liquid-solid system.
	Al-Wahaibi et al. [2007]	Polyacrylamide and sodium acrylate (Magnafloc 1011)	Stratified Flow	They examined the performance of DRP on oil-water in acrylic pipe of a 14 mm I.D.. The viscosity of used oil was 5.5 mPa s. The following results were noticed; 1- DRP gives longer time for stratified flow pattern and delays the transition to slug flow pattern by damping the interfacial waves. 2- Introducing DRP caused a decrease in pressure gradient, increase in water hold up. 3- 50% of DR was obtained.
	Al-Yaari et al. [2009]	(5-10-15 ppm) of: - Magnafloc - Polyethylene oxide	--	Studied the effect of adding two different DRPs (Magnafloc and polyethylene oxide) to two-phase oil-water flow by observing the flow pattern and pressure drop. They also examined the effect of salt content in the water on the performance of DRP. An acrylic horizontal pipe test section of 25.4 mm ID was used. They found that the injection of DRP with concentration of 10-15 ppm and high mixture velocity reduced the pressure drop and caused clear change in flow pattern. A negative salt effect on the DRP effectiveness was reported. At 5 ppm of DRP and at a water fraction range of (0.33–0.35) phase inversion point in dispersed flow regime occurred.
	Al-Yaari et	DRP	--	Conducted an experiment using horizontal pipe of 25.4 mm. Two-phase oil-water flow

	al. [2012]			have been tested with and without DRP. The aim of this study is to show the effect of DRP on the water hold up using conductivity probe. They found that when superficial water velocity (U_{SW}>0.5 m.s^{-1}) is larger than the superficial oil velocity (U_{SO}), the water holdup of oil-water with DRP is less than without DRP.
	Spedding et al. [2006]	--	--	Tested empirical correlations against two and three phase pipe flow data for the prediction of pressure drop. For three-phase flow empirical correlations, e.g. gas-oil-water, the pressure drop is predicted by treating the combined liquid phase as a single entity. As a result, four correlations were used for prediction three-phase intermittent SI type flows. They also found that existing two-phase moment balance models filled to predict the pressure drop of three-phase flow.
Three-Phase (Liquid-Liquid-Gas Flow)	Sifferman and Greenkorn [1981]	Three types of DRP were used; -Carboxymethyl cellulose (CMC) -Polyethylene oxide (POLYOX^{TM}) -Guar gum (Jaguar^{TM})	--	Carried out experiments on three-phase oil-polymer solution-sand mixture flows in a relatively large diameter pipes (0.027, 0.038, and 0.053 m); and flow rates were varied up to 0.0189 m^3.s^{-1}. They found results similar to those of the two-phase solid-liquid system.
	Kang et al. [1998]	Oil-soluble DRP	Stratified flow Slug flow Annular Flow	Studied the effect of DRP on pressure gradient and flow regime in horizontal and 2° upward inclined pipes. Experiments were carried out using three-phase CO_2-oil-water flows in a 10 cm I.D. and 18 m long pipe. The DRP concentrations was ranging from 0.0 to 75 ppm. The superficial gas velocities between 1.0 and 14.0 m.sec^{-1}, and the superficial liquid velocities between 0.03 and 1.5 m.sec^{-1}. They found that the drag reduction was 81% for the stratified flow, and 35% for the annular flow. Accordingly, they concluded that the drag reduction obtained for a certain concentration of DRPs depends on the water cut and flow

				patterns. In addition, they found that DRPs delay the stratified to slug flow transition at higher superficial liquid velocities.
	Moré et al. [2008]	Oil-soluble DRP Water-soluble DRP	Slug Flow	Carried out experiments on the effect of adding DRPs on three-phase gas-oil-water flows in a 10 cm I.D. and 36 m long pipe. The following parameters used; 1- Ranges of superficial liquid velocities and superficial gas velocities between 0.5-1.5 $m.s^{-1}$ and 4-10 $m.s^{-1}$ respectively. 2- Temperature and pressure were 30°C and 0.45 MPa respectively. 3- DRPs concentrations were varied from 0.0 up to 50 ppm. The following observations were noticed; 1- Adding DRPs to the flow resulted in decreasing the pressure drop and the flow pattern changed from slug to wavy stratified. 2- The amount of turbulence at the gas–liquid interface decreased with the addition of DRPs. 3- Negative behavior of oil-soluble DRP at dispersion (or emulsion) flow pattern.
	Langsholt [2012]	Oil-soluble DRP Water-soluble DRP	Stratified flow Slug flow Annular Flow	Conducted experimental studies on the influence of two types of DRPs (water- and oil-soluble) on three-phase gas-oil-water. The multiphase flows in 1° upward and 1° downward pipe, 10 cm ID, 25 m long pipe. Three flow patterns were examined. For the stratified flow and 1° downward pipe inclination, the results shown that the drag reduction increase with increasing the fraction of the DRPs. For the slug and annular flow, and 1° upward pipe inclination, the results shown that the water-soluble DRP was only marginally better than oil-soluble DRP. In terms of drag reduction, the results revealed that the drag reduction increased with increasing the DRP fraction in liquid. He also found that as the gas superficial velocity and the liquid superficial velocity increased, the drag reduction would increase.

2.4 Techniques used to study the Mechanisms of drag reduction by DRAs

Over the years, measurement of flow properties like phase velocities, vortices, induced turbulence, have been carried out with various techniques such as Impedance Capacitance, Hot-Wire Anemometry, Laser Doppler Velocimetry, Planar Doppler Velocimetry, Particle Image Velocimetry (PIV) …etc.

PIV is relatively a new non-intrusive, optical measurement technique that allows measurement of instantaneous velocity of single phase and multi-phase flows in two and three components. Its non-intrusive approach eliminates disturbances inherent in other approaches which makes it suitable for high speed flow with shocks, boundary-layer flow measurements as well as comprehensive study of laminar and turbulent flows. PIV enables qualitative determination on instantaneous velocity in the entire flow field with high spatial and restricted resolution which makes it relevant in studying the spatial structures in unsteady flows as opposed to single point measurement capability of conventional methods [Li F.C. and Hishida K. 2009; Raffel M. et al. 2007]. It is an indirect velocity measurement technique in the sense that the velocity of the flow field is determined from the measured tracer particle velocity [Raffel M. et al. 2007]. The reliability, accuracy and applicability to any optically accessible flow has made PIV one of the relevant diagnostic tools in industries and research as it extends the frontier of study into micro-fluids, spray atomization, combustion [Li F.C. and Hishida, K. 2009].

The numerous advantages portrayed by the PIV technique do not entirely obscure its shortcomings. PIV technique poses specialized challenges that require dexterity and adequate knowledge of fluid mechanics to overcome [Buchhave P. 1992]. It requires stringent measures in obtaining reliable results such as selection of seeding particles with matching densities to continuous phase. Moreover, PIV technique requires strict adherence to safety rules related to laser usage.

The basic PIV measurement involves seeding the flow with tracer particles, illuminating the seeded flow in the target area with light sheets from the light source and capturing the reflected light from the tracer particle as frames separated by time intervals by the camera. The frames are analyzed using different algorithms to determine the instantaneous velocity of the flow field. The analysis involves dividing the images into subsections termed interrogation areas (IA) containing fewer particles. Cross-correlation of two interrogation areas Ix and Ix+Δx pixel by pixel yields a signal peak, which represents common particle displacement ΔX. The velocity vectors were calculated by dividing each displacement vector by time delays between the two images i.e. $\overline{U} = \frac{\Delta X}{\Delta t}$. Sub-pixel interpolation is relevant in achieving accurate measurement of displacement and velocity. Vector map generated by repeating cross-correlation of IA over image pairs, undergoes further processing to determine the desired properties like vortex, streamlines etc.

Single-phase flows such as water flow over a solid or internal flow in pipes requires less stringent measures in analyzing with PIV than multiphase flows because the latter poses problems such as attenuation of light sheets by densely seeded flows, velocity differences associated with each phase in the flow. The complexity encountered in multiphase flows is brought by the interaction between the phases involved like gas-liquid, liquid-liquid, solid-liquid phases. Flow rate, bubble sizes and internal two-phase flow structure influences the process of surface flow generation and bubble parameters [Abdulmouti H. and Jassim E. 2013]. PIV analysis of multiphase flows requires the use of light sheet optics and separation of the phases (continuous and dispersed) in order to extract reliable information about the separate phases and the interaction between the phases [Saarenrinne P. et al. 2004]. The multiphase concept has led to various PIV techniques, which involve improved lighting and image acquisition and development of algorithms to cater for phase separation, size and orientation of dispersed phase, turbulence induced by dispersed phase etc.

Amongst PIV techniques used in literatures are PIV/LED, PIV/LIF, PIV/LIF/LED, micro-PIV, standard 2D-PIV, stereo-PIV, and Holographic PIV. The standard 2D-PIV (2D2C) measuring technique was used to study the flow characteristic in this study. This technique measures two velocity elements in a plane using a single CCD-camera.

PIV adopts the Lagrangian principle in its operation as it seemingly involves following of each particle across the flow field. The genesis of PIV was Laser Speckle Velocimetry,

which utilizes Young Fringes investigation to determine displacement from normal to lights dispersed sample faces under stress [Dudderar T.D. and Simpkins P.G. 1977].

Subsequently, PIV had been used for experimental purposes to determine flow velocity and other fluid properties. For example; cavitation flow in open channel [Tassin A.L. et al. 1995], flow in wet gas pipeline [Erickson D. and Twaite D. 1996], large scale stream discharge [Harpold A. A. and Mostaghimi S. 2004], liquid jet flow [Novotný J. et al. 2005], fluctuating aerated flow in slanted and even water pipes [Kabiri-Samani A. R. et al. 2007], turbulent bubbly blending layer flow [Ning T. et al. 2009].

The PIV measurement technique has evolved over the years owing to the need to improve on its accuracy and ability to take measurements in critical regions like boundary layers. Such improvements were seen in the components that constitute PIV analysis ranging from speed and number of cameras, various types of fluorescent tracer particles, light sources and optics to shutters, filters and synchronizers, with the aim of eliminating sources of errors and thereby achieve readings that almost depict the structure and dynamics of flows. The level of sophistication of the devices engenders the different available algorithms employed in evaluating images and determination of vectors and other desired quantities. It can be deduced that proper selection of components of PIV set-up and algorithms determine the reliability and accuracy of its measurement.

Hassan Y. A. et al. [1992] used the PIV technique to determine instantaneous velocities and other flow characteristics like vorticity of a bubbly flow in a rectangular vessel. The

liquid is mineral oil of density 0.878 g.cm^{-3} (25°C) and 69.0 centipoise viscosity seeded with a 70 μm diameter plastic spheres with bubbles induced by a needle. Deen N.G. [1999] determined turbulent properties such as strain rates and correlation between the dispersed and continuous phase of a bubble column by measuring instantaneous velocity in the continuous phase using regular PIV technique. Success was not achieved in determining the dispersed phase/ bubble velocity.

The Pseudo-turbulence in liquid induced by rising bubbles was measured by Lindken R. and Merzkirch W. [2002]. They used a novel PIV technique which combines three most used techniques namely PIV/LIF, digital masking and Shadowgraphs which complements one another by minimizing their individual drawbacks. The method was premised on high grey value of background intensity and use of one black-white (b/w) camera in capturing the image to be processed to calculate the velocity distribution of both liquid and bubble phases.

Aubin J. et al. [2004] investigated a liquid-gas two-phase flow for the motion of the liquid in an air impregnated liquid vessel agitated by 6-bladed pitched turbine for both upward and downward pumping mode using PIV. The time-averaged radial-axial velocity readings obtained were used to establish a relationship between aeration, average velocity and turbulent fields occurring in the liquid phase. The images obtained were analyzed with VISION+ (commercial software).

Harpold A. A. and Mostaghimi S. [2004] showed that the mean Reynolds stresses diminishes with the increase of Reynolds number and that the diminishing trend was more prominent in the seeded flow.

The momentous flow field in a motored compression ignition engine was investigated by Coupland J. M. et al. [2006]. They considered the flow as three-dimensional and measured velocity component using the combination of Holographic PIV (HPIV) and Object Conjugate Reconstruction (OCR). The whole set-up consists of optically designed diesel engine, holograph, CCD camera, seeding particles, optical-fiber probe and Fourier transform lens. The description of the holographic reconstruction image field and subsequent introduction of image shift were carried out by complex amplitude correlation calculation and OCR, respectively. Particle displacement was calculated by mapping each wave vector to corresponding image on the CCD array.

Ning T. et al. [2009] performed experimental investigation of gas-liquid two-phase flows of turbulent bubbly mixing layer flow with DRP through vertical channel using PIV technique. Also, comparisons had been conducted with pure water single-phase turbulent mixing layer flow with DRP.

Li F.C. and Hishida K. [2009] conducted a comprehensive overview of PIV techniques by illustrating with measurements in multiphase flows such as free surface flows, bubble flows and particle-laden flows with the aim of setting guidelines to aid research in multiphase flows. The review was centered on the interest areas namely enhancement of spatial resolution and accuracy of commonly used PIV, recent developments in relation to dimensions and velocity components of PIV techniques and advances in multiphase flow measurements using PIV techniques.

Abdulmouti H. and Jassim E. [2013] used PIV technique to investigate surface flows generated by bubble plume with the aim of broadening the scope of application of bubble

flow and two-phase flow, highlighted how the techniques of surface flow generation by bubble plume differs from single-phase liquid jet and single phase buoyant plume and how flow characteristics are related to bubble parameters. PIV/PTV and E-L numerical simulation modelling were used to capture the data of the field surrounding the bubble plume and the flow structure of various such as gas injection point, middle section and water surface of the bubble region.

Two different PIV/LIF methods in synchronization with two high-speed cameras were used to study the hydrodynamics and formation of slug in pipes by Czapp M. et al. [2012]. The stereo PIV/LIF method was used to determine 3-D water velocity amongst other parameters like flow rates, void fraction and axial vortex structures. While, the 2-D PIV/LIF method aligned with two high-speed cameras were used to determine the centerline axial velocity. Different flow regimes namely stratified, wavy, slug (high-pressure pulsating flow). Pipe flow was generated by varying inlet fluid (water and air) velocity introduced into horizontally placed transparent cylindrical pipe. An advanced cross-correlation scheme of 32 and 16 integration areas with 50% overlap and 3 refinement steps for iterative optimization were used. Weighting function was used to suppress edge phantom correlations, masking technique and the variation of the inlet water velocities of 0.505-1.506 $m.s^{-1}$ had 0.1% uncertainty. Comparisons were made between the two PIV methods and numerical simulation results were used to validate data such as turbulent intensities generated by both methods. It was noted that similar techniques of interfacial area and axial velocity were used by both methods to analyze the formation of slug.

CHAPTER 3

INSTRUMENTATION AND EXPERIMENTAL PROCEDURE

Instrumentation and experimental procedure reported in this chapter were used to study the effect of drag reducing polymers (DRPs) on the pressure gradient and flow patterns of fully developed single, two and three-phase flow, using 22.5 mm I.D. horizontal pipeline. In addition, the effects of mixture flow rates on the performance of DRPs were investigated. A multiphase flow loop was designed and constructed to achieve the objective of this study. The multiphase flow loop constructed in Research Institute (RI) building at the King Fahd University of Petroleum and Minerals. Detailed description of the flow loop is presented in section 3.2. All experiments conducted for this study were achieved by using tap water (aqueous phase), one type of kerosene known as ESCAID^{TM} 110 (oil phase) and atmospheric air. Detailed information about the three phases and the DRPs used is presented in section 3.1.

3.1 Fluids and DRPs Properties

The experimental loop was designed to examine different flow configurations; single-phase flow, two-phase flow, and three-phase flow. Atmospheric air was used as the gas-phase. Properties of air were determined based on temperature and pressure in the laboratory. Tap water was used in a closed circulating loop which was separated from oil and reclaimed in a separate tank. Properties of water were determined using NIST properties based on temperature and pressure in the laboratory.

ESCAID^{TM} 110 Fluid (one type of kerosene) has been selected to be the oil working fluid. The selection was based on its stable properties at the operating conditions of the loop and the low density to ease separation from water. Table 3.1 shows properties of ESCAID^{TM} 110 , tap water used, and air.

Table 3.1 Properties for oil (ESCAID^{TM} 110 Fluid), tap water, air.

Substance	Property	Typical Value	Test Based on
Properties of Oil (ESCAID^{TM}110)	Specific Gravity @ 15.6/15.6 °C	0.790 – 0.810	ASTM D 4052
	Kinematic Viscosity @ 40.0 °C, cSt	1.50-1.75	ASTM D445
Water	Density @ 25°C, kg/m^3	998	NIST
	Viscosity @ 25°C, Pa s	0.000985	NIST
Air	Density @ 25°C, kg/m^3	1.2	NIST
	Viscosity @ 25°C, Pa s	0.000018	NIST

ZETAG® 8165 (a copolymer of acrylamide and proprietary quaternized cationic monomer) was used as the water-soluble DRP. This means that in addition to acrylamide, it has a cation-anion repeating unit that dissociates in water. This is a polyelectrolyte flocculant produced by BASF–the Chemical Company, Germany. It is a

high molecular weight copolymer and available as a free-flowing white powder. Table 3.2 lists the properties of ZETAG® 8165. Figure 3.1 represents an increase in DRP viscosity at temperature equal to 25°C as its concentrations increased.

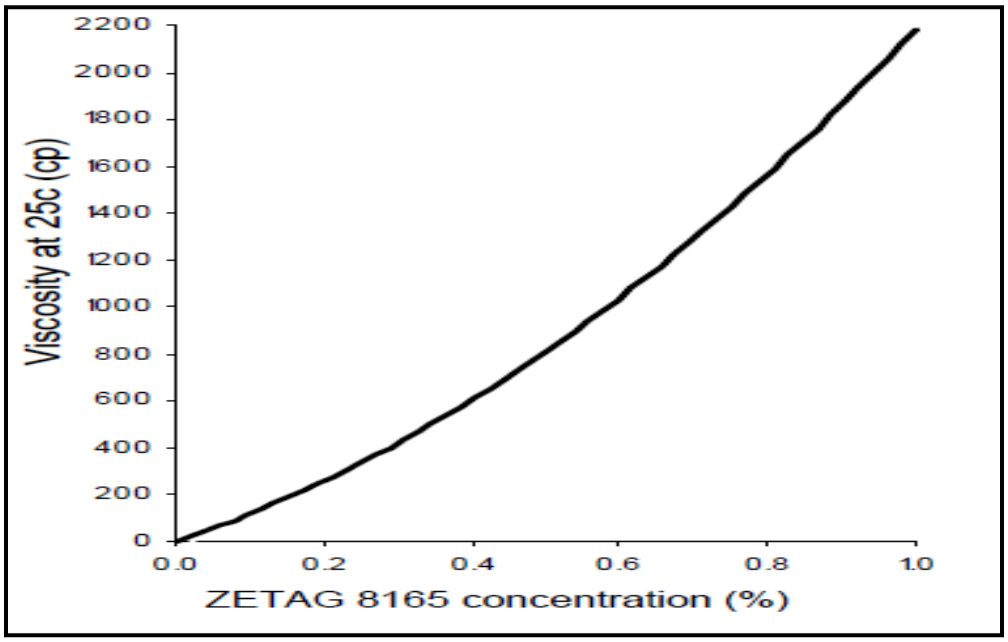

Figure 3.1 Viscosity versus solution concentration for ZETAG®8165 [Available at: Ciba Specialty Chemicals Corporation]

Table 3.2 Properties of water-soluble ZETAG®8165

Properties	Description
Product name	Polyacrylamide (PAM)
Appearance	Off-white granular solid
Molecular Weight	Very high
Bulk Density	0.7 $g.cm^{-3}$
PH of 0.5% solution	Approx. 3.5
Viscosity at 25°C	See Figure 3.1
Solubility	Water-soluble (Non-Newtonian)

Polyisobutylene (PIB), from Scientific Polymer Products, having ultrahigh molecular weight (2.8×10^6 $g.mol^{-1}$) and a linear rubbery (amorphous) structure [Choi and Jhon, 1996], was used as the oil-soluble DRP. It is made from the isobutylene [$CH_2=C(CH_3)_2$]

monomer only via cationic addition polymerization. Table 3.3 summarizes the properties of the above PIB.

Table 3.3 Physical properties of oil-soluble DRP (PIB)

Properties	Description
Product name	Polyisobutylene (PIB)
Supplier	Scientific Polymer Products, Inc.
Molecular Weight	0.85×10^{6} g.mol^{-1}
Description	Odorless clear slab
Specific Gravity	0.92 at 20°C
Solubility	Oil-soluble (Non-Newtonian)

3.2 Experimental Facility Design, Construction and Integrity

Turbulent drag reduction induced by dilute solutions of both water and oil-soluble DRPs in three-phase flow in a horizontal pipeline was investigated. The experimental facility in Figure 3.2 shows three-phase air-oil-water flow loop. It consists of two supply tanks of oil and water, two supply pumps (one for each liquid), pipes including test section, separation tank, return pump, air compressor, drag-reducing polymer (DRP) tanks, variable area flow meters, flow and pressure transmitter sensor, and data acquisition system. The two supply tanks and the separation tank have a volume of 1963 L each. More details of the installation and connections are shown in Figure 3.2. Technical specifications are summarized in Appendix A.

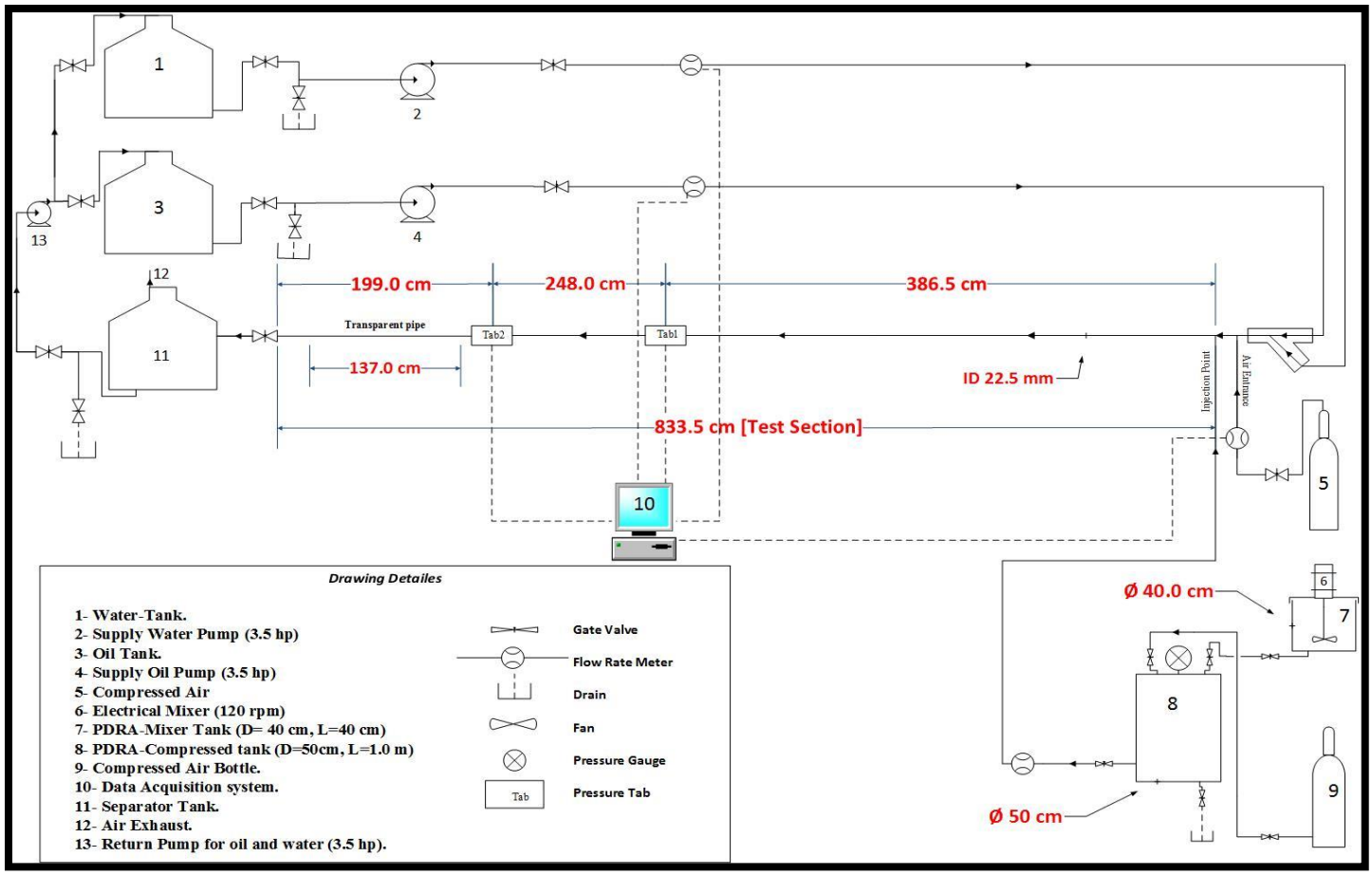

Figure 3.2 Multiphase Flow Facility

Figure 3.3 shows three variable speed pumps, capable of maintaining a steady and smooth flow rate and delivering oil or water at a maximum velocity of 2 m/s, were used. In the two phase (air-water or air-oil) experiments, one pump connected to the water tank, and the other to the oil (ESCAID^{TM}110) tank supplied the corresponding phases to the test loop. Each experimental run achieved steady flow in 2 min. Then the flow rates, pressure drops, and the observed flow pattern were recorded. The exiting oil-water mixture is accumulated in the air-oil-water separation tank. After the completion of an experiment, the third pump returns the segregated oil and water from the separation tank to the respective mother tank. The separation tank is kept open to the atmosphere, which gives air a chance to discharge outside the tank. Whereas, oil and water segregation happened by gravity due to density difference. The DRP-mixed oil and water, in each trial, were discarded to maintain the DRP concentration in the test section at the desired experimental value. Flow rates of air, oil and water can be controlled by increasing or decreasing the speed of the pump/compressor drivers using the speed control panel or by using control valves.

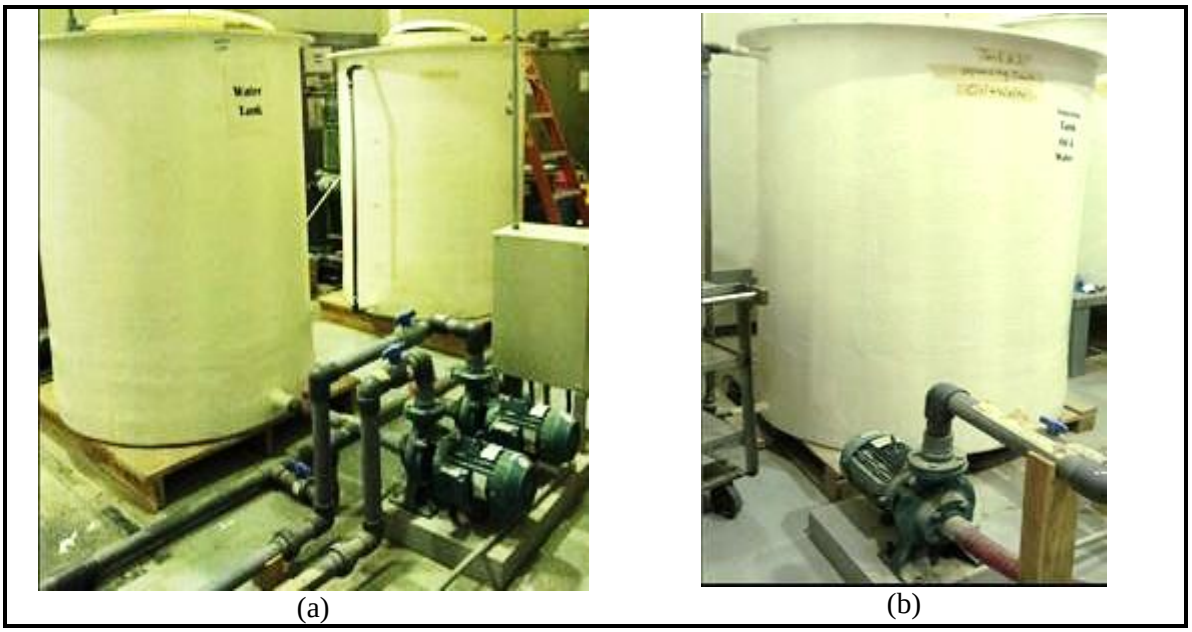

(a) (b)

Figure 3.3 a) Two supplying tanks and two supplying pumps. b) Separation tank and return pump

The wet/wet differential pressure transmitter sensor (PX 157) consists of a solid-state piezoresistive sensing element, which is electrostatically attached to a glass pedestal. This arrangement avoids the effects of induced stress and vibration. This sensor has an accuracy of ± 0.75% (of full scale). It is connected to two pressure tabs (Tab 1 and Tab 2). These tabs, Tab 1 and Tab 2, are located at a distance of 3.865 m and 6.345 m, respectively, from the inlet. The distance between two pressure tabs is 2.48 m. See Figure 3.4A. The ratio of test section length to internal diameter (of 22.5 mm) is taken from the start of the test section until Tab 2. This ratio is 282.

Before entering the test section, the oil and water phases were mixed at the Y-shaped fitting. One branch of the Y-shaped fitting is angled at 45° to shorten the developing length and minimize the mixing phenomenon (where two fluid streams were mixed together through certain distance before they segregated). The T-shaped fitting mixed air

with the oil-water mixture as previously shown in Figure 3.2. The test section is 22.5 mm ID and 8.33 m long pipe and consists of two parts; the first part is PVC pipe (ASTM D-1785) and was used to monitor the pressure. The other part is made of transparent Plexiglas of the same diameter and was used for visual observation and capturing the flow pattern. It is installed near the end of the test section.

State-of-the-art flow transmitter sensors and piston-type variable area flow meters were used. See Figure 3.4B. The flow transmitter sensors have an accuracy of ± 2% (of full scale). Their flow rates were varied as follows:

i. 0.0073–0.0414 $m^3.min^{-1}$ for the water phase;

ii. 0.0076–0.0388 $m^3.min^{-1}$ for the oil phase; and

iii. 0.0540–0.9817 $m^3.min^{-1}$ for air phase.

The output of the sensors (flow transmitter sensors and wet/wet differential pressure transmitter sensor) was recorded at a rate of 1 Hz for a test duration using the data acquisition system. See Figure 3.4C. An interface program (LABVIEW) was used to save the data acquired by these sensors. The characteristics of the sensors and data acquisition system are summarized in Appendix A, Table A2.

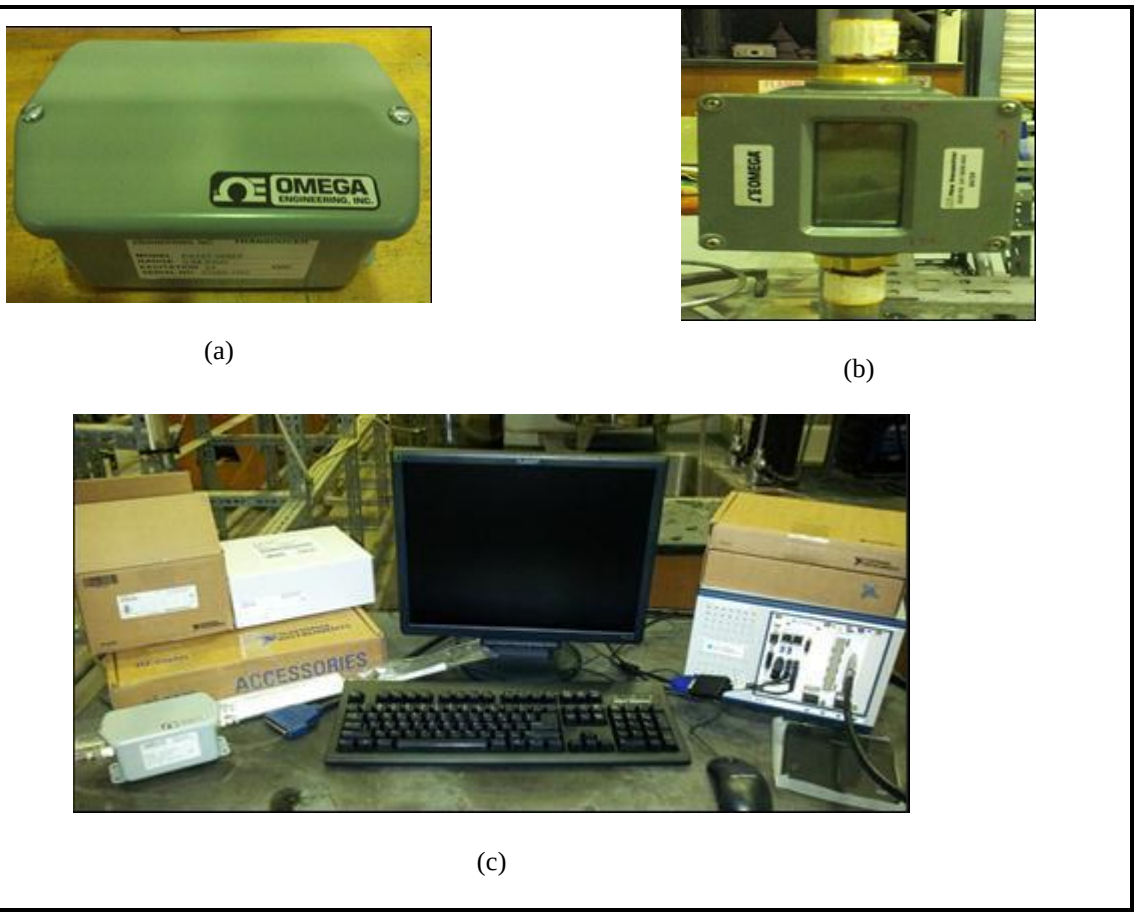

(a)

(b)

(c)

Figure 3.4 A) Wet\wet differential pressure transmitter sensor, B) Flow transmitter sensor, C) Data acquisition system.

The water-soluble ZETAG®8165 DRP powder passes through three stages; mixing, shifting, and injecting. A 50 gram of the above DRP, which are in solid-phase, was first dissolved in tap water using a 50 L stainless steel tank and a low speed mixer that was operated at 120 rpm for 6 hours to prepare a 1000 ppm master solution, following the method described by Warholic et al. [1999]. The above master polymer solution was gravity-transferred to a 157 L stainless steel tank to avoid DRP degradation. Note that pump-transfer introduces shear degradation of polymer. After transferring the whole DRP master solution, the tank was pressurized up to 2 bars. Then, it was injected into the

test section through a 2 mm side hole located 60 cm far from the mixing point. The effects of the water-soluble ZETAG® 8165 DRP on fluid flow were investigated by varying the feed concentration of the master solution up to 190 ppm in some cases, and recording the corresponding pressure drops for the three cases, which are single, two and three-phase flow.

For PIB master solution preparation, same procedure adapted for preparing the ZETAG® 8165 master solution was implemented. The only difference is the PIB was originally in liquid-phase and a 1440 ppm master solution in ESCAID™110 was prepared a day before the test. The effects of the oil-soluble PIB DRP on fluid flow were evaluated following the procedure adopted for the water-soluble ZETAG® 8165. However, the feed concentration of the master solution were varied up to 340 ppm in some cases. Figure 3.5 shows schematics of the method by which the DRPs introduced to the flow.

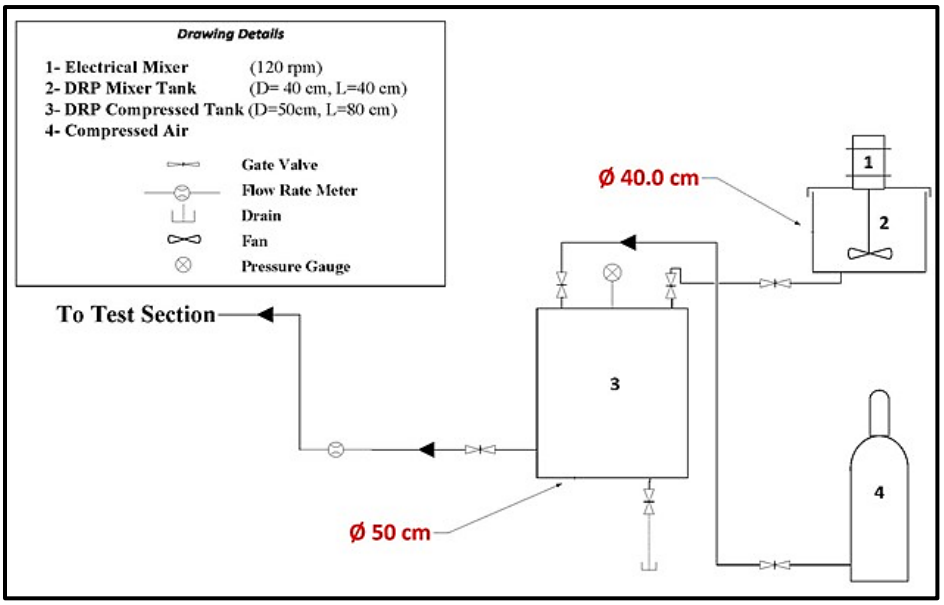

Figure 3.5 Method of injecting the Drag Reducing Polymers to the multiphase flow test section

The PIV setup as shown in Figure 3.6 was made up of a Ray power continuous wave laser was placed to illuminate the test section from below, a Speed sense 9040 (CCD) phantom camera with 1,600 X 1,280 pixels and 8-bits resolution, which was placed at the right angle to the laser. In addition to that, a Phantom Camera Control application (PCC studio) and Dantec Dynamics Studio (DynamicStudio) software were used for image recording and PIV analysis, respectively. The camera was positioned in front of the test section and perpendicular to the laser position to avoid off-axis recording of images.

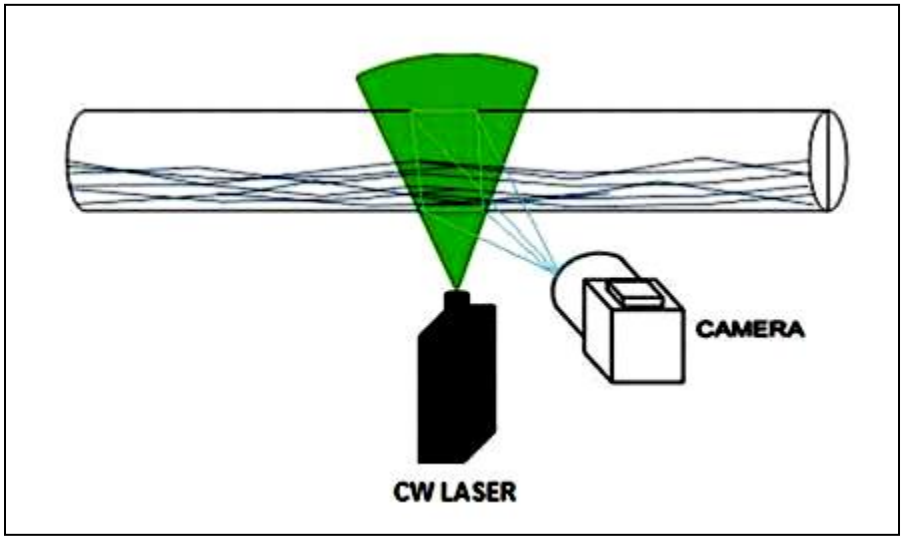

Figure 3.6 Schematics of PIV setup, and transparent part of the test section.

3.3 Experimental Procedure

3.3.1 Definitions

The concentration of water-soluble DRP injected during the experiments can be calculated according to Equation 3.1. In this equation, DRP flow rate is divided by total liquid flow rate multiplied by concentration of master solution of 1000 ppm. Same equation can be used for the case of oil-soluble DRP. The only difference is the concentration of master solution, which is 1440 ppm.

$$C_{DRP} = \frac{Q_{DRP.}}{Q_{total}} \times 1000 \tag{3.1}$$

where;

C_{DRP}: DRP concentration, ppm

Q_{DRP}: Flow rate of the DRP to be added, $m^3.s^{-1}$

Q_{Total}: Total Liquid flow rate in the test section, $m^3.s^{-1}$

The percentage drag reduction (%DR) along the pipeline affected by adding DRPs can be expressed as:

$$\%DR = \frac{\Delta P_1 - \Delta P_2}{\Delta P_1} \times 100\% \tag{3.2}$$

where ΔP_1 is the pressure drop measured in the absence of drag reducing polymer and ΔP_2 is the pressure drop measured with drag reducing polymer.

According to Darcy-Weisbach equation, the head loss in single- and two-phase fully developed and turbulent pipe flow is proportional to the power of 1.8 of the liquid velocity. This equation is given as [Weisbach 1845]:

$$\frac{\Delta h_L}{\Delta L} = \frac{\Delta P}{\Delta L \gamma} = f \frac{U^2}{2gD} \tag{3.3}$$

where

Δh_L : Head loss (m)

ΔP : Pressure drop (Pa)

γ : Specific weight of fluid ($N.m^{-3}$) $\gamma = \rho g$

f : Fanning friction factor, $f = 0.046\,\mathrm{Re}^{-0.2}$

U : Average liquid velocity ($m.s^{-1}$)

ΔL : Distance between pressure tabs (m)

D : Pipe diameter (m)

g : Gravity acceleration ($m.s^{-2}$)

For the three-phase flow, the head loss is calculated using Equation 3.4:

$$\frac{\Delta h_L}{\Delta L} = \frac{\Delta P}{\Delta L \gamma_m} = f_m \frac{U_m^2}{2gD} \tag{3.4}$$

where

Δh_L : Head loss (m)

ΔP : Pressure drop (Pa)

γ_m : Mixture specific weight ($N.m^{-3}$), $\gamma_m = \rho_m g$

f_m : The mixture fanning friction factor, $f_m = 0.046\,\mathrm{Re}_m^{-0.2}$

U_m : The mixture velocity, $m.s^{-1}$, $U_m = V_{SW} + V_{SO}$

Mixture Reynolds number and mixture properties, such as density and viscosity, are given as follows:

$$Re_m = \frac{\rho_m \times D \times U_m}{\mu_m} \tag{3.5}$$

$$\rho_m = (\rho_{Water} \times water\ cut) + (\rho_{Oil} \times (1 - water\ cut)) \tag{3.6}$$

$$\mu_m = (\mu_{Water} \times water\ cut) + (\mu_{Oil} \times (1 - water\ cut)) \tag{3.7}$$

$$water\ cut = \frac{Q_{Water}}{Q_{Water} + Q_{Oil}} \tag{3.8}$$

where

Re_m : Mixture Reynolds number.

μ_m : Dynamic mixture viscosity (N.s.m^{-2})

ρ_{Water} : Water density (Kg.m^{-3})

ρ_{Oil} : Oil density (Kg.m^{-3})

Q_{Water} : Volumetric water flow rate (m^3.s^{-1})

Q_{Oil} : Volumetric oil flow rate (m^3.s^{-1})

To evaluate the effect of adding DRP on the head loss, Equations 3.3 or 3.4 were substituted in Equation 3.2 as follows:

$$\%DR = \frac{\gamma\Delta h_{L-1} - \gamma\Delta h_{L-2}}{\gamma\Delta h_{L-1}} \times 100\%$$

$$\frac{\%DR}{100\%} = \left[1 - \frac{\Delta h_{L-2}}{\Delta h_{L-1}}\right]$$

$$\Delta h_{L-2} = \Delta h_{L-1}\left[1 - \frac{\%DR}{100\%}\right] \quad (3.9)$$

where

Δh_{L-1}: Head loss calculated in the absence of DRP per meter length, (m/m).

Δh_{L-2}: Head loss calculated after adding the DRP per meter length, (m/m).

The amount of saving in energy consumption, due to adding DRP, is an important part of comprehensive energy analysis. This can be mathematically expressed as:

$$W_{PS} = Q_m \gamma_m \left(\Delta h_{L-1} - \Delta h_{L-2} \right) \tag{3.10}$$

where

W_{PS} : Saving in power consumption per meter length ($W.m^{-1}$).

Q_m : Mixture volumetric flow rate ($m^3.m^{-1}$). $Q_m = Q_{Water} + Q_{Oil}$

The percentage saving in energy consumption per length can be mathematically expressed as:

$$\%W_{PS} = \frac{W_{PS}}{W} \times 100\% \tag{3.11}$$

where

W : Power consumption per meter length ($W.m^{-1}$), $W = Q_m \gamma_m \Delta h_{L-1}$

3.3.2 Calibration

Calibrations are essential after finishing building the multiphase flow loop. The read-out of the sensors, i.e. flow transmitter sensors and wet/wet differential pressure transmitter sensor, should be calibrated by comparing it with the actual value.

Figures 3.7A, 3.7B, 3.7C, 3.7D, and 3.7E show the calibration curves for air, water, oil, water-soluble DRP, and oil-soluble DRP flowmeters, respectively.

Figures 3.8A, 3.8B and 3.8C represent a comparison between calculated frictional pressure gradient using Darcy-Weisbach equation versus measured pressure gradient at various fluid velocity. The comparisons show a good agreement between the measured and the calculated values. The calculated frictional pressure gradient is shown previously in Equation 3.3.

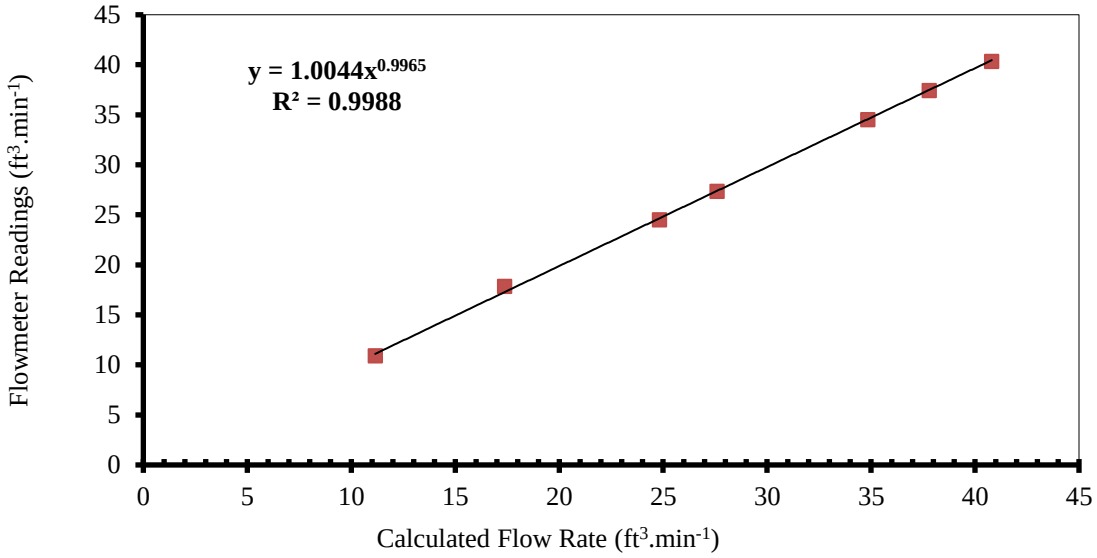

Figure 3.7A Air flow meter calibration

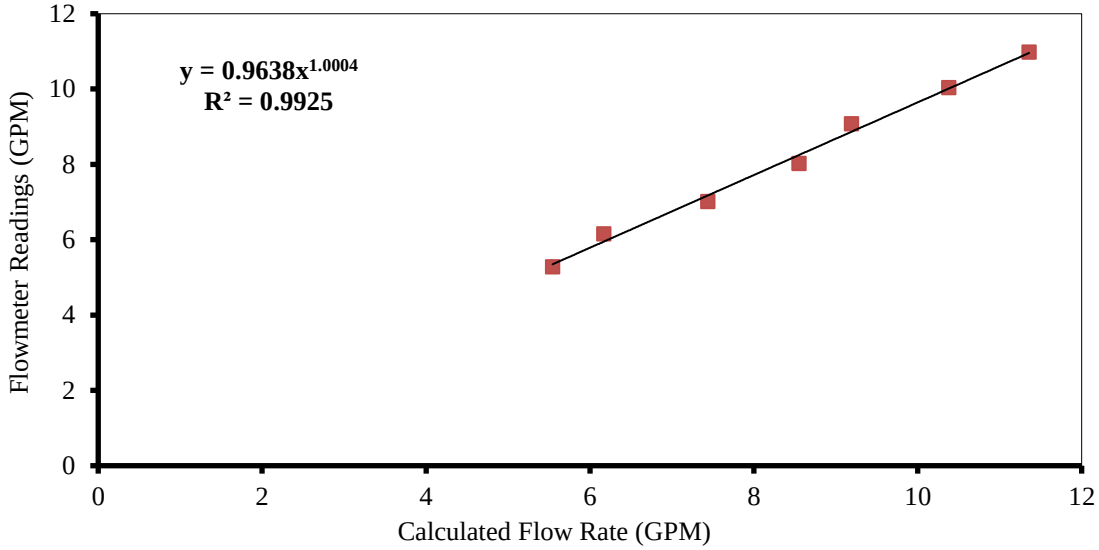

Figure 3.7B Water flow meter calibration

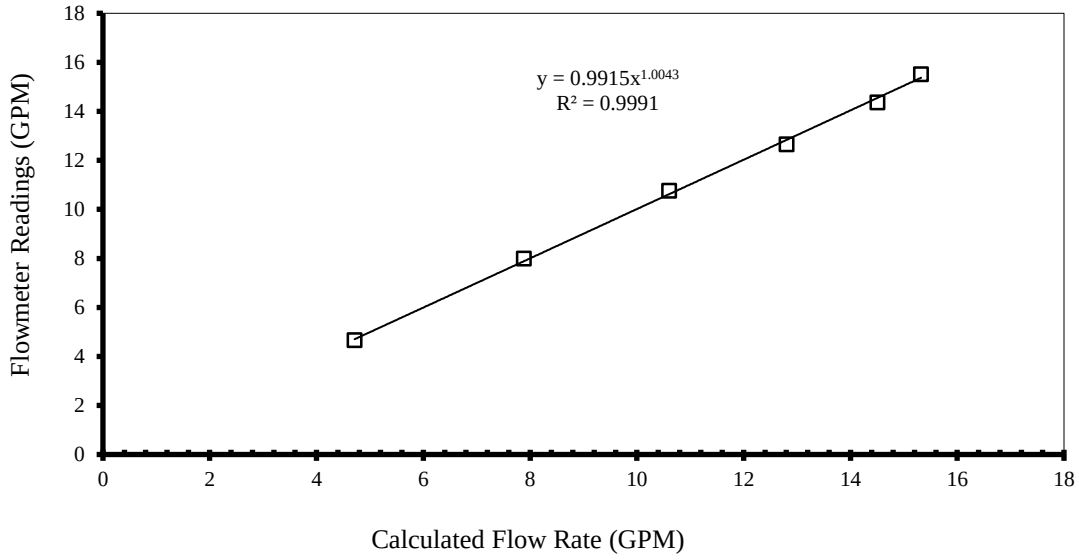

Figure 3.7C Oil flow meter calibration

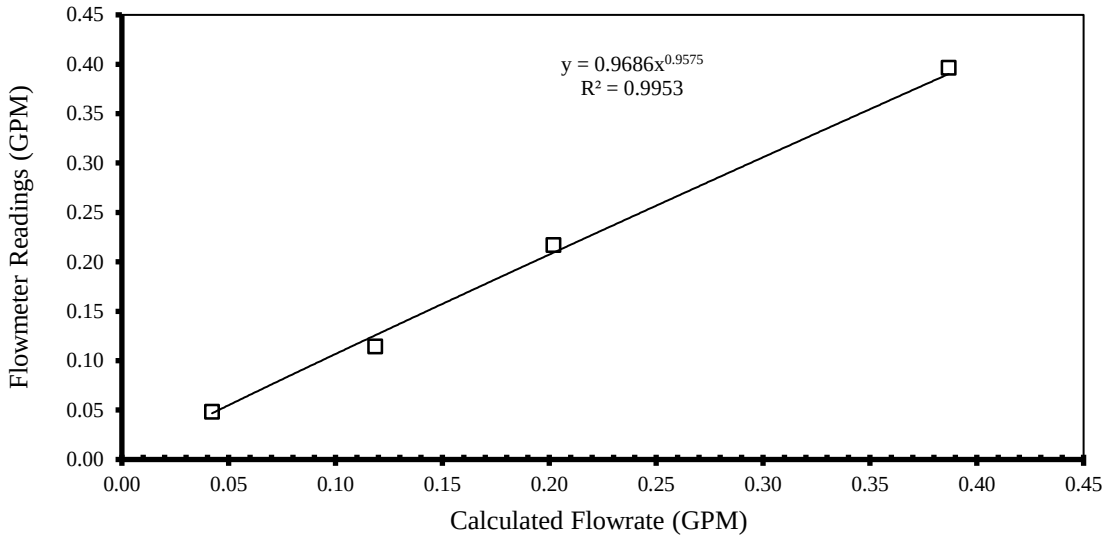

Figure 3.7D Water-soluble DRP flow meter calibration

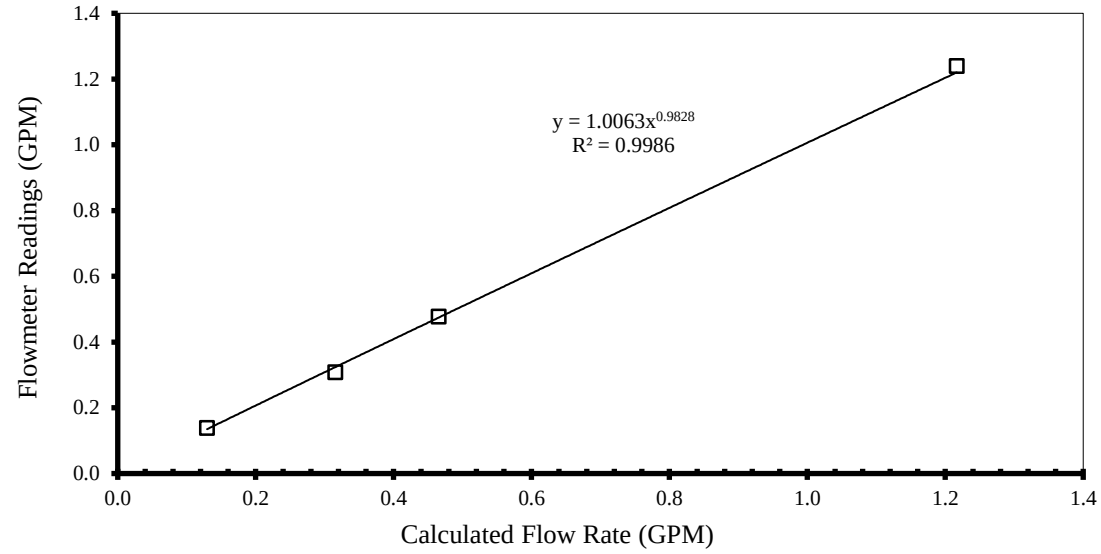

Figure 3.7E Oil-soluble DRP flow meter calibration

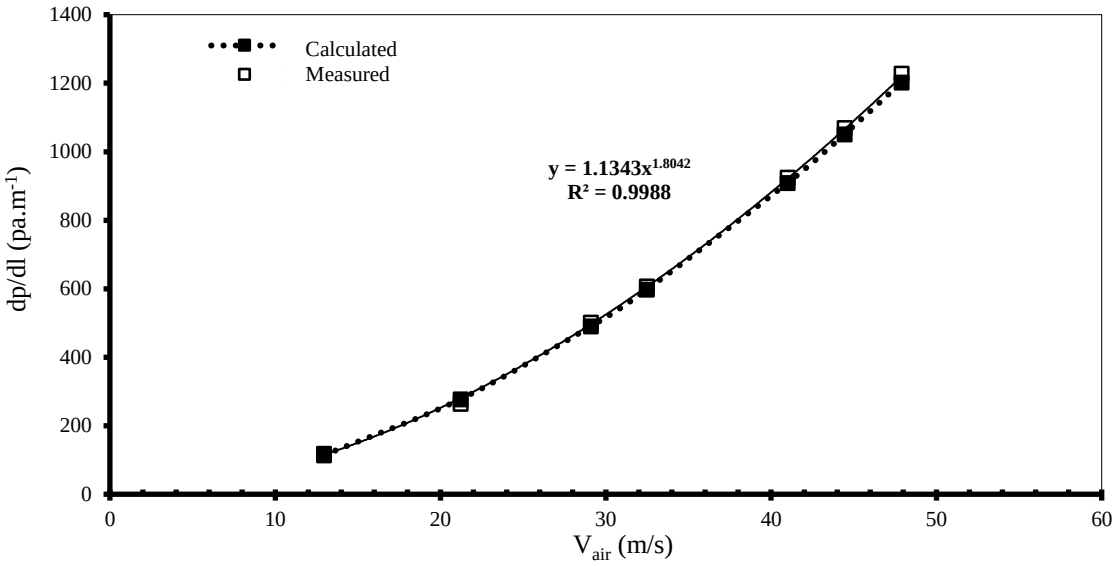

Figure 3.8A Variation of pressure gradient versus single-phase air velocity

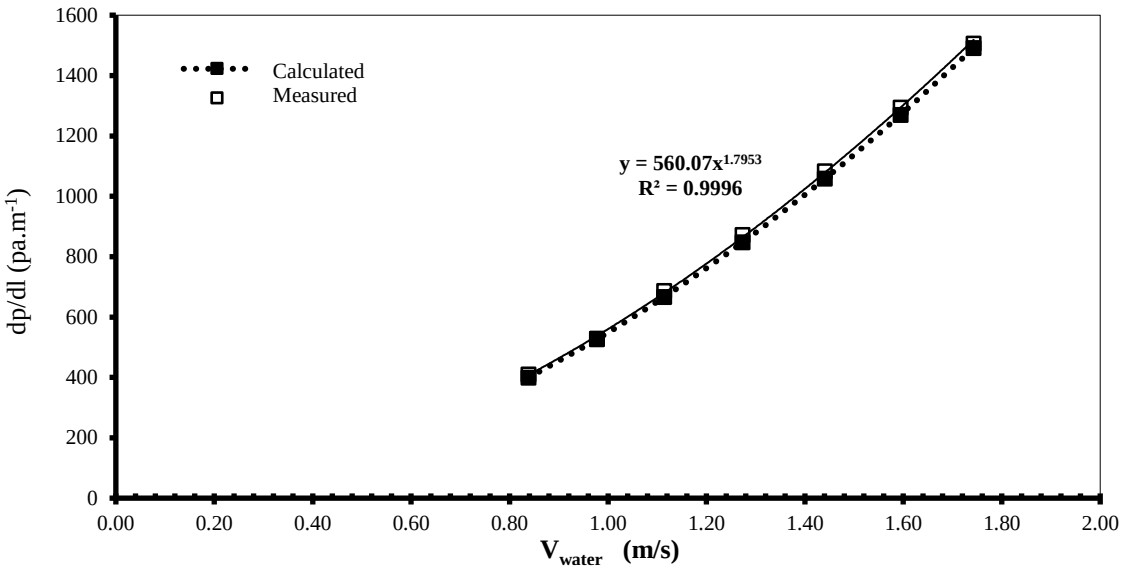

Figure 3.8B Variation of pressure gradient versus single-phase water velocity

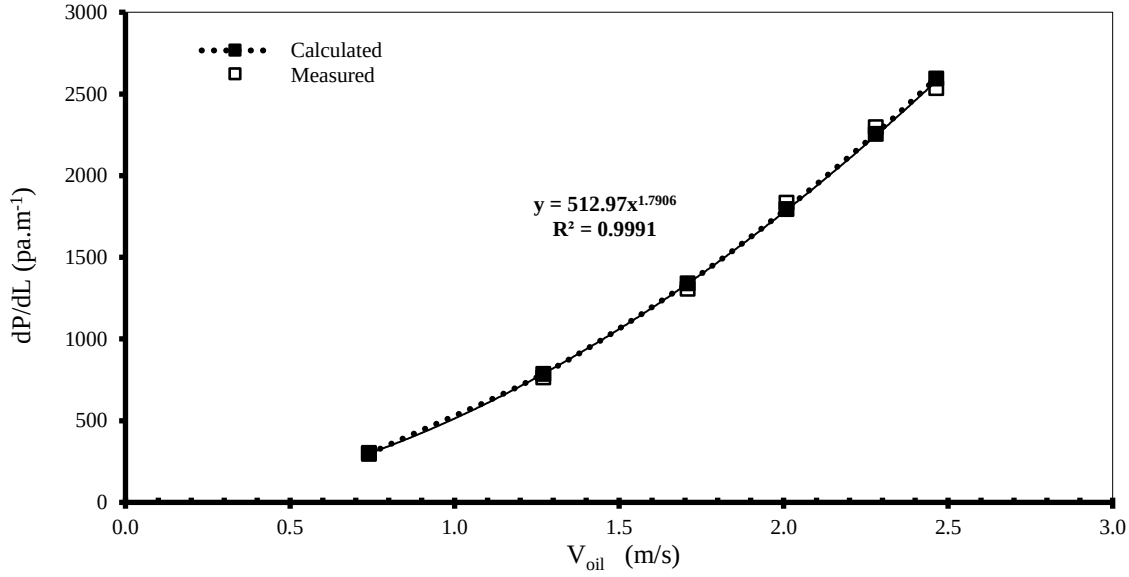

Figure 3.8C Variation of pressure gradient versus single-phase oil velocity

3.3.3 Experimental Procedure for Single-Phase

The Procedure followed while performing single-phase water experiment was as following;

i. Detailed description of the setup used are demonstrated earlier in Chapter 3.
ii. One of the supply tanks was completely filled with tap water.
iii. A concentration of 1000 ppm of master solution was prepared by mixing 50 gram of water-soluble DRP, which is in solid phase, with 50 liters of tap water.
iv. Then, this solution was shifted to the pressurized tank by help of gravity. When all the solution transfers to the pressurized tank, the solution was pressurized up to 2 bar. Schematics of the method by which the DRPs introduced to the flow are shown earlier in Chapter 3, Figure 3.6.
v. All necessary calibrations for the sensors (e.g.; wet-wet pressure differential gauge and flow transmitter sensor) were done before starting the experiments.
vi. For the case of injection DRP to the test section, no circulation of the accumulated quantity in the separation tank was allowed.

The Procedure followed for performing single-phase oil experiment was as following;

i. The other supply tank was filled with oil.
ii. Same equipment used for mixing the water-soluble DRP is used again for injecting oil-soluble DRP, which is obtained from the manufacturer in liquid-phase.

iii. The concentration of master solution was approximately 1440 ppm.

iv. The tanks used to inject the oil-soluble DRP were cleaned to make sure that there is now traces of water-soluble DRP.

v. The flow meter device used to measure the oil-soluble DRP flow rate was calibrated.

vi. For the case of injection DRP, the circulation of the accumulated quantity in the separation tank was not allowed.

3.3.4 Experimental Procedure for Two-Phase

The Procedure followed for the case of two-phase air-water experiment was as following;

i. One of the supply tanks was completely filled with tap water.

ii. The compressed-air cylinder was fully pressurized.

iii. A concentration of 1000 ppm of water-soluble DRP master solution was prepared.

iv. The air and water were mixed at the beginning of the test section at various flow rate values as shown previously in Figure 3.2.

v. Water-soluble DRP injected immediately after the mixture of air and water.

vi. For the case of injection water-soluble DRP, no circulation of the accumulated quantity in the separation tank was allowed.

The Procedure followed for the case of two-phase air-oil experiment was as following;

i. The other supply tank was filled with oil.

ii. The compressed-air cylinder was fully pressurized.

iii. The concentration of oil-soluble DRP master solution was approximately 1440 ppm.

iv. The tanks used to inject the oil-soluble DRP were cleaned to make sure that there is now traces of water-soluble DRP.

v. The mixing between air and oil happened at same location mentioned earlier for the case of air and water.

vi. Oil-soluble DRP injected immediately after the mixture of air and oil.

vii. For the case of injection oil-soluble DRP, no circulation of the accumulated quantity in the separation tank was allowed.

3.3.5 Experimental Procedure for Three-Phase

The Procedure followed for the case of three-phase air-oil-water experiment was as following;

i. Two supply tanks were completely filled with tap water and oil.

ii. The compressed-air cylinder was fully pressurized.

iii. A concentration of 1000 ppm of water-soluble DRP master solution was prepared.

iv. The air and water were mixed at the beginning of the test section at various flow rate values as shown previously in Figure 3.2.

v. Water-soluble DRP injected immediately after the mixture of air, oil, and water.

vi. For the case of injection water-soluble DRP, no circulation of the accumulated quantity in the separation tank was allowed.

The Procedure followed for the case of three-phase air-oil-water experiment was as following;

i. Two supply tanks were filled with water and oil.

ii. The compressed-air cylinder was fully pressurized.

iii. The concentration of oil-soluble DRP master solution was approximately 1440 ppm.

iv. The tanks used to inject the oil-soluble DRP were cleaned to make sure that there is now traces of water-soluble DRP.

v. The mixing between air, oil, and water happened at same location mentioned in the previous case.

vi. Oil-soluble DRP injected immediately after the mixture of air, oil, and water.

For the case of injection oil-soluble DRP, no circulation of the accumulated quantity in the separation tank was allowed.

CHAPTER 4

UNCERTAINITY ANALYSIS

4.1 Introduction

The purpose of experimental measurements is to characterize the performance of a process and to determine a specific quantity of the measured value. In general, imperfections in the experiment will help in increasing error in the result. Consequently, we can say that no test or measurement is performed perfectly without a margin of error. Thus, the true value is unknown, and the error corresponds to that value is unknown as well. In order to obtain the true value, the result of the experimental measurement, which represents an approximation of the true value, must be accompanied with a statement of the uncertainty. According to Dieck [2002], the uncertainty analysis is a numerical method used to find the potential error that would exists in all data.

Errors in the result of experimental measurement may be thought of as arising from two sources, a random component and a systematic component. Random component, systematic component, and the combination of these two errors will be discussed in more detailed below. Also, the uncertainty analysis of the experimental results of this study will be included below.

4.1.1 Random Uncertainty

Random variation of observations, which called random effect, is well known error in the experimental measurements. This error arising from variation in repeated measurements which taken under nominally the same conditions. Random uncertainty points out the limits of these random errors and is based on the standard deviation of the data (SX) as shown in Equation 4.1.

$$S_x = \left[\frac{\sum_{j=1}^{N} \left(X_j - \overline{X} \right)^2}{N-1} \right]^{0.5} \tag{4.1}$$

Where: N: is number of data sets.

Xj: is the jth data set.

$\bar{X}$: is the average of the data sets.

N-1: is the degree of freedom of the data sets.

The standard deviation of the data average ($S_{\bar{X}}$) is calculated as

$$S_{\overline{X}} = \frac{S_X}{\sqrt{N}} \tag{4.2}$$

4.1.2 Systematic Uncertainty

This error arising from the imperfect correction of systematic effects. This type of error remains constant while a measurement is repeated under the same circumstances and their effect is to introduce a bias or offset between the true value and the experimentally obtained mean value. Systematic errors (b_j) for a particular instrument, which is often provided by the manufacturer, are combined using the following equation.

$$B_R = \left[\sum_{j=1}^{N} \left(b_j^2 \right) \right]^{0.5} \tag{4.3}$$

where:

B_R: is the combined systematic uncertainty component.

4.1.3 Combined Uncertainty at 95 % Confidence Level

To quantify the accuracy of the experimental measurements and to estimate the overall measurement uncertainty, the random uncertainty and the systematic uncertainty are combined, and it can be calculated by

$$U_{95} = \pm t_{95} \left[\left(\frac{B_R}{2} \right)^2 + \left(S_{\bar{X}} \right)^2 \right]^{0.5} \tag{4.4}$$

where: U_{95}: Combined uncertainty at 95% confidence level.

t_{95}: Population-t distribution at a 95% confidence interval of a measurement.

The Random Uncertainties, Systematic Uncertainties, and the Combined Uncertainties of the experimental measurements performed in this study are listed in Table 4.1.

Table 4.1 Instruments uncertainty analysis

Parameter	Instrument	Supplier	Random Uncertainty	Systematic Uncertainty	Combined Uncertainty
DRP flow rate	Rotameter (7200 series)	KING Instrument CO.	0.32%	1.00%	1.18%
Oil flow rate	Flow transmitter sensor (FLR D series)	OMEGA	0.37%	0.50%	0.88%
Water flow rate	Flow transmitter sensor (FLR D series)	OMEGA	0.19%	0.50%	0.63%
Gas flow rate	Flow transmitter sensor (FLR D series)	OMEGA	0.49%	0.50%	1.10%
Pressure drop	wet/wet differential pressure transmitter (PX 157 series)	OMEGA	0.04%	0.75%	0.75%

CHAPTER 5

EXPERIMENTAL RESULTS OF SINGLE-PHASE WATER AND OIL WITH DRPs

5.1 Introduction

In this chapter, the performance of the water-soluble DRP was evaluated by conducting a series of experiments using water as the single-phase with and without ZETAG®8165. These experiments have been presented for oil and water flowing in a 22.5 mm I.D. and 8.33 m long PVC horizontal pipe. The objective of this investigation was to determine the maximum drag reduction and the corresponding DRP concentration (after which no further reduction could occur).

Consequently, the effectiveness of the oil-soluble DRP PIB for the single-phase oil flow was assessed by following the procedure applied to the analogue water flow. PIB was gently mixed with ESCAID™110 to form a master solution of 1440 ppm.

5.2 Results and discussion

5.2.1 Single-Phase Water Flow With and Without Water-Soluble DRP

In these tests, the DRP flow rate was varied and the water flow rate was kept constant. Figure 5.1A shows the following common trend for each Re. The pressure gradient dP/dL, in the presence of the DRP, first very steeply dropped; then it fairly flattened as the DRP flow rate Q_{pol} increased, indicating minor influence of Q_{pol} on dP/dL. This particular initial drop in dP/dL occurred corresponding to almost the same threshold value of DRP flow rate, and showed to be directly related to Re as follows:

$$dP/dL\,|_{39620} > dP/dL\,|_{35522} > dP/dL\,|_{26363} > dP/dL\,|_{20178}$$

The above finding also holds for dP/dL without the DRP; however, with DRP the initial dP/dL was much lower. The introduction of the DRP further sharply decreased the DRP-free dP/dL. Therefore, both findings can be connected to increase in turbulence level. This reduction happens due to the ability of the DRP molecules to extend such that they become comparable in size to the turbulent eddies. This extension in polymer aggregate or entanglement helps in dampening the propagation of turbulence, i.e. for a defined Re and DRP flowrate, the hydrodynamic size of the DRP molecules protracted through uncoiling. This dampened the turbulent eddies which may increase the thickness of viscous laminar sublayer, and streamlined the velocity field. Hence, the dP/dL decreased.

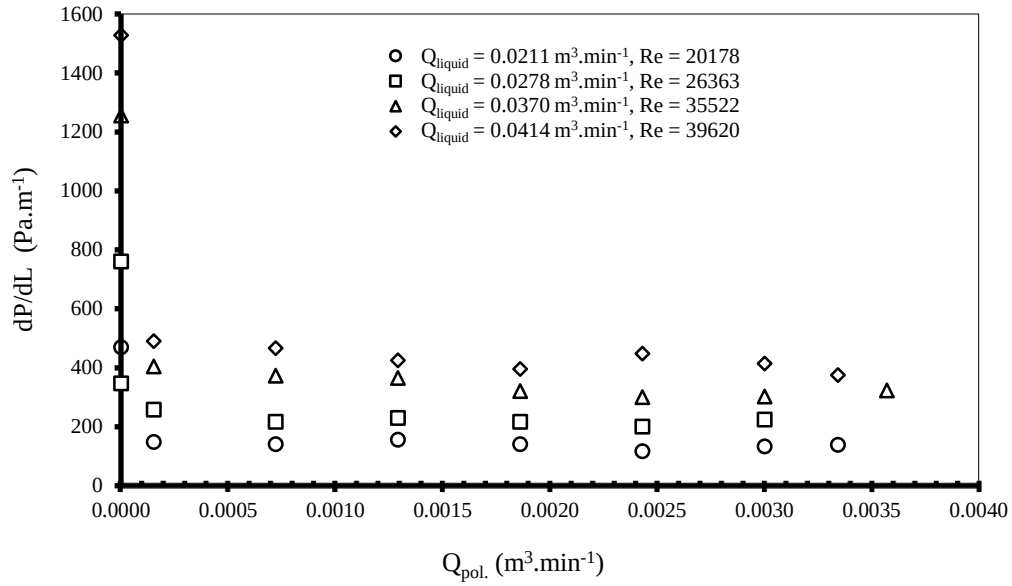

Figure 5.1A Pressure gradient of single-phase water flow versus polymer flow rate using water-soluble DRP at different water flow rate.

Figure 5.1B shows the effect of injecting DRP for different cases. A maximum drag reduction of 76% occurred at relatively high Reynolds number (35,522). The addition of water-soluble DRP ZETAG® 8165 clearly minimized the effect of turbulence activity, and decreased the pressure gradient and increased the %DR. See Figures 5.1A and 5.1B. The increment in %DR with increasing DRP concentration was positive. Also, a fluctuation trend was observed in the percentage drag reduction. This could be due to turbulent activities which affects the DRP aggregates. However, no more reduction occurred above a critical concentration. Therefore, for the water-soluble DRP in single-phase water flow, the critical (effective) concentration obtained is 64 ppm.

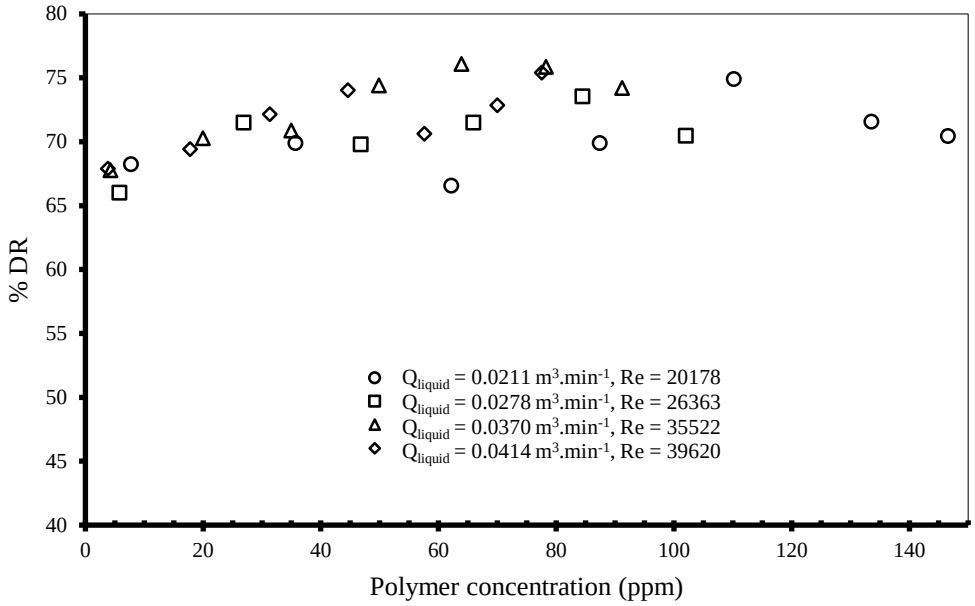

Figure 5.1B Percentage drag reduction versus polymer concentrations for single-phase water flow at water-soluble DRP flow rate of 0.0 - 0.0033 $m^3.min^{-1}$ and at different water flow rate.

5.2.2 Single-Phase Oil Flow With and Without Oil-Soluble DRP

Figure 5.2A shows the variation of pressure gradient with oil flow rate corresponding to the DRP flow rate of Q_{pol} = 0.0024 $m^3.min^{-1}$. The results proved that the oil-soluble polymer produced a reasonable percentage drag reduction. Figure 5.2B reports %DR as a function of PIB concentration, which was varied by varying Q_{liquid} from 0.0107 to 0.0350 $m^3.min^{-1}$; Q_{pol} was fixed at 0.0024 $m^3.min^{-1}$. It shows at maximum liquid flow rate, the percent drag reduction is 41%. While at relatively low liquid flow rate, the percent drag reduction is increased up to 80%. This high percentage may attributed to high concentration of oil-soluble DRP existed when the liquid flow rate was at its minimum

value. The high percentage also can be attributed to the level of turbulence and the effectiveness of the DRP at that particular flow rate.

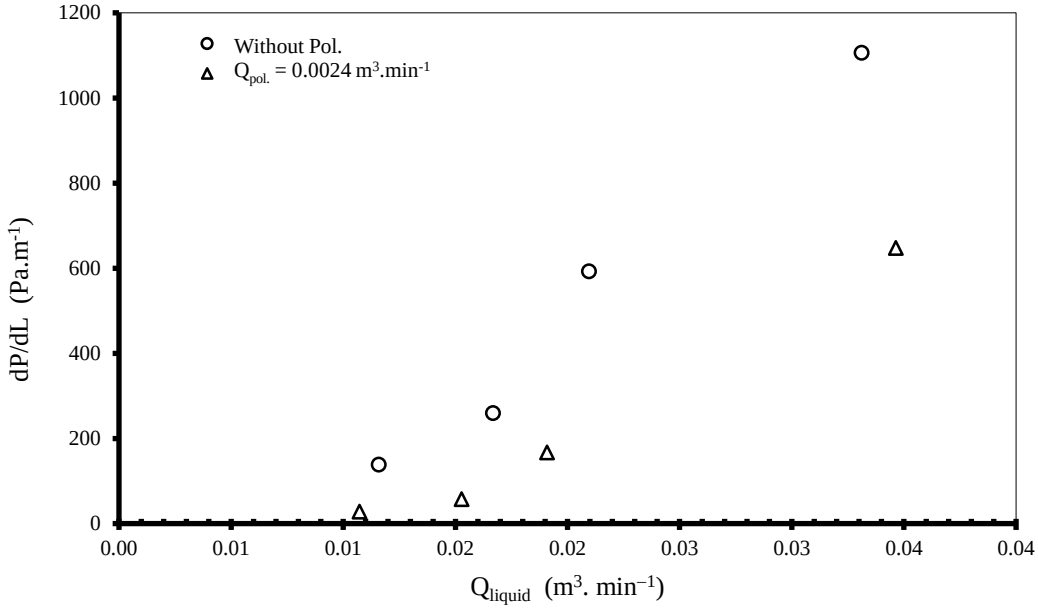

Figure 5.2A Pressure gradient of single-phase oil flow versus liquid flow rate at maximum oil-soluble DRP flow rate.

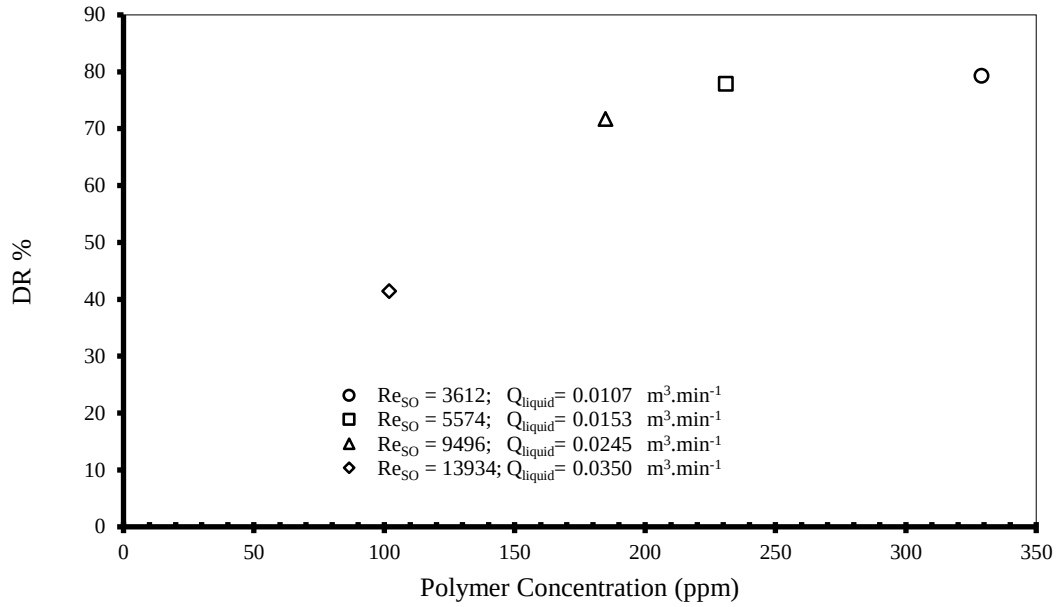

Figure 5.2B Percentage drag reduction versus polymer concentration for single-phase oil flow with oil-soluble DRP at maximum polymer flow rate (Q_{pol} = 0.0024 $m^3.min^{-1}$) with various oil flow rate.

Figures 5.3A and 5.3B show the pressure gradient as a function of polymer flow rate, and %DR as a function of oil-soluble PIB concentration, respectively. Here, the oil flow rate Q_{liquid} was fixed at 0.0388 $m^3.min^{-1}$. Figure 5.3B shows that at maximum oil-soluble DRP flow rate the percent drag reduction is around 35%. This finding qualitatively matches Figure 5.2B.

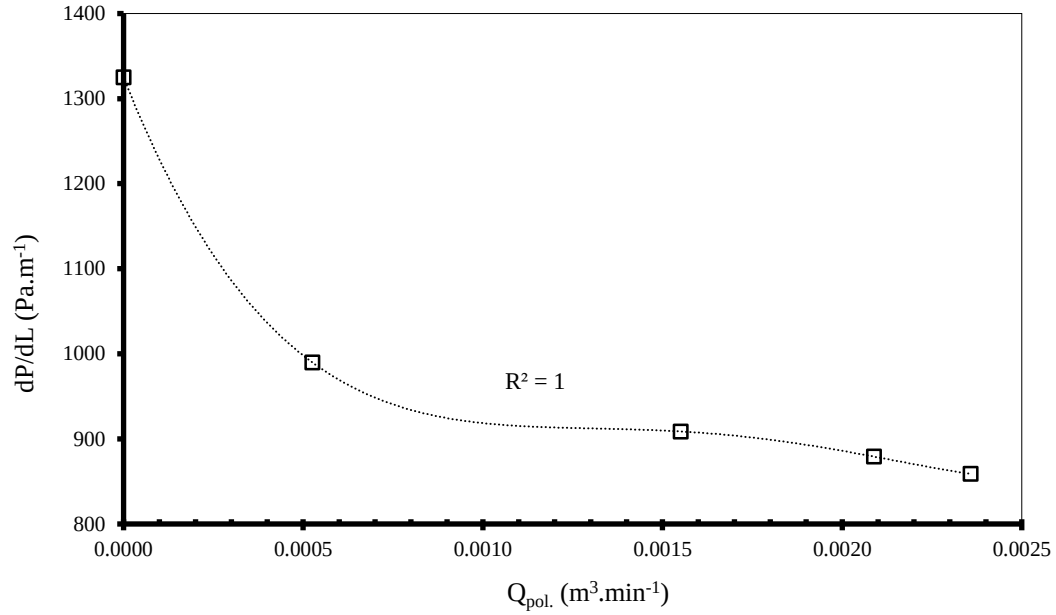

Figure 5.3A Pressure gradient of single-phase oil flow versus polymer flow rate at maximum oil flow rate Q_{liquid} = 0.0388 m^3/min; Re = 16795 (dotted curve represents third order polynomial cure).

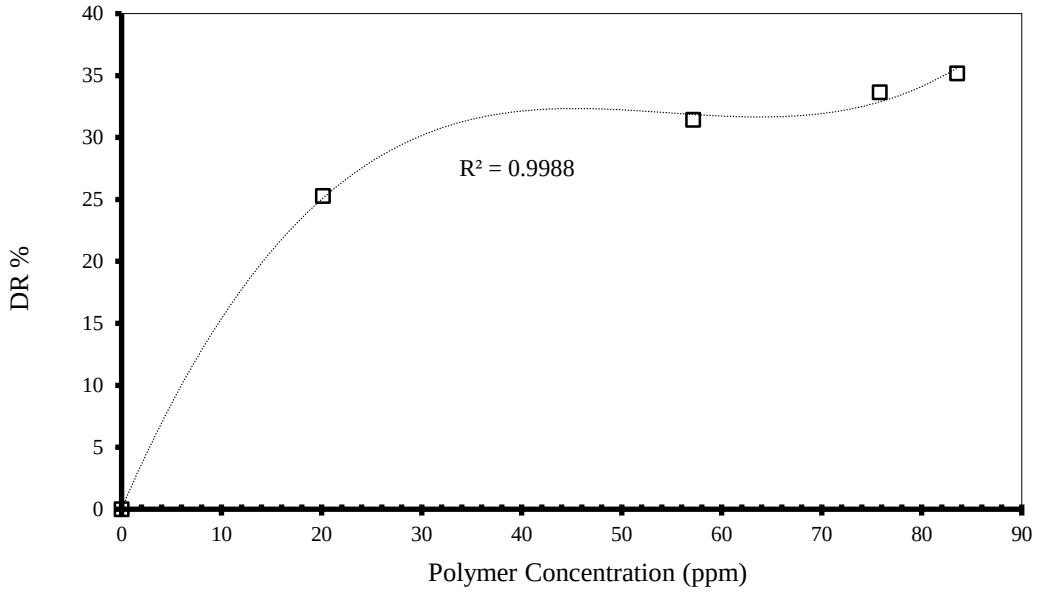

Figure 5.3B Percentage drag reduction versus polymer concentration for single-phase oil flow with oil-soluble DRP ($Q_{pol.}$ = 0.0 - 0.0024 m^3/min), and at maximum oil flow (Q_{liquid} = 0.0388 m^3/min; Re = 16795), dotted curve represents third order polynomial cure.

5.2.3 Comparison between Single-Phase Water and Oil Flow

Figure 5.4 compares the effect of Reynolds number on %DR of single-phase water and oil flows, in the presence of ZETAG® 8165 (polar) and PIB (nonpolar) DRPs, respectively. The following two different trends were observed. For the water flow, %DR initially increased with the increase in Re_{SL}; then it asymptotically flattened. On the contrary, for the oil flow, it sharply decreased in an approximately linear fashion. At Re_{SL} = 12000, %DR for both flows turned out to be the same (~50%). Re_{SL} was varied by varying the corresponding water and oil flow rates.

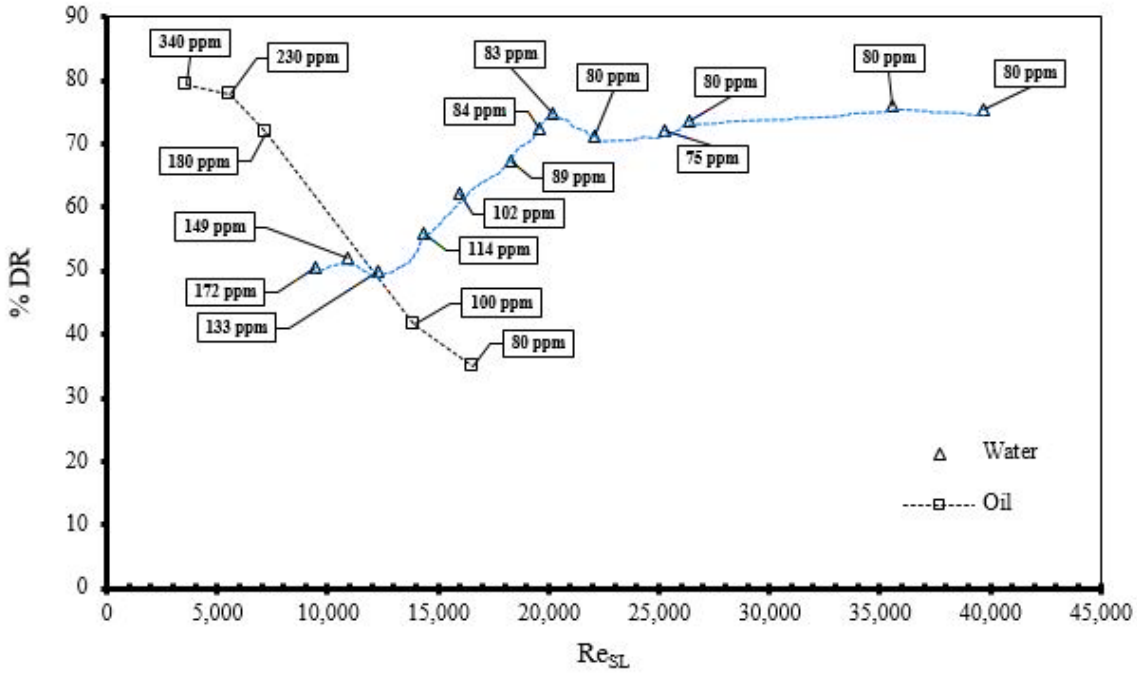

Figure 5.4 Comparison between single-phase water flow and single-phase oil flow (Tables 4A and 4B), dotted curve represents third order polynomial cure.

5.2.4 Single-Phase DRP Degradation Tests

Figure 5.5A investigates the shear-induced degradation of PIB at 120 ppm in the single-phase flow of ESCAID^{TM}110 (oil) at 0.0294 $m^3.min^{-1}$. The oil was circulated in the loop at this flow rate for 3.4 hours. The resulting degradation was evaluated by monitoring dP/dL as a function of time. The greater is dP/dL, the higher is the degradation of the DRP.

Figure 5.5B shows the analogous experiment for the single-phase water flow with ZETAG® 8165 (acrylamide-quaternized cationic monomer copolymer) under comparable test conditions. However, the circulation time was extended. In the first day, it was for 3.5 hours and in the second day, it was for another 5 hours. Both day fairly flat trend lines, compared with that of Figure 5.5A, confirm that shear-induced degradation of ZETAG® 8165 is much less than that of PIB. This degradation behavior is attributed to the respective different chemical structures of these DRPs. See Figure 5.6A.

An important feature was observed in the first and second day stability behavior of the water-soluble DRP. See Figure 5.5B. In the second day it showed to be more stable than the first day. The shear-degraded polymer chains assembled overnight because of dipole-dipole interaction and formed associative polymer clusters. The mechanism of this cluster formation is shown in Figure 5.6B. These clusters served as energy sinks and saved the main polymer backbones from being affected by the shear introduced by the delivery pump.

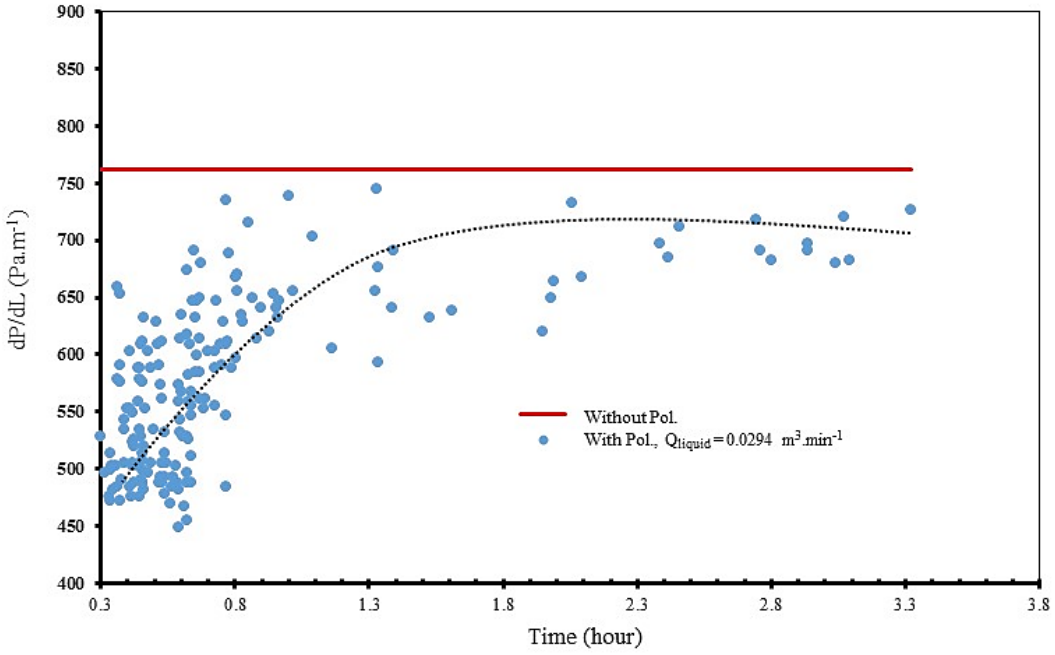

Figure 5.5A Polymer degradation test for single-phase oil flow at constant oil flow rate and at oil-soluble DRP concentration of 120 ppm (dotted curve represents the time-average value).

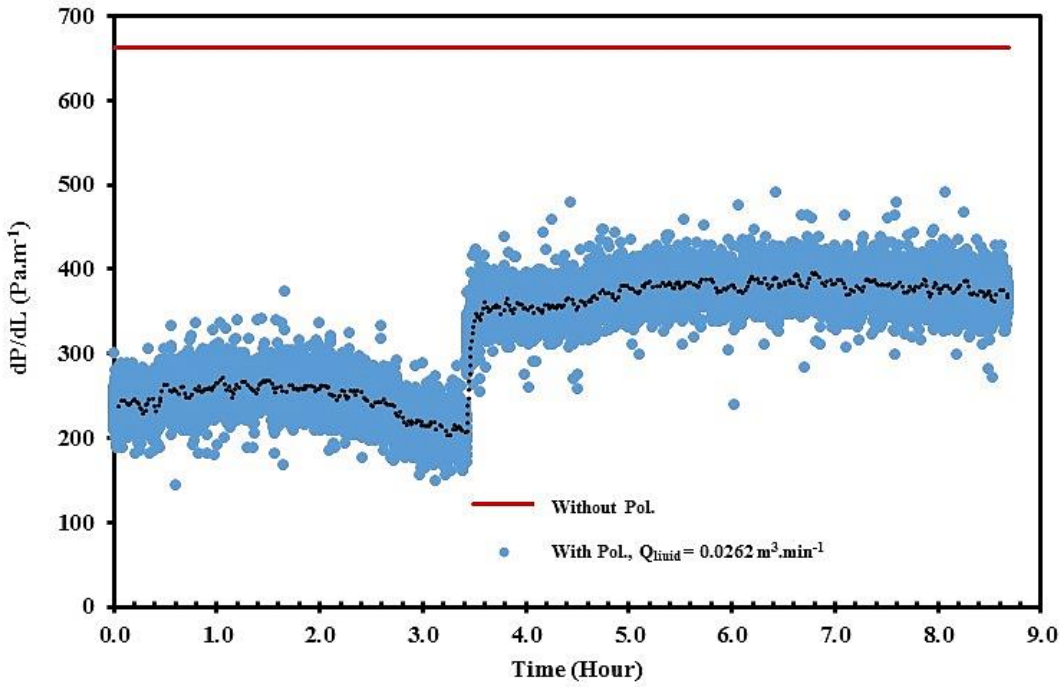

Figure 5.5B Polymer degradation test for single-phase water flow at constant water flow rate and at water-soluble DRP concentration of 120 ppm (dotted curve represents the time-average value).

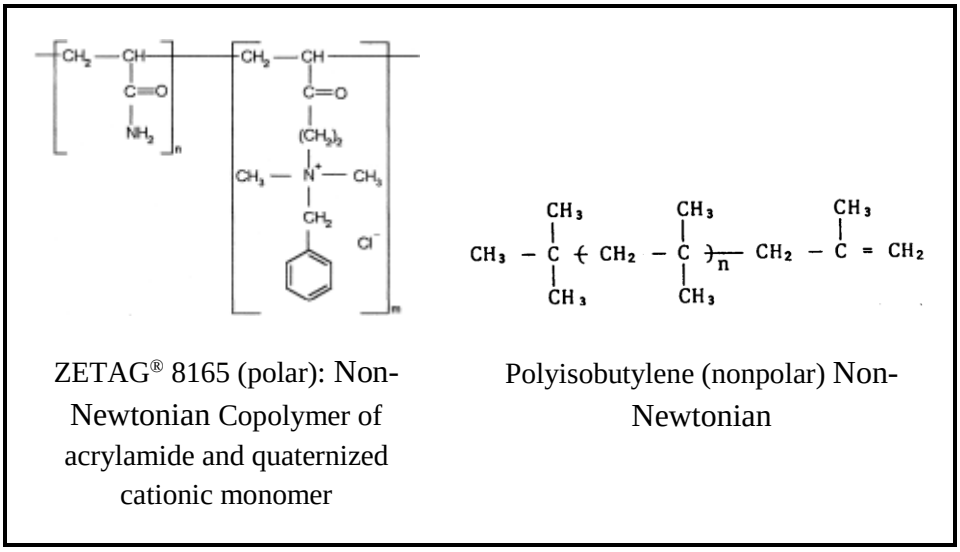

Figure 5.6A Comparison of chemical structures of ZETAG® 8165 and polyisobutylene (PIB).

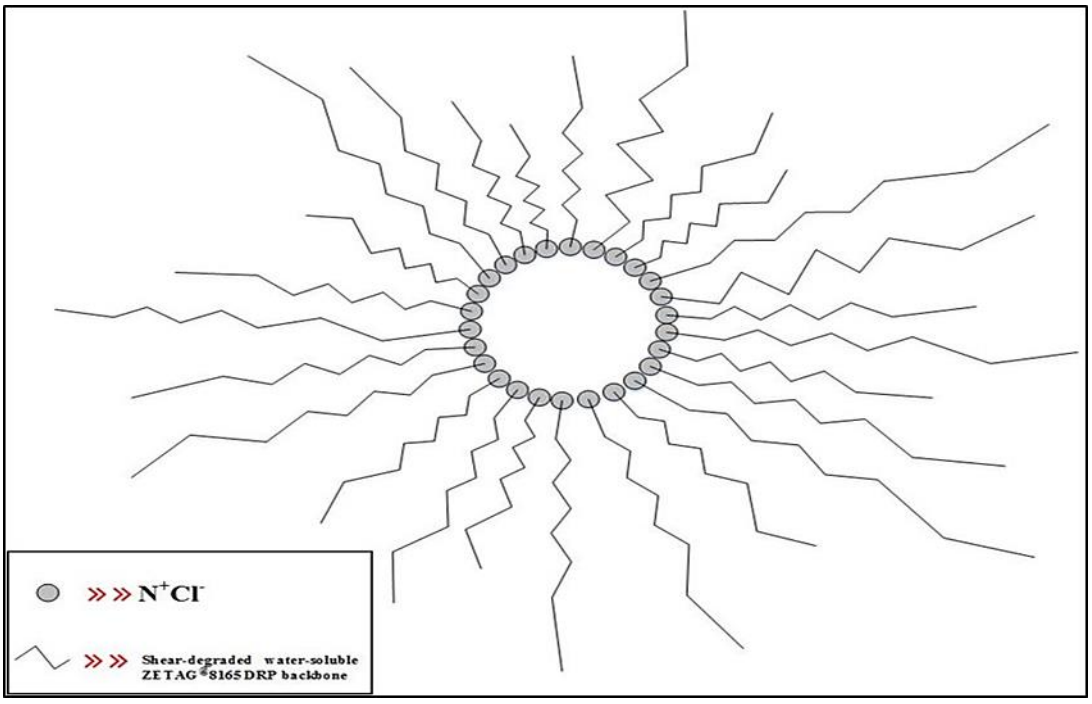

Figure 5.6B Postulated mechanism of associative cluster formation.

5.3 Conclusion

In this Chapter a series of experiments were conducted to determine the influence of water-soluble and oil-soluble drag reducing polymers (DRPs) in single-phase water and oil flows, respectively. These experiments have been presented for oil and water flowing in a 22.5 mm I.D. and 8.33 m long PVC horizontal pipe. The effect of water flow rate, oil flow rate, DRPs types and concentrations on pressure gradient and percentage drag reduction were investigated.

For case of single-phase water flow, the results showed a large reduction in pressure gradient due to water-soluble DRP at high liquid mixture superficial velocity. The drag reduction achieved when water-soluble DRP used is 76%.

However, a contrary performance was presented for the case of single-phase oil flow with oil-soluble DRP. At maximum liquid superficial velocity, the drag reduction dropped to 34 %.

A polymer degradation tests for both water-soluble DRP and oil-soluble DRP were also performed. Under similar conditions, using oil-soluble or water-soluble may not results in same drag reduction.

CHAPTER 6

EXPERIMENTAL RESULTS OF TWO-PHASE AIR-OIL AND AIR-WATER FLOW WITH DRPs

6.1 Introduction

This Chapter presented the results of the conducted experiments for pressure drop and flow pattern of two-phase air-water and air-oil flows with DRPs.

However, the performance of the water-soluble and oil-soluble DRPs was evaluated by conducting a set of experiments of two-phase flow using a combination of air-water and air-oil. The objective of this investigation was to determine the effect of DRPs on the flow patterns and the maximum drag reduction.

Consequently, a comparison between the two types of DRPs based on the effectiveness in damping the turbulence activities and other factors related to the DRP chemical structure.

6.2 Results and Discussion

6.2.1 Two-Phase Air-Water flow with and Without Water-Soluble DRP

Figure 6.1A investigates the two-phase air-water flow with and without the water-soluble DRP ZETAG® 8165. In this investigation, the DRP flow rate Q_{pol} was varied using the following three pairs of constant water and air flow rates:

i. $Q_{liquid} = 0.0190\ m^3.min^{-1}$ and $Q_{air} = 0.0793\ m^3.min^{-1}$;

ii. $Q_{liquid} = 0.0227\ m^3.min^{-1}$ and $Q_{air} = 0.0793\ m^3.min^{-1}$; and

iii. $Q_{liquid} = 0.0265\ m^3.min^{-1}$ and $Q_{air} = 0.0934\ m^3.min^{-1}$.

Under the above flow conditions, the observed flow pattern without the DRP showed to be slug flow (existence of large air bubbles, tending to approach the pipe diameter, separated by water slugs) with high slugging frequency, which decreased with the increasing level of DRP injection. Note that the level of DRP injection increased as its flow rate Q_{pol} increased. The pressure gradient dP/dL versus Q_{pol}, with respect to each pair of Q_{liquid} and Q_{air}, varied showing a common trend. dP/dL initially decreased rapidly up to a critical Q_{pol}. Exceeding this value, it flattened, indicating a fairly minor effect of Q_{pol} on dP/dL. However, in each case, the decrease in dP/dL occurred for a very low value of Q_{pol}, that is, a very low dosage of the DRP.

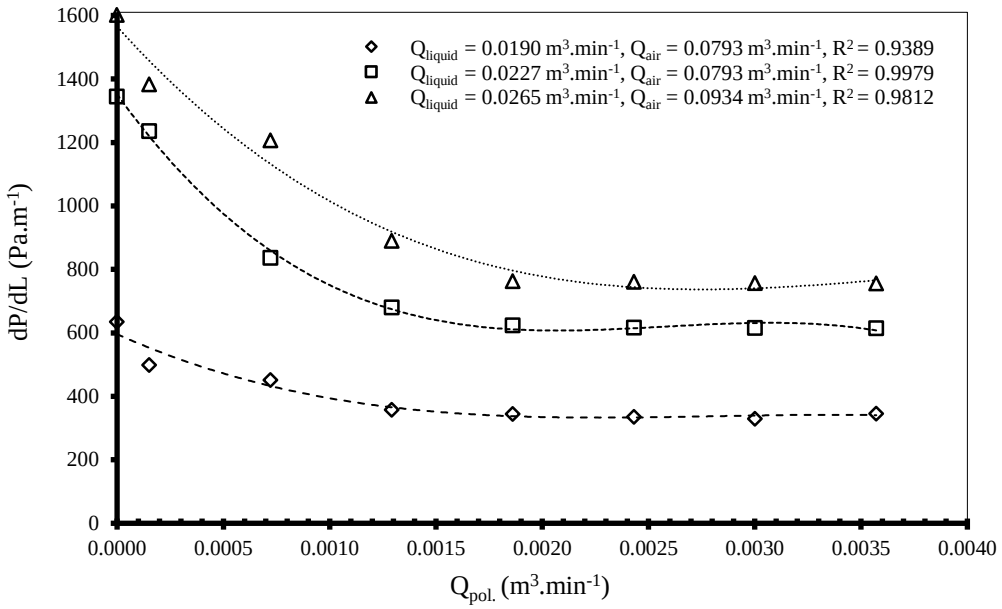

Figure 6.1A Pressure gradient of two-phase air-water flow versus polymer flow rate (water-soluble DRP) at constant water flow rate, constant air flow rate, and variant DRP flow rate. Range of DRP concentrations were; ◊ 0 – 186 ppm; □ 0 – 157 ppm; Δ 0 – 134 ppm (dotted curve represents third order polynomial cure).

Figure 6.1B is an alternative equivalent representation of Figure 6.1A data. Here, each dP/dL and the related Q_{pol} have been converted respectively to the corresponding %DR and water-soluble DRP dosage (ppm). The %DR versus DRP dosage (ppm), with respect to each pair of Q_{liquid} and Q_{air}, varied showing a common trend. %DR initially increased rapidly up to a critical DRP concentration. Beyond this value, it became asymptotic, showing insignificant influence of DRP dosage on %DR. This particular finding, exhibited in the presence of air, matches the single-phase %DR versus DRP dosage relation, already reported in the literature, i.e. Choi and Jhon [1996] and Al-Sarkhi and Hanratty [2001]. This means that the introduction of air did not transpose the fundamental relation between %DR and DRP dosage.

The asymptotic %DR and the corresponding critical DRP dosage can be listed as follows:

i. %DR = ~45 and DRP dosage = ~70 ppm (for Q_{liquid} = 0.0190 $m^3.min^{-1}$ and Q_{air} = 0.0793 $m^3.min^{-1}$);

ii. %DR = ~53 and DRP dosage = ~80 ppm (Q_{liquid} = 0.0227 $m^3.min^{-1}$ and Q_{air} = 0.0793 $m^3.min^{-1}$); and

iii. %DR = ~52 and DRP dosage = ~75 ppm (Q_{liquid} = 0.0265 $m^3.min^{-1}$ and Q_{air} = 0.0934 $m^3.min^{-1}$).

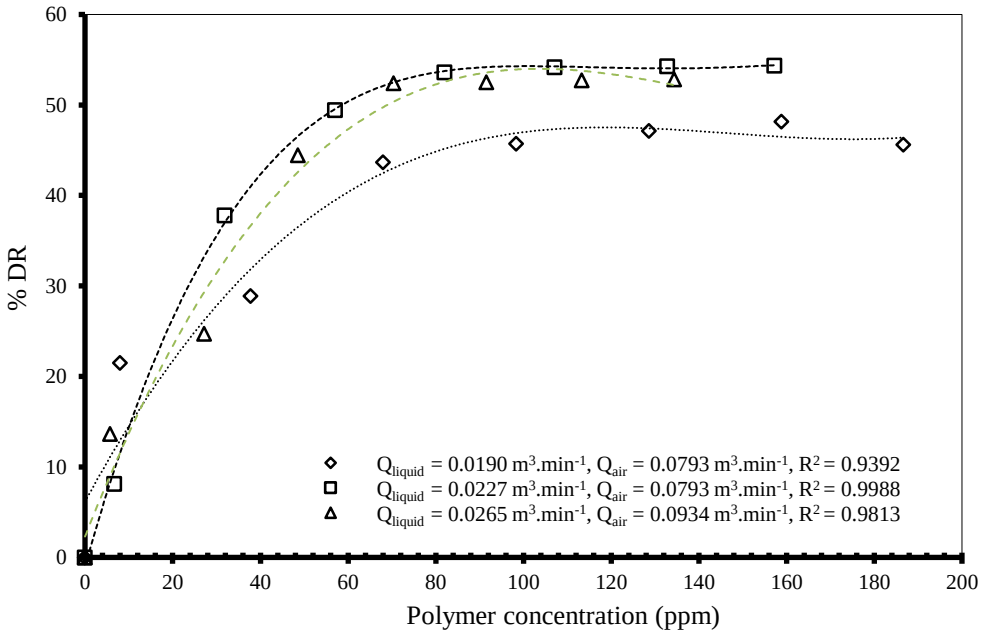

Figure 6.1B Percentage drag reduction versus polymer concentration (water-soluble DRP) for air-water flow (dotted curve represents third order polynomial cure).

Figure 6.2A studies the two-phase air-water flow with and without the water-soluble DRP ZETAG® 8165 under the following experimental conditions:

i. $Q_{pol} = 0.0\ m^3.min^{-1}$ (no DRP dosage) and $Q_{liquid} = 0.0190\ m^3.min^{-1}$; and

ii. $Q_{pol} = 0.0036\ m^3.min^{-1}$ (190 ppm dosage of DRP) and $Q_{liquid} = 0.0190\ m^3.min^{-1}$.

In the above study, the pressure gradient dP/dL was recorded as the air flow rate Q_{air} was continually increased. Note that the increase in Q_{air} indicates the related increase in the fluid flow turbulence and changes in the water flow pattern. In either of the aforementioned situation, the dP/dL versus Q_{air} showed a common trend. dP/dL increased as Q_{air} increased, and the DRP dosage significantly affected the dP/dL versus Q_{air} relation. The plot shifted to the right, and dP/dL appreciably decreased for the same value of Q_{air} (turbulence level). Therefore, as the air flow rate increased, the effect of DRP showed to be significant by reducing the pressure gradient.

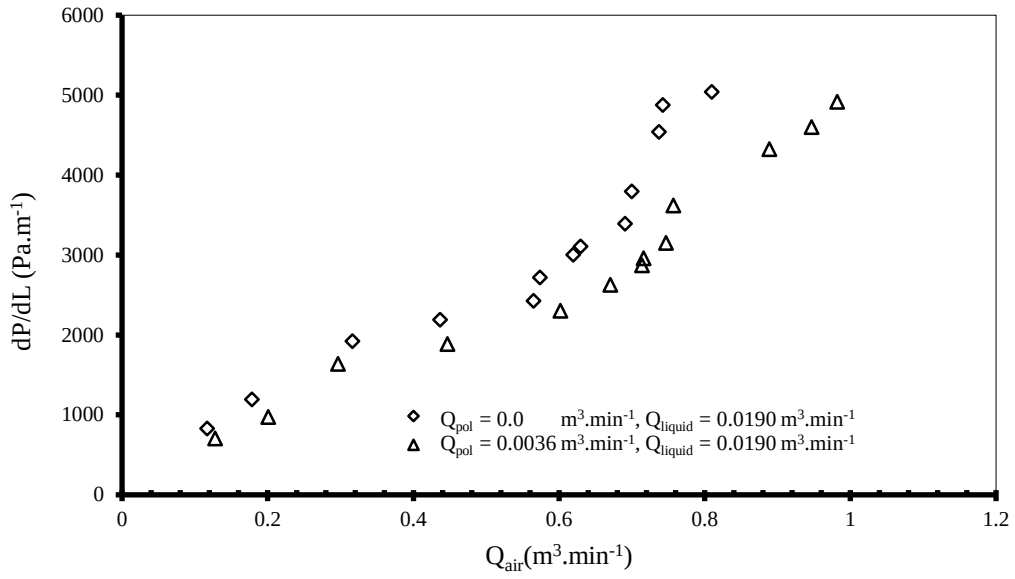

Figure 6.2A Pressure gradient of two-phase air-water flow versus air flow rate at constant water flow rate and at constant water-soluble DRP flow rates at concentration of 190 ppm.

Figure 6.2B illustrates the %DR behavior for the two-phase air-water flow. Here, the Reynolds number based on superficial gas velocity Re_{SG} was varied by varying the air flow rate Q_{air}. The %DR, for Q_{pol} = 0.0036 $m^3.min^{-1}$ (190 ppm dosage of DRP) and Q_{liquid} = 0.0190 $m^3.min^{-1}$, decreased with the increase of Re_{SG}. Therefore, the increase in the intensity of turbulence and the associated mixing decreased %DR in ZETAG® 8165-mediated air-water flow. The above DRP dosage showed to be unable to dampen the growth of eddy population with increasing Q_{air}.

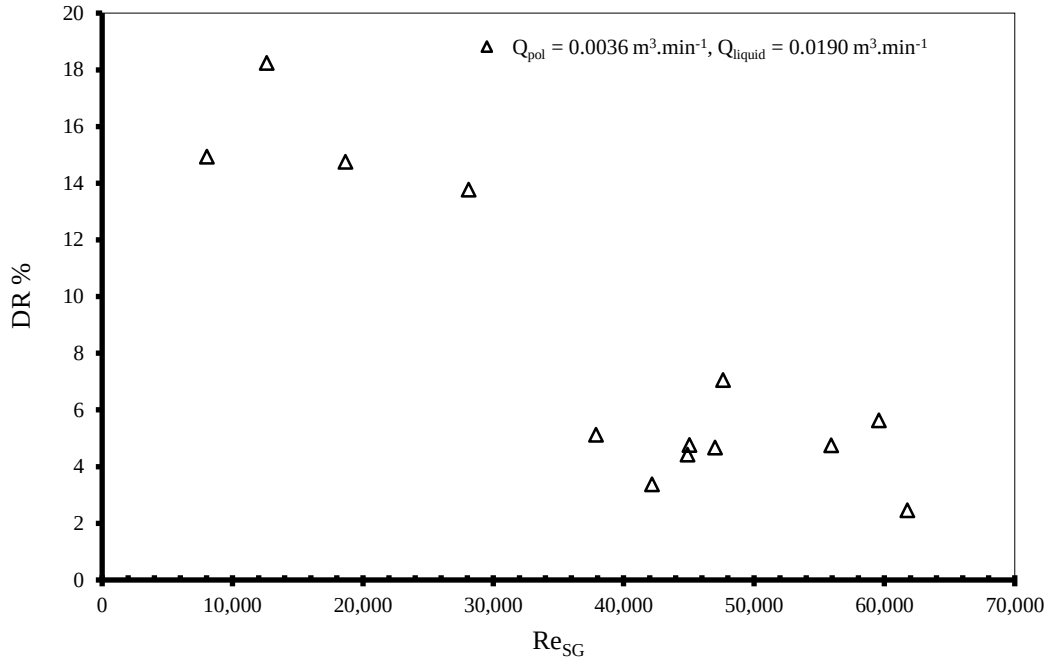

Figure 6.2B Percentage drag reduction versus Reynolds number based on gas superficial velocity (water-soluble DRP) for air-water flow.

The non-asymptotic first part of Figure 6.1A shows that the reduction in dP/dL is appreciably sensitive to fairly low Q_{pol}. Therefore, Figure 6.3A experimental design was applied using a very low dosage of ZETAG® 8165 (4.2 ppm) to the high frequency air-water slug flow. See Figures 6.3A and 6.3B. The findings are overall similar to those of Figures 6.2A and 6.2B, respectively. However, the effects are more pronounced in this case. Notwithstanding, the following result turned spectacular, which, to the best of our knowledge, has not been reported in the literature. The comparison of Figure 6.2B and Figure 6.3B results shows that the drag reduction performance by water-soluble ZETAG® 8165 at a low concentration (4.2 ppm) well exceeded that at a high concentration (190 ppm). This finding can be ascribed to the change in DRP external environment, that is, flow pattern, polarity, and phase morphology that surrounded the

DRP molecules. See Figure 6.4. Water (a single-component fluid) and ZETAG® 8165 are both polar. Therefore, here air interacted with a continuum of polar fluid.

Consequently, the hydrodynamic size of the DRP molecules, dictated by the extent of uncoiling, affected the capacity for dampening the turbulent eddies, streamlining the velocity field, and eventually increasing the thickness of viscous laminar sublayer. Accordingly, the %DR varied.

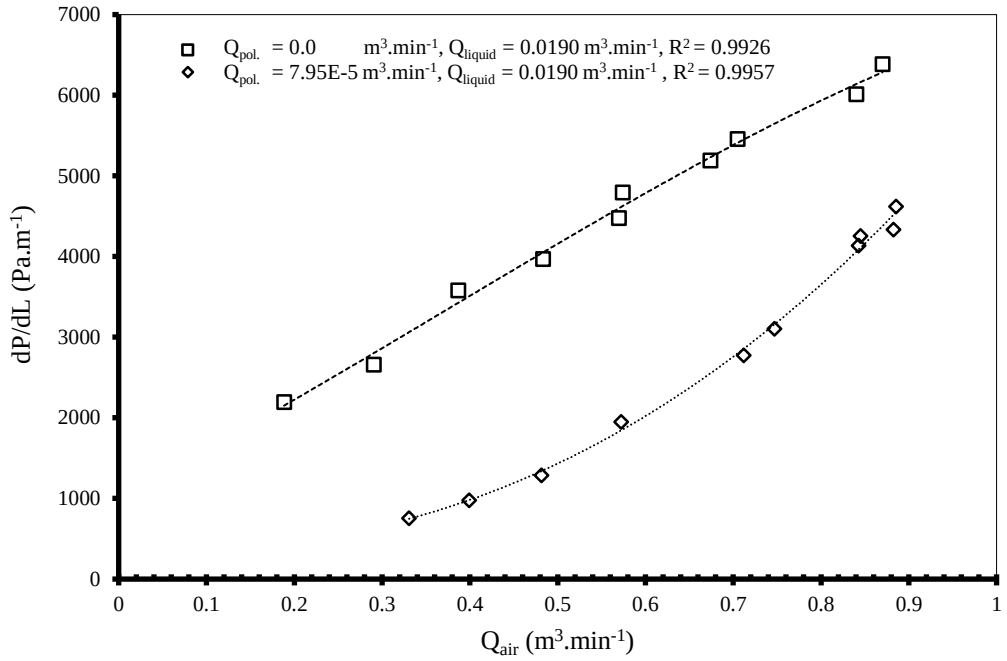

Figure 6.3A Pressure gradient of two-phase air-water flow versus air flow rate at constant water flow rate and at constant water-soluble DRP flow rate at concentration of 4.2 ppm (dotted curve represents third order polynomial cure).

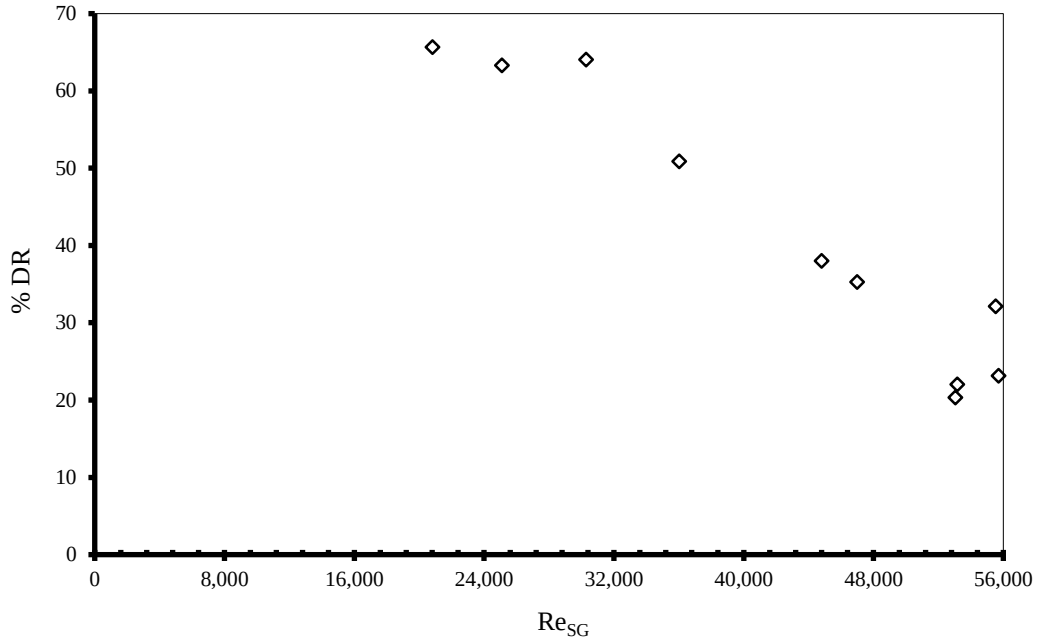

Figure 6.3B Percentage drag reduction versus Reynolds number based on gas superficial velocity (water-soluble DRP) for air-water flow at Q_{liquid} = 0.019 m^3/min, and at Q_{liquid} = 9.75E-5 m^3/min.

$$-(CH_2-CH-CO-NH_2)_n-(CH_2-CH-\{CO-(CH_2)_2-N^+-(CH_2)_2-CH_2-Ph\}\{Cl^-\})_m$$

$$+ H^+-OH^-$$

$$\Downarrow$$

$$-(CH_2-CH-CO-NH_2)_n-(CH_2-CH-\{CO-(CH_2)_2-N^+-(CH_2)_2-CH_2-Ph\}\{OH^-\})_m$$

$$+ H^+-Cl^-$$

Figure 6.4 Change in polarity, environment, and phase morphology of water.

6.2.2 Two-Phase Air-Oil flow With and Without Oil-Soluble DRP

Figure 6.5A evaluates the two-phase air-oil flow with and without the oil-soluble DRP PIB under the following experimental conditions:

i. $Q_{pol} = 0.0\ m^3.min^{-1}$ (no PIB dosage) and $Q_{liquid} = 0.0106\ m^3.min^{-1}$; and

ii. $Q_{pol} = 0.0013\ m^3.min^{-1}$ (184 ppm dosage of PIB) and $Q_{liquid} = 0.0106\ m^3.min^{-1}$.

Note that the dosage of PIB is comparable with that of ZETAG® 8165. Here, ESCAID™110 (kerosene)—consisting of mainly C_{10} to C_{16} aliphatic branched and straight chain hydrocarbons—and PIB are both nonpolar. Therefore, air in these experiments interacted with a continuum of nonpolar multi-component fluid.

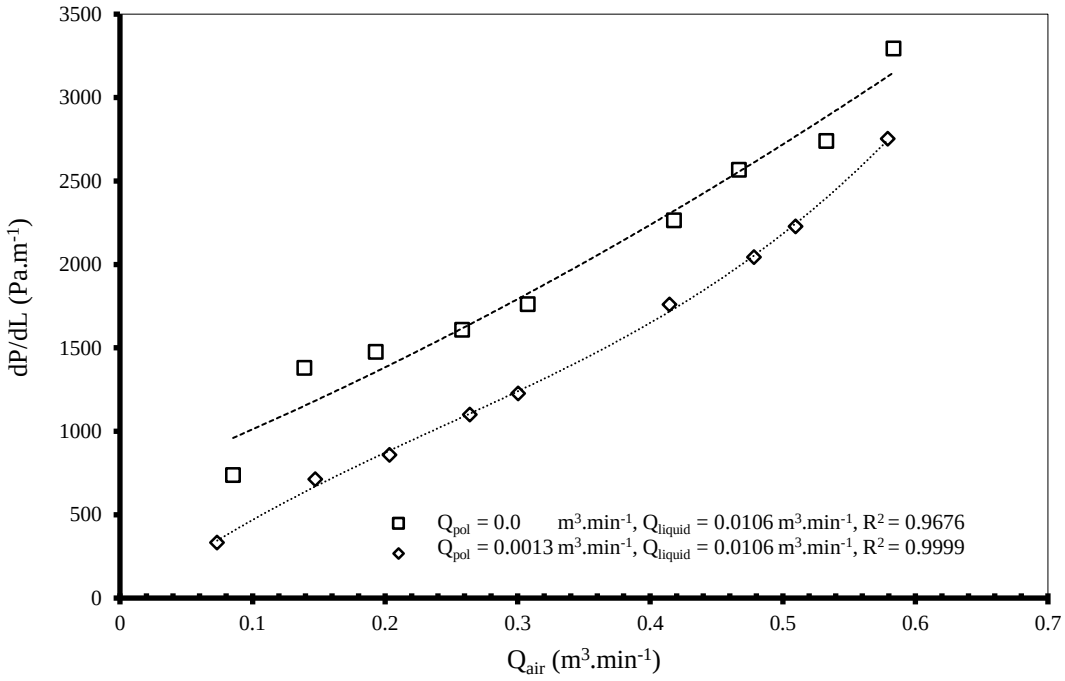

Figure 6.5A Pressure gradient of two-phase oil-air flow versus air flow rate at constant oil flow rate and at constant oil-soluble DRP flow rate (dotted curve represents third order polynomial cure).

Figure 6.5A demonstrates that as the air flow rate increased, the effect of DRP became noticeable by reducing the pressure gradient. Figure 6.5B illustrates that the %DR, for Q_{pol} = 0.0013 $m^3.min^{-1}$ (184 ppm dosage of DRP) and Q_{liquid} = 0.0106 $m^3.min^{-1}$, decreased with the increase of Re_{SG}. These air-oil flow findings qualitatively match those of air-water flow. See Figures 6.2A and 6.2B, respectively. Hence, the role played by the applied DRP (polar or nonpolar) and air on the continuum of fluid (polar or nonpolar) essentially remains the same. Hence, the previous explanation of results also holds.

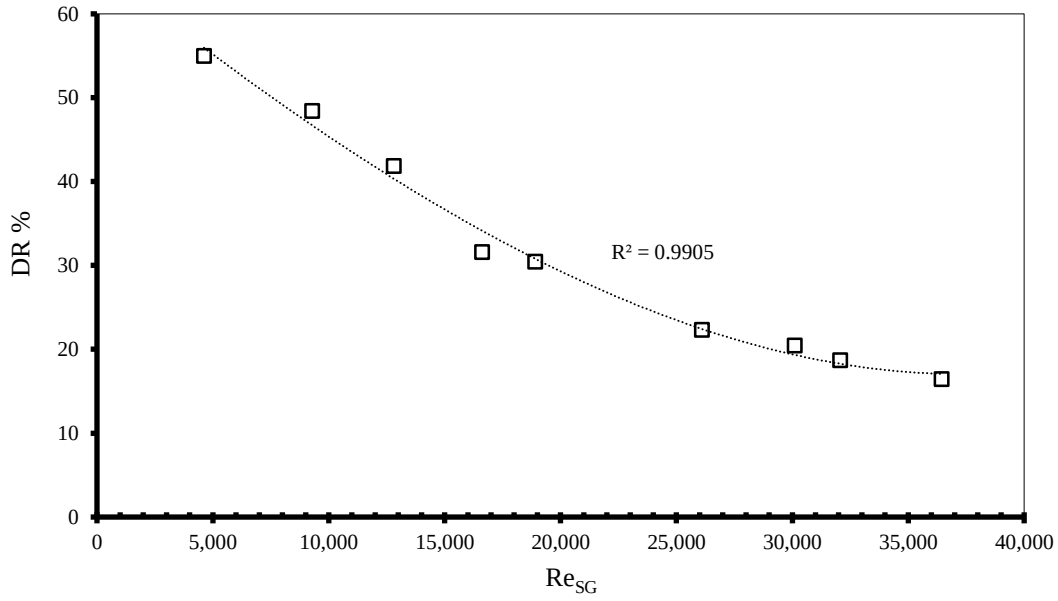

Figure 6.5B Percentage drag reduction versus Reynolds number based on gas superficial velocity for air-oil flow at constant liquid flow rate (Q_{liquid} = 0.0106 m^3/min) and at constant oil-soluble DRP flow rate ($Q_{pol.}$ = 0.0013 m^3/min), dotted curve represents third order polynomial cure.

The introduction of PIB affected the flow pattern as follows. It delayed the transition from low frequency to high frequency slug flow and the appearance of annular flow. On the other hand, Appendix B, Table B2 summarizes the influence of air flow rate on the oil phase flow pattern. As the air flow rate increased, the flow pattern changed from slug flow (existence of large air bubbles, tending to approach the pipe diameter, separated by water slugs) to annular flow (where water flows on the wall of the pipe as a film, with some liquid entrained in the core, and air flows in the center). In fact, as the superficial air velocity V_{SG} increased from 3.07 to 21.40 $m.sec^{-1}$, the air layer expanded its boundaries, potentially increasing the interfacial and wall stresses. Hence, the increasing air flow rate decreased %DR. Another possible explanation is that the above DRP dosage showed to be unable to dampen the growth of eddy population with increasing Q_{air}. Hence, the increasing Q_{air} decreased %DR.

6.2.3 Comparison between Two-Phase Air-Water and Air-Oil Flow

Figure 6.6 illustrates the %DR behavior for the two-phase air-water and air-oil flows. Here, the Reynolds number based on superficial gas velocity Re_{SG} was varied by varying the air flow rate Q_{air}, and Re_{SW} = 9199 and Re_{SO} = 3929 were used for water and oil (ESCAID^{TM}110), respectively. The %DR versus Re_{SG} variational trend for water and oil, in the presence of air (a much lighter gaseous phase), mutually differed. For water, it gradually increased; then it flattened. By contrast, for oil it continually decreased. Also, at Re_{SG} (superficial air velocity-based Reynolds number) = 12000, %DR for both flows

turned out to be the same (~45%). For Re_{SL} and Re_{SG} > 12000, %DR for ZETAG® 8165-mediated water flow showed to be much higher than that of PIB-mediated oil flow. In other words, the increase in the intensity of turbulence and the associated mixing improved %DR in ZETAG® 8165-mediated water flow. However, the opposite occurred for the PIB-mediated oil flow. The degradation behavior of ZETAG® 8165 versus PIB may be partially accountable for this. According to Al-Sarkhi and Hanratty [2001], the DRP aggregate probably disintegrated due to the impingement of a very high air velocity on the fluid continuum, which degraded the PIB chain. Recollect the opposite finding of Figure 6.2B in this context (190 ppm dosage of DRP), where the liquid flow rate and air flow rate were higher than the above case.

Figures 5.4 and 6.6 findings add new insight into the conventional drag-reducing mechanism. Drag reduction depends on the following factors. One is the DRP state that includes:

i. The hydrodynamic size of the DRP molecules, dictated by the extent of uncoiling; and
ii. The chemical structure of the DRP (polar versus nonpolar, homo- versus copolymer, etc.), its molecular weight, and backbone stability.

The other factor is DRP external environment that comprises:

i. The fluid flow pattern, polarity, and phase morphology that surround the DRP molecules; and
ii. The intensity of turbulence and the associated mixing phenomena.

The resultant interaction of the above two factors affect the capacity for dampening the turbulent eddies, streamlining the velocity field, and eventually increasing the thickness of viscous laminar sublayer. These events finalize the %DR. The judicious experimental design, that is, increasing the intensity of turbulence and the associated mixing through variation of Re_{SL} and Re_{SG} enabled us to propose the above explanation. Therefore, the drag reduction mechanism consolidated in the present two-phase air-water flow also holds in Section 6.3.1.

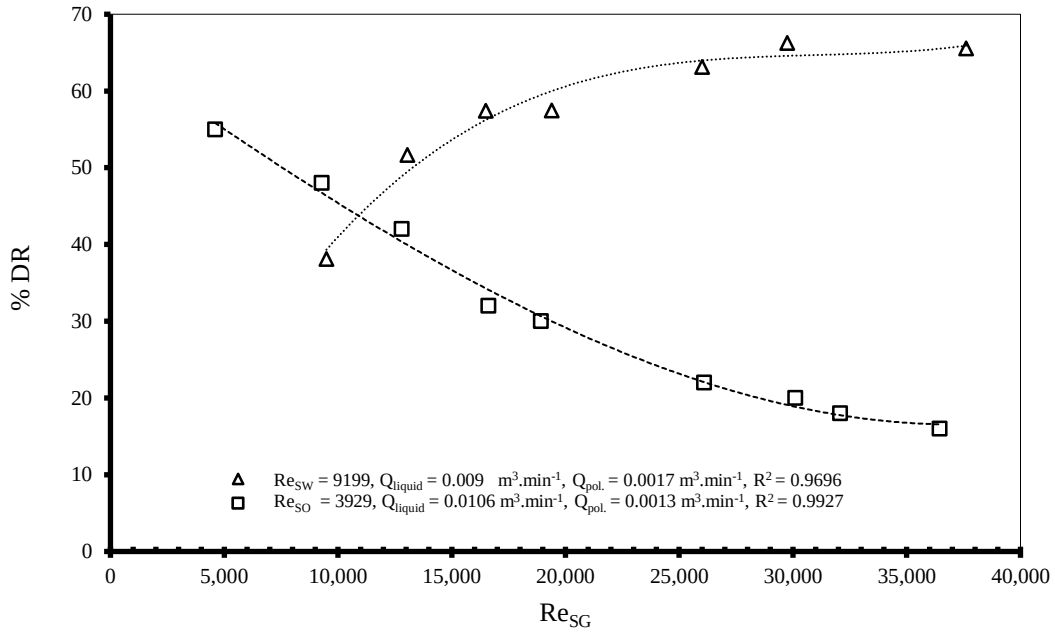

Figure 6.6 Comparison between two-phase air-water flow and two-phase air-oil flow (Tables 4A and 4B) at constant water-soluble DRP and oil-soluble DRP of 190 ppm and 184 ppm, respectively (dotted curve represents third order polynomial cure).

6.3 Conclusion

A series of experiments have been conducted to examine the effect of selected water - and oil-soluble DRPs on percentage drag reduction and flow patterns in two-phase air-water and air-oil flow. These experiments have been conducted using a 22.5 mm I.D. and 8.33 m long PVC horizontal pipe.

The overall performance of the water-soluble DRP is better than the oil-soluble DRP. For example, the maximum %DR of water-soluble ZETAG® 8165 DRP was 66 for two-phase flow. While, the maximum %DR for oil-soluble DRP was 55 for two-phase flow. In addition, Appendix B, Tables B1 and B2 represent that the DRPs injected into the two-phase fluids changed the flow patterns except for flows at very high superficial air velocity. However, the air-water flow findings qualitatively match those of air-oil flow. See Figures 8B and 10B, respectively. Hence, the role played by the applied DRP (polar or nonpolar) and air on the continuum of fluid (polar or nonpolar) essentially remains the same.

Moreover, this chapter add new insight into the conventional drag-reducing mechanism in terms of two factors. One is the DRP state that includes; the hydrodynamic size and chemical structure of the DRP. The other factor is the DRP external environment such as fluid flow patterns and intensity of turbulence. These two factors appeared clearly in Figures 6.2B and 6.3B were the water-soluble ZETAG® 8165 DRP at a low concentration well exceeded that at a high concentration.

CHAPTER 7

EXPERIMENTAL RESULTS OF AIR-OIL-WATER FLOW WITH DRPs

7.1 Introduction

In this Chapter, the performance of the water-soluble and oil-soluble DRPs was evaluated by conducting a set of experiments of three-phase air-oil-water flow. The objective of this investigation was to determine the effect of DRPs on the flow patterns and the maximum drag reduction. Consequently, a comparison between the two types of DRPs based on the effectiveness in damping the turbulence activities and other factors related to the DRP chemical structure had been done.

7.2 Results and Discussion

7.2.1 Three-Phase Air-Oil-Water Flow with and without Water-Soluble DRP

The three-phase air-oil-water slug flow experiments were conducted by varying the air flow rate and keeping the water and oil flow rates and the water-soluble DRP ZETAG® 8165 concentration constant. The following two sets of experiments were performed.

The first set, which refers to Figure 7.1A, studied the three-phase air-oil-water flow with and without the water-soluble DRP, by monitoring dP/dL as a function of Q_{air}, under the following experimental conditions:

i. Q_{pol} = 0.0 $m^3.min^{-1}$ (no DRP dosage), Q_{water} = 0.0189 $m^3.min^{-1}$, and Q_{oil} = 0.0076 $m^3.min^{-1}$ (total flow rate is Q_{liquid} = 0.0260 $m^3.min^{-1}$); and

ii. Q_{pol} = 0.0030 $m^3.min^{-1}$ (115 ppm dosage of ZETAG® 8165), Q_{water} = 0.0160 $m^3.min^{-1}$, and Q_{oil} = 0.0076 $m^3.min^{-1}$ (total flow rate is Q_{liquid} = 0.0260 $m^3.min^{-1}$).

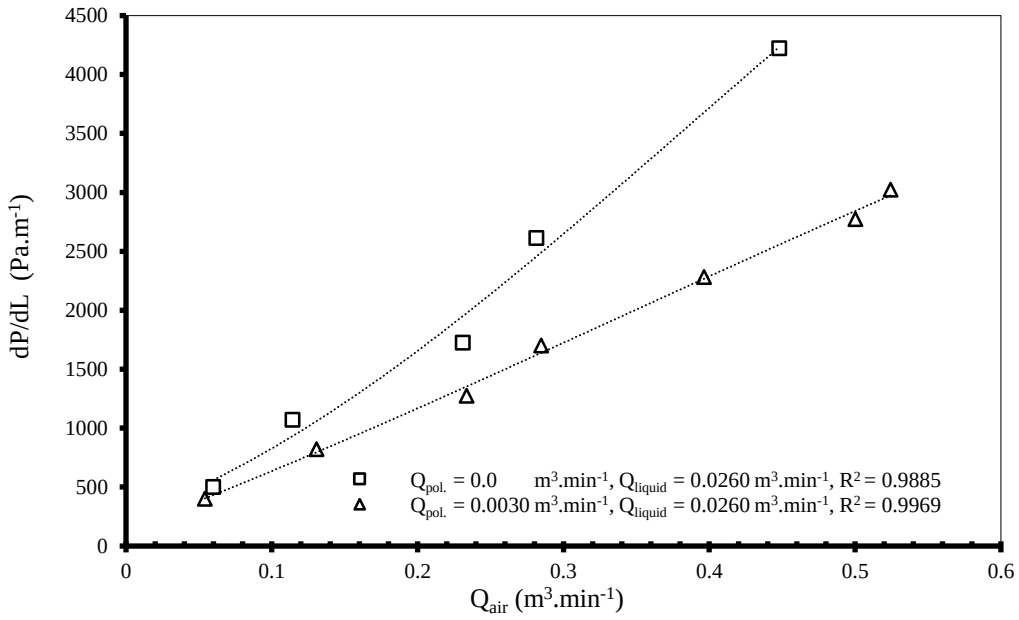

Figure 7.1A Pressure gradient of three-phase air-oil-water flow with and without water-soluble DRP (DRP concentration is 115 ppm) versus air flow rate at constant oil flow rate and at constant water flow rate. For □ (Q_{water} = 0.0189 $m^3.min^{-1}$, Q_{oil} = 0.0076 $m^3.min^{-1}$); Δ (Q_{water} = 0.0160 $m^3.min^{-1}$, Q_{oil} = 0.0076 $m^3.min^{-1}$), dotted curve represents third order polynomial cure.

The above figure shows that ZETAG® 8165 reduced the pressure gradient for each air flow rate applied. However, the above effect on the pressure gradient decreased as the air flow rate increased. This finding qualitatively matches that of air-water and air-oil flows. See Figures 6.3A and 6.5A, respectively.

Figure 7.1B shows that the %DR, for Q_{pol} = 0.0030 $m^3.min^{-1}$ (115 ppm dosage of ZETAG® 8165) and Q_{water} = 0.0160 $m^3.min^{-1}$, Q_{oil} = 0.0076 $m^3.min^{-1}$ (total flow rate is Q_{liquid} = 0.0260 $m^3.min^{-1}$) increased with the increase of Re_{SG}. This is an insightful result and agrees with the report of Langsholt [2012]. However, it is strikingly opposite to what

the two-phase air-water and air-oil flows demonstrated. See Figures 6.3B and 6.5B, respectively.

In fact, the main source of pressure gradient reduction was the existence of water-soluble DRP in the water layer, which was governed by wall shear stress reduction and interfacial shear reduction between phases.

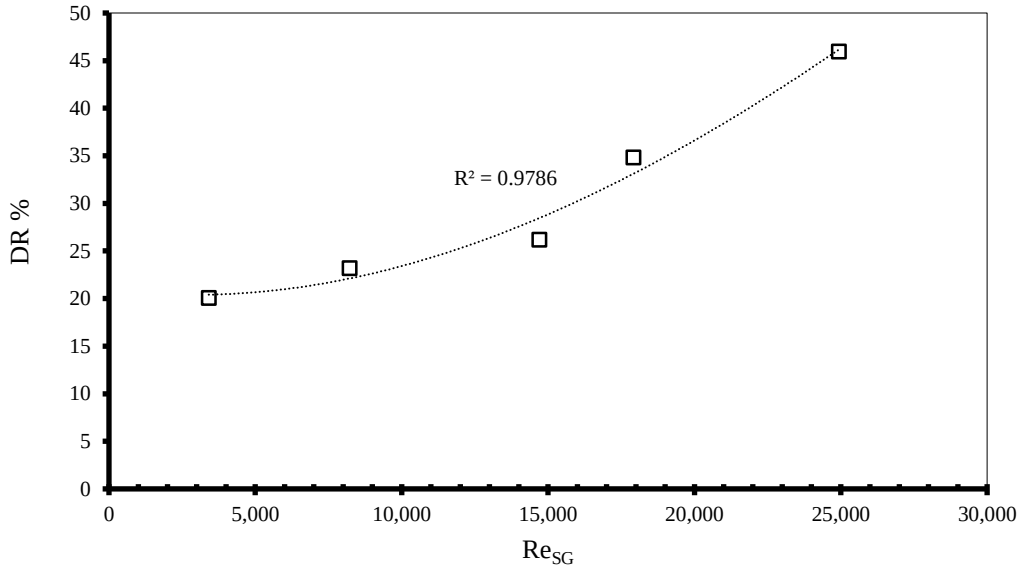

Figure 7.1B Percentage drag reduction versus Reynolds number based on gas superficial velocity at DRP concentration of 115 ppm ($Q_{pol.}$ = 0.0030 m^3/min) for three phase air-oil-water flow with water-soluble DRP at Q_{water} = 0.0160 $m^3.min^{-1}$ and Q_{oil} = 0.0076 $m^3.min^{-1}$ (Q_{liquid} = 0.0260 m^3/min), dotted curve represents third order polynomial cure.

The second set, which concerns Figure 7.2A, was conducted as follows:

i. Q_{pol} = 0.0 $m^3.min^{-1}$ (no DRP dosage), Q_{water} = 0.0076 $m^3.min^{-1}$, and Q_{oil} = 0.0189 $m^3.min^{-1}$ (total flow rate is Q_{liquid} = 0.0266 $m^3.min^{-1}$);

ii. Q_{pol} = 0.0 $m^3.min^{-1}$ (no DRP dosage), Q_{water} = 0.0111 $m^3.min^{-1}$, and Q_{oil} = 0.0179 $m^3.min^{-1}$ (total flow rate is Q_{liquid} = 0.0290 $m^3.min^{-1}$); and

iii. Q_{pol} = 0.0030 $m^3.min^{-1}$ (103 ppm dosage of ZETAG® 8165), Q_{water} = 0.0081 $m^3.min^{-1}$, and Q_{oil} = 0.0179 $m^3.min^{-1}$ (total flow rate is Q_{liquid} = 0.0290 $m^3.min^{-1}$).

The above figure also shows that ZETAG® 8165 reduced the pressure gradient for each air flow rate applied. This finding qualitatively matches what Figure 7.1A demonstrated. Also, see Langsholt [2012].

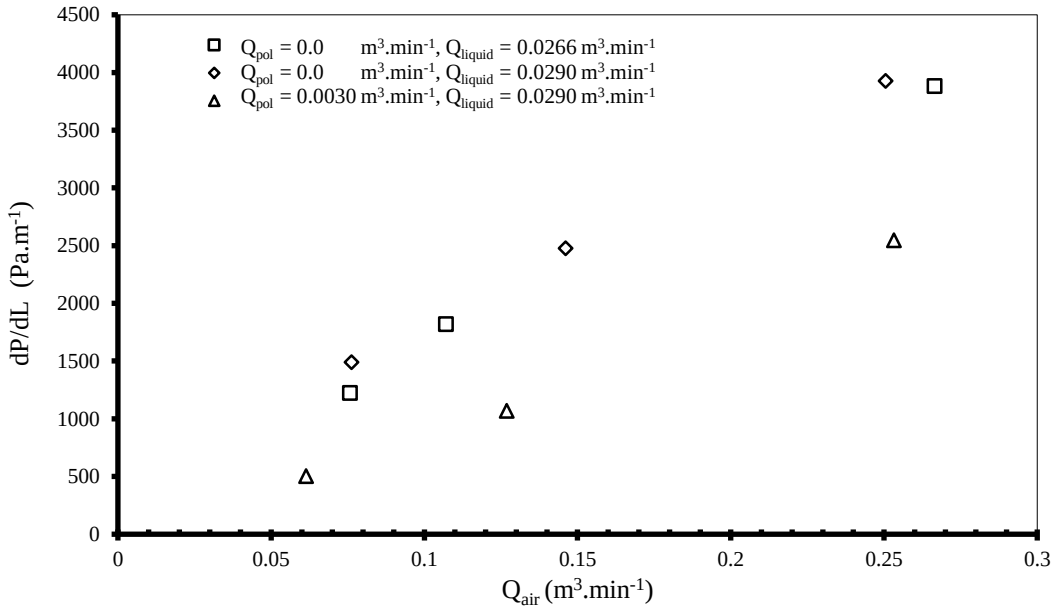

Figure 7.2A Pressure gradient of three-phase air-oil-water flow versus air flow rate with and without water-soluble DRP (DRP concentration is 103 ppm). For □ (Q_{water} = 0.0076 $m^3.min^{-1}$, Q_{oil} = 0.0189 $m^3.min^{-1}$); ◊ (Q_{water} = 0.0111 $m^3.min^{-1}$, Q_{oil} = 0.0179 $m^3.min^{-1}$); Δ (Q_{water} = 0.0081 $m^3.min^{-1}$, Q_{oil} = 0.0179 $m^3.min^{-1}$).

Figure 7.2B illustrates that the %DR, for Q_{pol} = 0.0030 $m^3.min^{-1}$ (103 ppm dosage of ZETAG® 8165), Q_{water} = 0.0081 $m^3.min^{-1}$, and Q_{oil} = 0.0179 $m^3.min^{-1}$ (total flow rate is Q_{liquid} = 0.0290 $m^3.min^{-1}$) increased with the increase of Re_{SG}. It can be indicated that DRP ZETAG® 8165 is able to absorb the turbulence activity near the pipe wall and at the phases interface. This conforms to the previous finding of Figure 7.1B, as well as the three-phase fluid system studied by Sifferman and Greenkorn [1981]. The Set 1 and Set 2 %DR experiments can be compared as follows:

i. %DR = 20, Re_{SG} = ~4,000; %DR = 28, Re_{SG} = 16,000; and dosage of ZETAG® 8165 = 115 ppm (Set 1, Figure 7.1B); and

ii. %DR = 38, Re_{SG} = 4,000; %DR = 67, Re_{SG} = 16,000; and dosage of ZETAG® 8165 = 103 ppm (Set 2, Figure 7.2B).

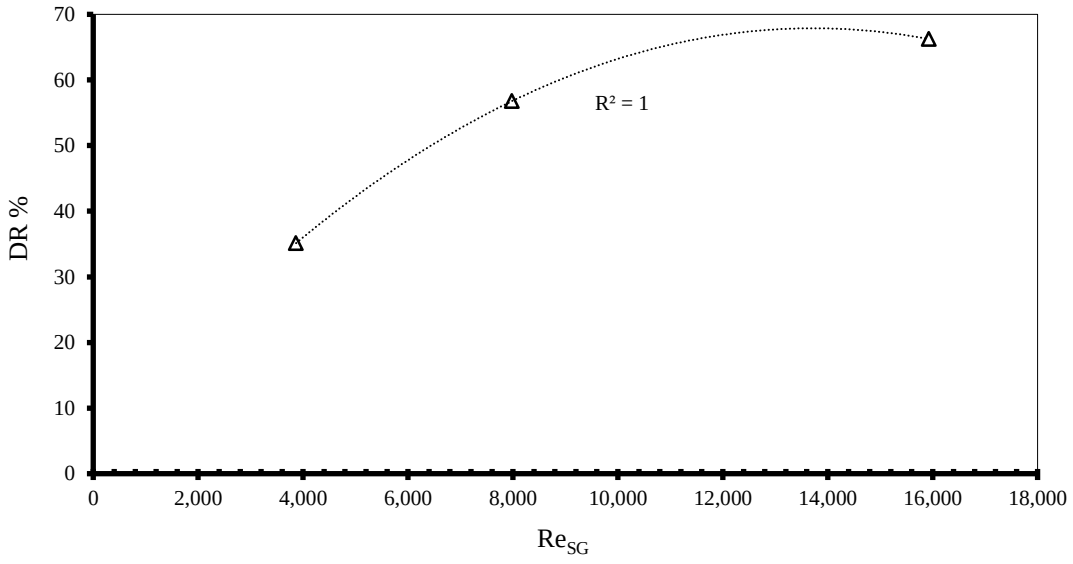

Figure 7.2B Percentage dag reduction versus Reynolds number based on gas superficial velocity at DRP concentration of 103 ppm ($Q_{pol.}$ = 0.0030 m^3/min) for three-phase air-oil-water with water-soluble DRP at Q_{water} = 0.0081 $m^3.min^{-1}$and Q_{oil} = 0.0179 $m^3.min^{-1}$ (Q_{liquid} = 0.0290 m^3/min), dotted curve represents fifth order polynomial cure

The above comparison reveals that in the three-phase air-oil-water slug flow, the water-soluble DRP ZETAG® 8165 even at a lower concentration showed much higher %DR at a higher mixture velocity Q_{liquid}. In addition to previously mentioned factors, the ZETAG® 8165 entanglements can damp the propagation of turbulence in case of lower water flow rate (Figure 7.2B) more effectively than the case of higher water flow rate (Figure 7.1B).

7.2.2 Three-Phase Air-Oil-Water Flow with and without Oil-Soluble DRP

Figure 7.3A, investigated the three-phase air-oil-water flow with and without the oil-soluble DRP PIB, by monitoring dP/dL as a function of Q_{air}, under the following experimental conditions:

i. Q_{pol} = 0.0 $m^3.min^{-1}$ (no PIB dosage), Q_{water} = 0.0106 $m^3.min^{-1}$, and Q_{oil} = 0.0190 $m^3.min^{-1}$ (total flow rate is Q_{liquid} = 0.0296 $m^3.min^{-1}$);

ii. Q_{pol} = 0.0023 $m^3.min^{-1}$ (110 ppm dosage of PIB), Q_{water} = 0.0106 $m^3.min^{-1}$, and Q_{oil} = 0.0166 $m^3.min^{-1}$ (total flow rate is Q_{liquid} = 0.0295 $m^3.min^{-1}$);and

iii. Q_{pol} = 0.0023 $m^3.min^{-1}$ (110 ppm dosage of PIB), Q_{water} = 0.0190 $m^3.min^{-1}$, and Q_{oil} = 0.0083 $m^3.min^{-1}$ (total flow rate is Q_{liquid} = 0.0296 $m^3.min^{-1}$).

The above figure demonstrates that PIB decreased the pressure gradient for each air flow rate experimented. This finding qualitatively conforms to that of air-water, air-oil, and air-oil-water flows. See Figures 6.3A, 6.5A, 7.1A and 7.2A, respectively. However, the

depression in dP/dL, in this case is not as pronounced as that observed with the water-soluble ZETAG® 8165-mediated air-oil-water flow.

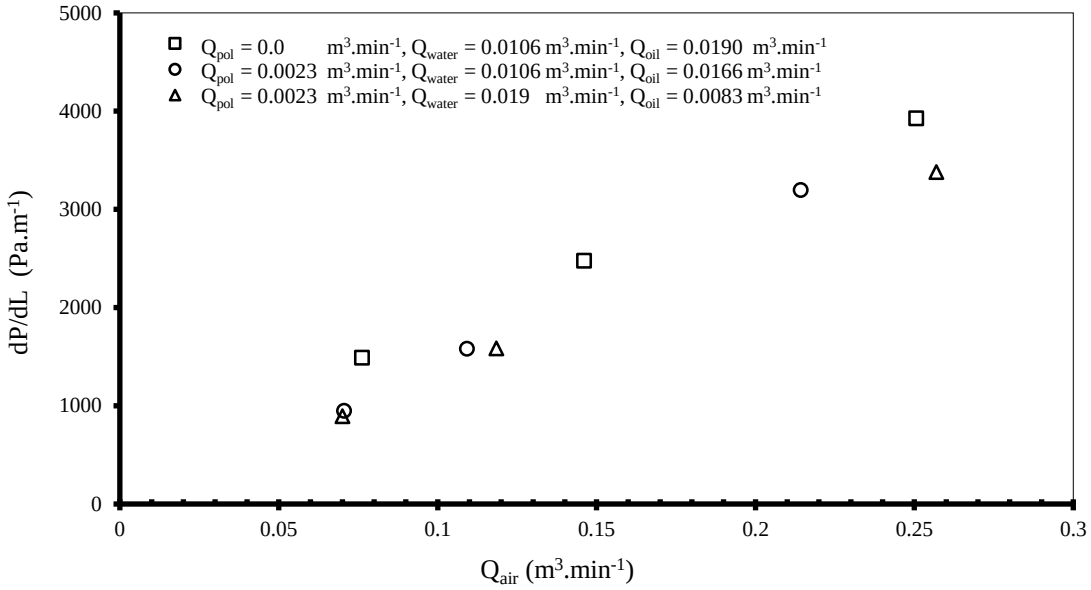

Figure 7.3A Pressure gradient of three-phase air-oil-water flow with and without oil-soluble DRP versus air flow rate at DRP concentration of 110 ppm. Where: □ (Q_{liquid} = 0.0296 $m^3.min^{-1}$); ○ (Q_{liquid} = 0.0295 $m^3.min^{-1}$); Δ (Q_{liquid} = 0.0296 $m^3.min^{-1}$).

Figure 7.3B, shows that the %DR, for Q_{pol} = 0.0023 $m^3.min^{-1}$ (110 ppm dosage of PIB), Q_{water} = 0.0166 and 0.0190 $m^3.min^{-1}$, and Q_{oil} = 0.0166 and 0.0083 $m^3.min^{-1}$ (total flow rate is Q_{liquid} = 0.0296 $m^3.min^{-1}$), fairly coincided with a common trend line and decreased with the increase of Re_{SG}. This is an interesting result; it is supported by the report of Langsholt [2012] and the findings of the two-phase air-water and air-oil flows in Figures 6.2B, 6.3B, and 6.5B. However, it is amazingly contrary to what the two-phase air-water flow as well as the three-phase ZETAG® 8165-mediated air-oil-water flow

exhibited. See Figures 6.1B, 7.1B, and 7.2B, respectively. The Figure 7.3B finding can be addressed as follows.

The increasing air flow rate, that is, Re_{SG} generated a larger amplitude of roll waves. These waves increased the air-oil interface, oil-water interface and wall stresses, which reduced the existing %DR.

The following can be concluded by comparing Figure 7.2B with Figure 7.3B. The water-soluble DRP ZETAG® 8165, because of structural difference, can better dampen the turbulent eddies than the oil-soluble DRP PIB. Also, according to Daas et al. [2006], the ability of the former to decrease the roughness at the air-water interface, oil-water interface and resist the wall stresses is much better than that of the latter.

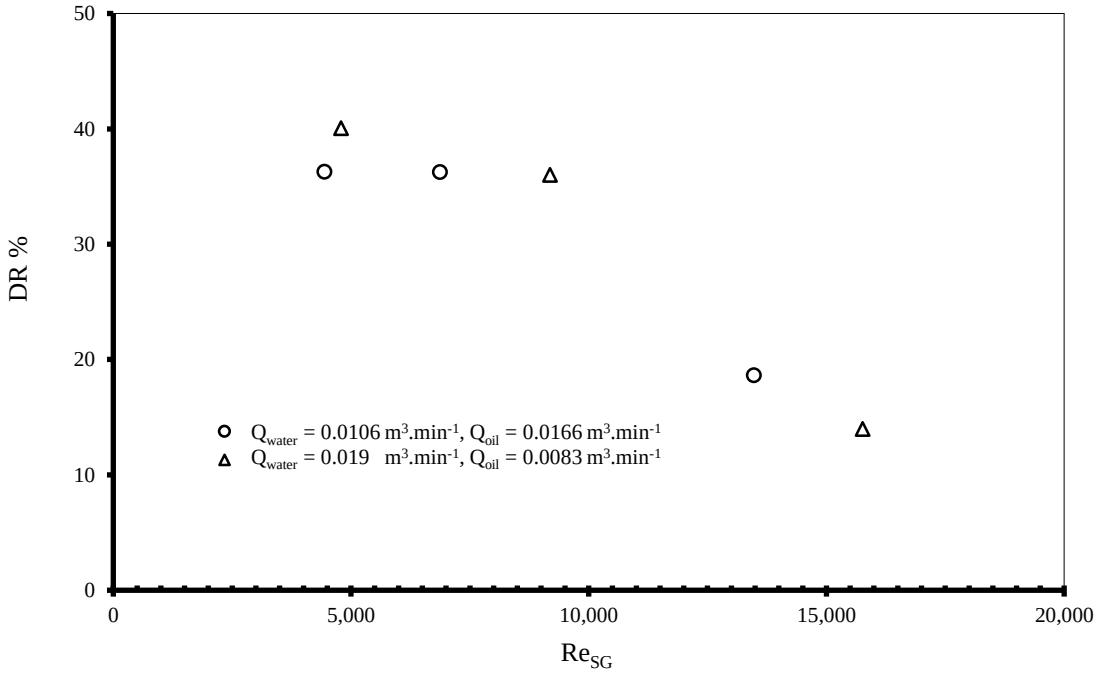

Figure 7.3B Percentage drag reduction versus Reynolds number based on gas superficial velocity at Q_{liquid} = 0.029 $m^3.min^{-1}$, Q_{pol} = 0.0023 $m^3.min^{-1}$, where oil-soluble DRP concentration is 110 ppm.

7.2.3 Effect of DRP on Fluid Flow Pattern

Appendix B, Tables B1 and B2 list the experimental test matrix and the variation of flow patterns before and after the injection of the two experimental DRPs (ZETAG® 8165 and PIB). The following findings can be listed for most cases:

i. The DRPs injected into the two- and three-phase fluids changed the flow patterns except for flows at very high superficial gas velocity V_{SG} or Reynolds number Re_{SG}. They also reduced the pressure gradient dP/dL under all the experimental conditions.

ii. Visual observations revealed that both DRPs delayed (i) the transition from low to high frequency slug flow, and (ii) the appearance of annular flow, particularly for the two-phase and three-phase flows.

iii. The DRPs, depending on the slug flow frequency, altered the numbers of slugs SN that passed the transparent part of the test section. For low frequency slug flow (SLF), SN was fewer than that of the average slug flow (S). For the high frequency slug flow (SHF), SN was much higher than the average slug flow (S). With the DRP, SN was fewer than that without the DRP, which concurs with the investigations of Thwaites et al. [1976] and Al-Sarkhi and Soleimani [2004]. This result can be related to the increase in bubble velocity behind the slug, which, in turn, increased the liquid thickness that enhanced the shedding rate and the slug destabilization.

iv. At a very high V_{SG} and in the presence of water-soluble DRP, an annular flow changed to a high frequency slug flow (SHF). However, for the oil-soluble DRP,

the %DR decreased at the highest value of V_{SG}, and the flow pattern did not change. According to Al-Sarkhi and Hanratty [2001], the DRP aggregate disintegrated due to the impingement of a very high air velocity on the fluid continuum, which degraded the DRP chain.

7.3 Conclusion

A series of experiments have been conducted to examine the effect of selected water- and oil-soluble DRPs on percentage drag reduction and flow patterns in three-phase air-oil-water flow. These experiments have been conducted using a 22.5 mm I.D. and 8.33 m long PVC horizontal pipe.

It was shown that the DRPs were affecting positively in three-phase flow experiments. One of the deliverable results indicates that an increase in DRPs concentrations results in an increase in percentage drag reduction up to certain limit then it fairly flattened.

Referring to Appendix B, Tables B1 and B2, and Figures 5.5A and 5.5B, the overall performance of the water-soluble DRP is better than the oil-soluble DRP due to the ability of the former to decrease the roughness at the phases interface and resist the wall stresses is much better than that of the latter. Also, the maximum %DR of water-soluble ZETAG® 8165 DRP were 66 for three-phase flow. While, the maximum

%DR for oil-soluble DRP were 40 for three-phase flow. In addition, Tables C1 and C2 represent that the DRPs injected into the three-phase fluids changed the flow patterns except for flows at very high superficial air velocity. On the other hand, the water-soluble DRP ZETAG® 8165, because of chemical composite difference, can better dampen the turbulent vortices than the oil-soluble DRP PIB.

CHAPTER 8

PIV EXPERIMENTAL RESULTS WITH COMPARISON WITH NUMERICAL RESULTS

8.1 Introduction

This chapter presents experimental investigations conducted to understand the mechanism of drag reducing polymers (DRPs). Water-soluble DRP has been used as an example. However, the same analysis also applies to oil-soluble DRP. In particular, the influence of water-soluble DRP in single and two-phase (stratified-wavy) flows on flow field characteristics has been investigated. These experiments have been presented for water and air-water flowing in a horizontal PVC 22.5 mm I.D., 8.33 m long pipe. The effects of liquid flow rates and DRP concentrations on streamlines, and the instantaneous velocity were investigated by using Particle Image Velocimetry (PIV) technique. A comparison of the PIV results was performed by comparing them with the computational results obtained by FLUENT software.

The PIV analyses were carried out on the Dantec Dynamics studio. Firstly, images were imported as an ensemble to make analyses faster and calibration which maps image view

to object view was done without calibration images by taking advantage of the prior knowledge of the pipe diameter. Then, sequence of analysis as depicted in Figure 8.1 was applied to the ensemble.

The analysis sequence starts with image pre-processing which is usually done to enhance the quality of the images. This was achieved by background subtraction and image balancing. The former was carried out to eliminate background noises while the latter was done to reduce non-uniformity of illumination.

Thereafter, the Adaptive Correlation scheme was adopted from the numerous schemes available in the Dantec Dynamics studio software to determine velocity vectors because it's accurate, easy to apply and does not push the limit of PIV signals by over-processing. The scheme contains algorithms required for image processing from cross-correlation, vector validation to image post-processing to yield reliable vector maps.

Then, cross-correlation was carried out by specifying final IA as 32 x 32 pixels with 3 refinement steps, 50% horizontal and vertical overlap and Gaussian Window function to remove small noise due to cyclic nature of FFT. Vector validation was achieved by setting stringent conditions like peak to height ratio to 1.3 in the Peak validation algorithm to identify spurious vectors. This was combined with Local Neighborhood Validation which replaces the spurious vectors based on the interpolation from the surrounding good vectors. The interrogation area offset was adopted to obtain accurate velocity from the mean displacement vectors by three-point symmetric algorithm (Central difference offset).

The post processing was achieved with the use of High Accuracy and Deforming Windows scheme which offers the following benefits: use a signal analysis approach without image interpolation, optimize the signal strength by window off-set, optimize signal strength by capturing particle drop-out due to velocity gradients, achieve bias free measurements through improved super-pixel interpolation, achieve high sub-pixel accuracy independent of correlation peak unlike Gaussian and Parabolic fit, and minimize displacement estimate errors by use of adaptive deforming windows.

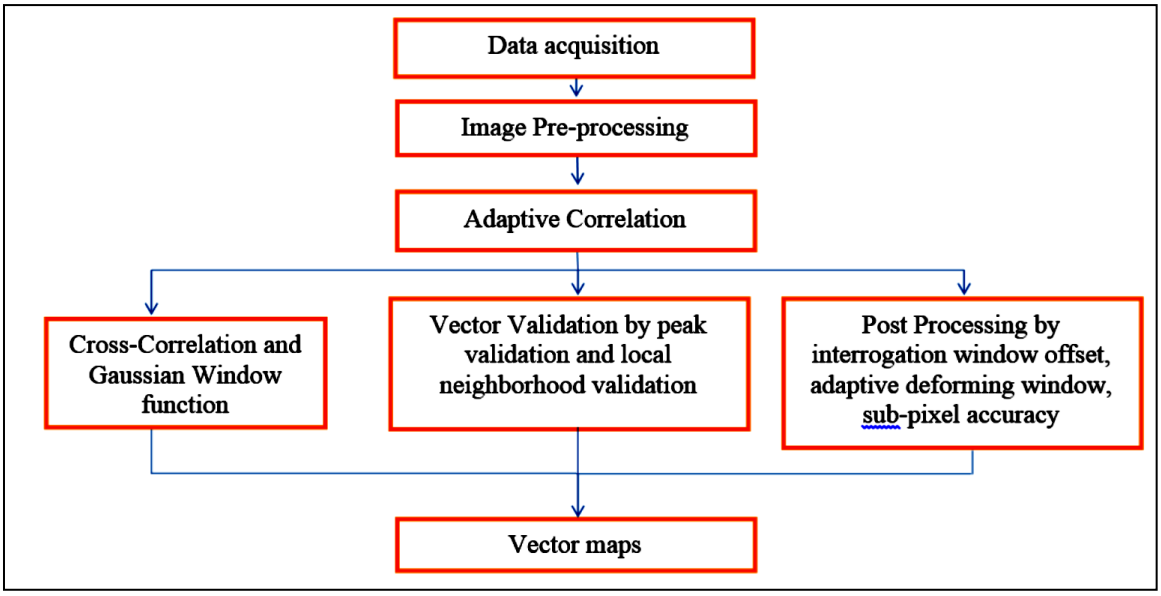

Figure 8.1 Sequence of analysis for PIV

Asides the instantaneous velocities that were obtained from the generated Vector map for each image, flow characteristics such as vortices, streamlines, and average velocity map can also be determined. Vorticity is the description of the local spinning motion of the

flow field, and is mathematically defined as the curl (rotational) of the flow velocity vector as shown in Equation 8.1 [Schlichting H. and Gersten K. 2003].

$$\overline{\omega} = curl(\overline{V}) = \nabla X\overline{V} = \left(\frac{\partial W}{\partial y} - \frac{\partial V}{\partial z}\right)\hat{i} + \left(\frac{\partial U}{\partial z} - \frac{\partial W}{\partial x}\right)\hat{j} + \left(\frac{\partial V}{\partial x} - \frac{\partial U}{\partial y}\right)\hat{k} \tag{8.1}$$

The previous equation represents a 3-D flow field which gives local spin around each axis. By using PIV, the velocity vector is really a projection of the 3-D velocity field onto the experimental plane. Lack of information about the third velocity component, W, only the rotation about the z-axis (in x-y plane) can be obtained. For a 2-D velocity field, vorticity equation (Equation 8.1) reduces to:

$$\omega_z = \left(\frac{\partial V}{\partial x} - \frac{\partial U}{\partial y}\right)\hat{k} \tag{8.2}$$

The turbulence intensity (TI) with and without DRP was also measured. According to Schlichting H. and Gersten K. [2003], the turbulent velocity map can be decomposed into average velocity $\overline{U}$, which is measure directly by using DynamicStudio software, and velocity fluctuation vector u', which can estimated based on data variance using the aforementioned software.

$$u = \overline{U} + u' \tag{8.3}$$

The level of turbulence can be quantified by calculating the turbulence intensity parameter as following:

$$TI_u = \frac{u'}{\overline{U}} \cong \frac{\sigma_u}{\overline{\mu}_u} \tag{8.4}$$

$$TI_v = \frac{v'}{\overline{V}} \cong \frac{\sigma_v}{\overline{\mu}_v} \tag{8.5}$$

where;

TI_u : Turbulence Intensity in the streamwise.

TI_v : Turbulence Intensity in the spanwise.

u', v' : standard deviation of the velocity fluctuations at a certain location over a specified time.

$\overline{U}, \overline{V}$: mean of the velocity at same location over the same time period.

$\overline{\mu}_u, \overline{\mu}_v$: mean velocity for u and v components $\overline{\mu}_u = \frac{1}{n}\sum_{i=1}^{n} u_i$ (8.6)

σ_u, σ_v : variance for u and v components $\sigma_u^2 = \frac{1}{n-1}\sum_{i=1}^{n}\left(u_i - \overline{\mu}_u\right)^2$ (8.7)

8.2 Experimental Setup and Procedure

A detailed experimental setup have been described in Chapter 3, section 3.2. The procedure followed in running the single-phase experiment, for instance, the pipe was filled with water, which seeded with tracer particles, with and without DRP, and the PIV reading was taken from the transparent part of the test section. The image-videos were recorded first by using the Phantom Camera Suite (PCC). This software used to adjust the recorded videos settings such as; resolution, exposure time, frame rate per second…etc, based on the flow rate. The field of view (FOV) of 46 x 12.5 mm was illuminated by the

laser at 4.0 mJ and the camera was adjusted to bring it in focus. Camera Intensity Calibration (also known as Camera Section Reference) was performed at 1,630 x 1,200 resolution, sample rate of 200 fps, and with the exposure time set at maximum value. The flow without seeding particle was recorded after which it was seeded with 10 µm Hollow Glass Sphere (HGS). Images of the flow introduced at different flow rates were recorded at resolution of 1248 x 544 pixels, and sample rates 900 frame.s^{-1} over 30 sec duration.

8.3 Results and Discussion

8.3.1 Experimental Investigation for Single-Phase Water Flow by Using PIV Technique

Experiments were performed for single-phase water flow seeded with tracer particles with and without DRP for certain range of water flow rates. PCC software, laser, and high-speed camera were used to capture high resolution video in the transparent portion of the test section. For the purpose of examining PIV accuracy, Equation 8.8 was used to draw analytical curve for laminar single-phase water flow as shown in Figure 8.2. In this figure, the minimum experimental superficial velocity can be attained was 0.1958 m.sec^{-1}, which gives Reynolds number of 4959. This value of Reynolds number falls in the turbulent region. Furthermore, the range of superficial velocities were between 0.1958 up 0.3986 m.sec^{-1} or in Reynolds number between 4959 up to 10,096.

$$U_{Laminar} = 2V_{ave}\left[1 - \frac{r^2}{R^2}\right] \quad (8.8)$$

For the purpose of showing the effect of adding DRP to single-phase water flow by using PIV technique, Figure 8.3 represents a number of experiments for single-phase water with DRP which it had same flow characteristics as in Figure 8.2. It can be observed that the addition of water-soluble DRP clearly minimizes the effect of turbulence activity and the trend of the data became close to the laminar velocity profile near the pipe wall still but/not the same. In fact, when DRP was mixed with the liquid in a pipeline in parts per million (ppm) level, it changes the flow structure in turbulent flow by suppressing the formation of turbulent bursts and the propagation of the turbulent eddies, and in turn increasing the thickness of the laminar sub-layer near the pipe wall. In other words, DRPs streamline turbulent flows and reduce the Reynolds stresses at the wall as shown in Figures 8.4 and 8.5.

The percentage drag reduction at various concentrations of DRP, for single-phase water flow at water flow rate of (0.50-0.77) $x10^{-2}$ $m^3.min^{-1}$ and at water-soluble DRP flow rate of 0.717 $x10^{-3}$ $m^3.min^{-1}$, was around 45%. The constant percentage drag reducing percentage indicates that the increment in DRP concentrations has no effect.

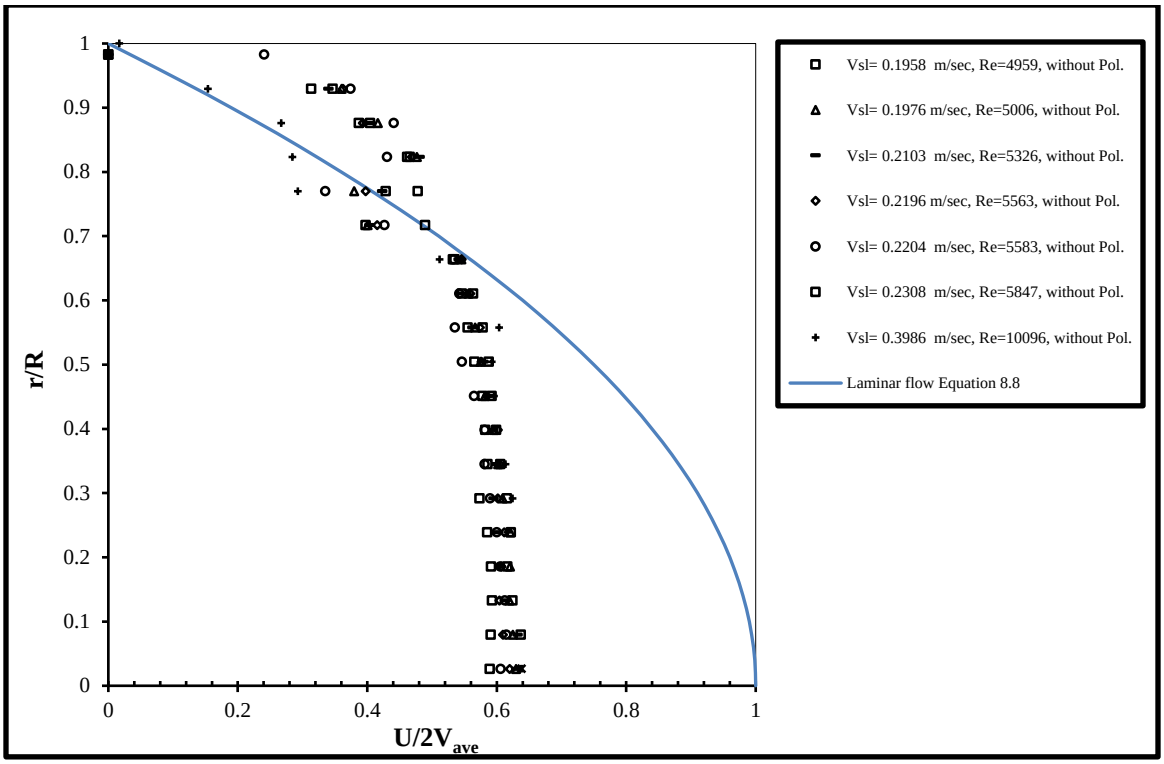

Figure 8.2 PIV results for single-phase water flow without DRP

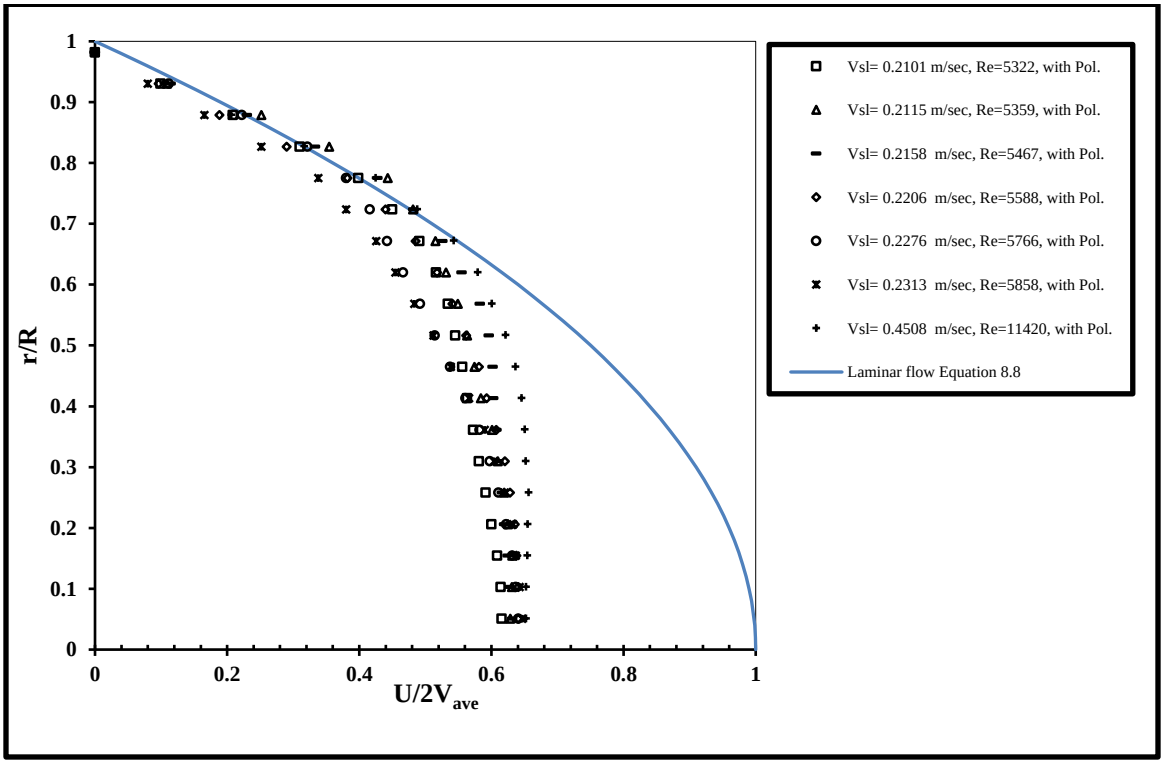

Figure 8.3 PIV results for single-phase water flow with DRP

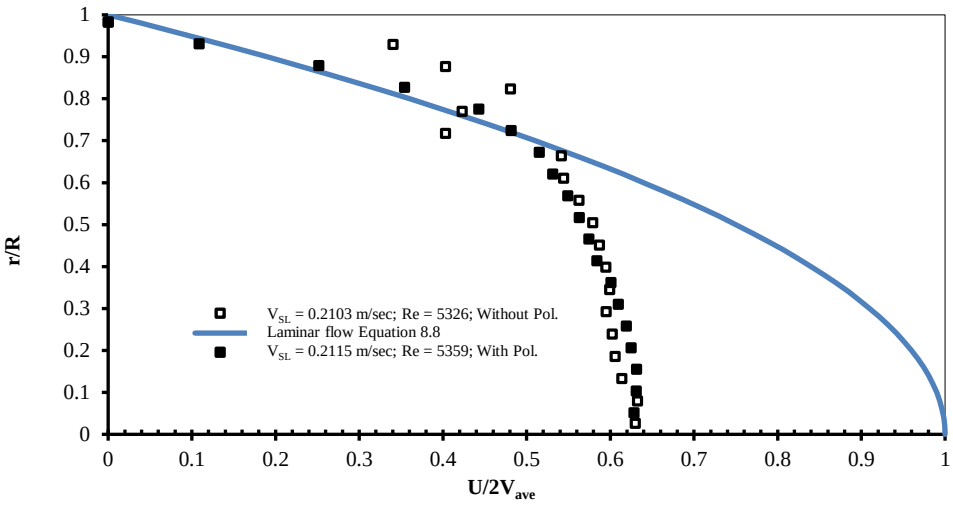

(a)

Streamlines

V_{SL}= 0.2103 m.sec^{-1}; Re=5326; Without DRP

V_{SL}= 0.2115 m.sec^{-1}; Re=5359; With DRP

(b)

Vorticity

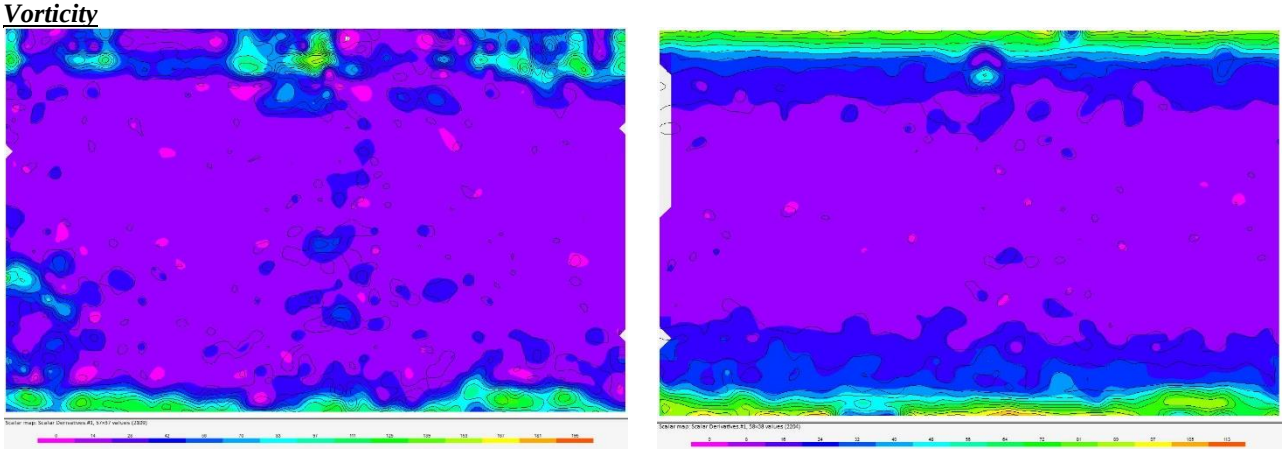

V_{SL}= 0.2103 m.sec^{-1}; Re=5326; Without DRP

V_{SL}= 0.2115 m.sec^{-1}; Re=5359; With DRP

(c)

Turbulence Intensity in Streamwise (T.I.u)

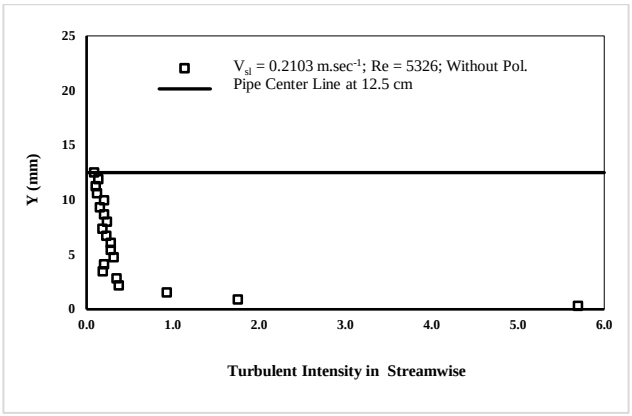

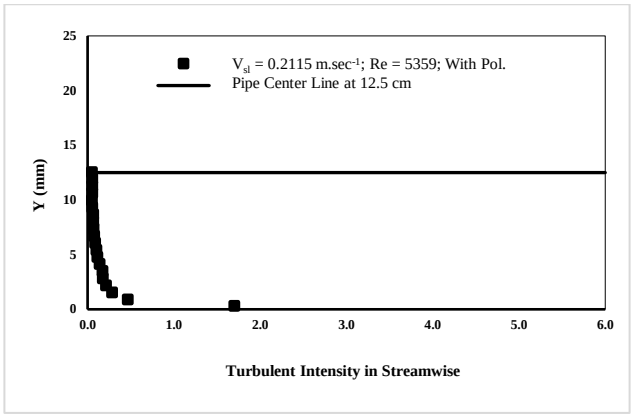

V_{SL}= 0.2103 m.sec^{-1}; Re=5326; Without DRP

V_{SL}= 0.2115 m.sec^{-1}; Re=5359; With DRP

(d)

Turbulence Intensity in Spanwise (T.I.v)

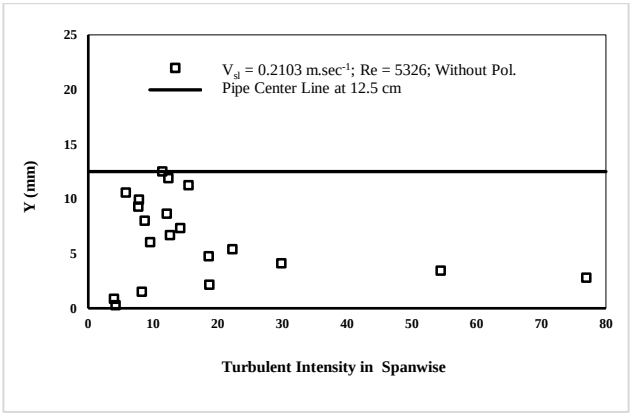

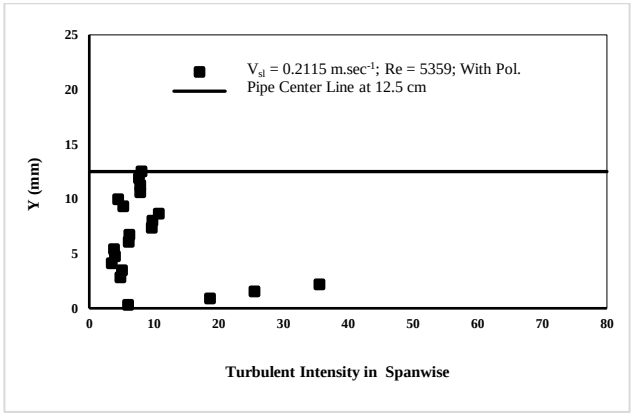

V_{SL}= 0.2103 m.sec^{-1}; Re=5326; Without DRP

V_{SL}= 0.2115 m.sec^{-1} ; Re=5359; With DRP

(e)

Figure 8.4 PIV results for single-phase water flow with and without DRP

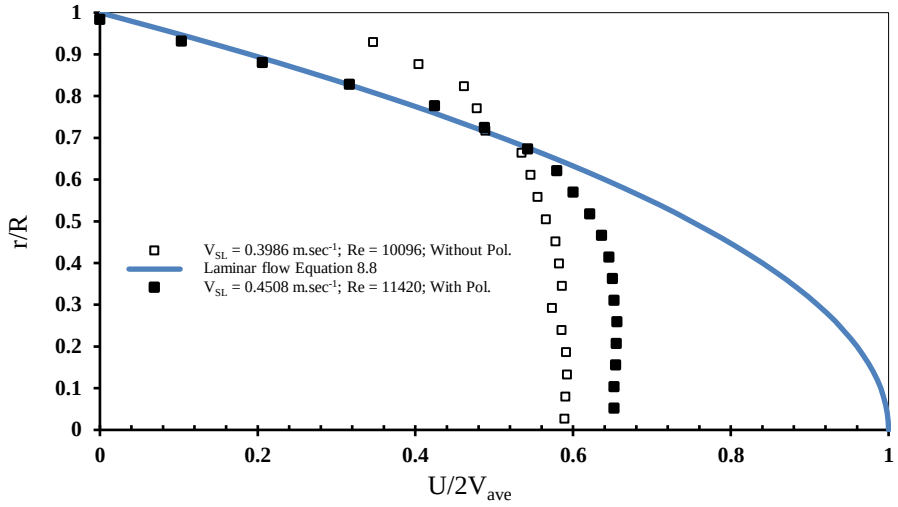

(a)

Streamlines

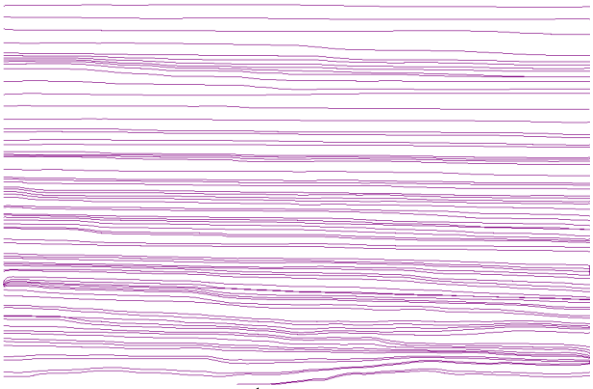

V_{SL}= 0.3986 m.sec^{-1}; Re=10096; Without DRP

V_{SL}= 0.4508 m.sec^{-1}; Re=11420; With DRP

(b)

Vorticity

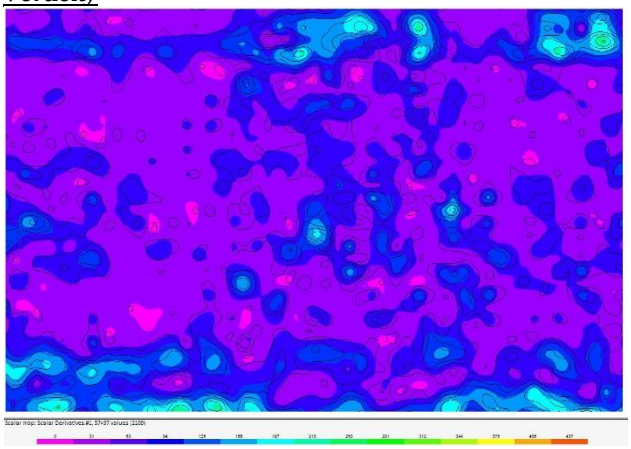

V_{SL}= 0.3986 m.sec^{-1}; Re=10096; Without DRP

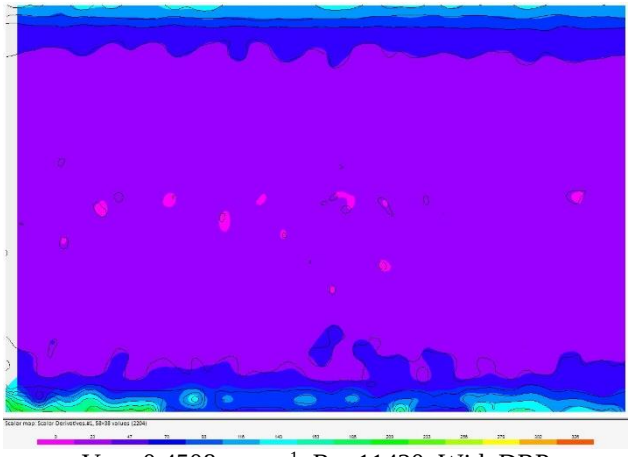

V_{SL}= 0.4508 m.sec^{-1}; Re=11420; With DRP

(c)

Turbulent Intensity in Streamwise (T.I.u)

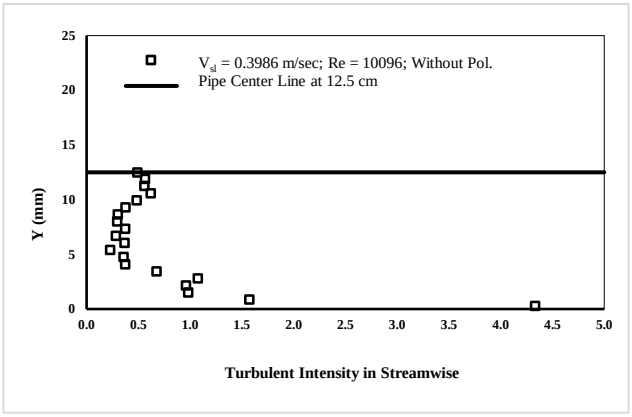

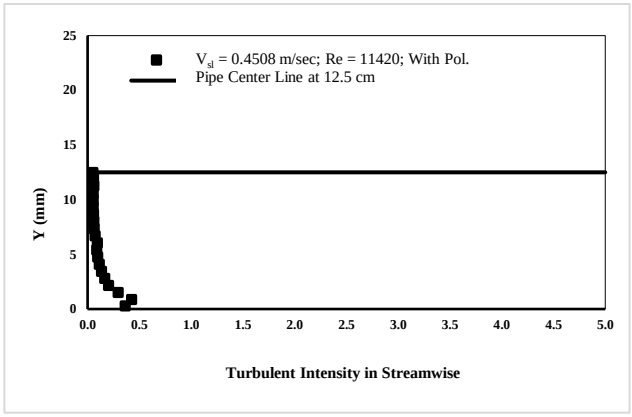

V_{SL}= 0.3986 m.sec^{-1}; Re=10096; Without DRP

V_{SL}= 0.4508 m.sec^{-1}; Re=11420; With DRP

(d)

Turbulent Intensity in Spanwise (T.I.v)

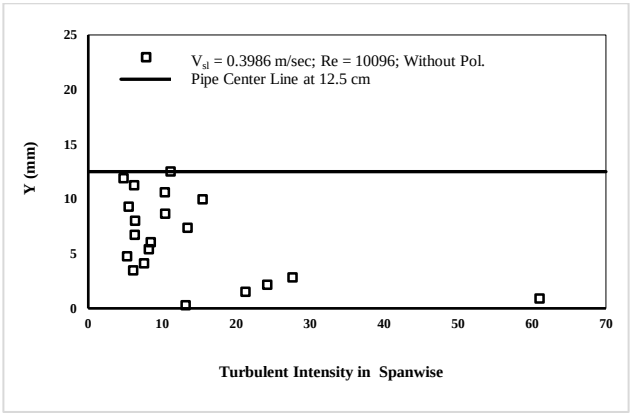

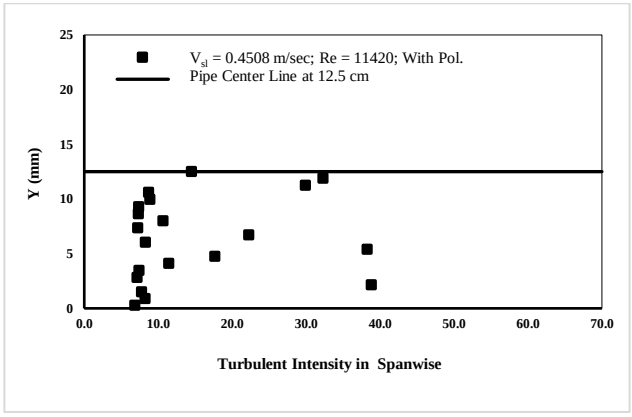

V_{SL}= 0.3986 m.sec^{-1}; Re=10096; Without DRP

V_{SL}= 0.4508 m.sec^{-1}; Re=11420; With DRP

(e)

Figure 8.5 PIV results for single-phase water flow with and without DRP.

8.3.2 Comparisons between FLUENT Software and PIV for single-Phase Water Flow

For further verification of the powerful of PIV technique in obtaining the velocity profile, the experimental data obtained by the aforementioned technique was compared with the FLUENT software results. A computational fluid dynamic (CFD) software package (FLUENT) was used to numerically predict the velocity distribution. This software was used to illustrate the solution of a 2D turbulent and laminar single-phase water flow. As shown in Figure 8.6, the flow inside a pipe of diameter 25 mm and a length of 5 m. The velocity profile has been examined towards the end of the 5 m pipe, which satisfied the entrance length theory, in order to get the fully developed flow. Due to symmetry, only half portion of the pipe was modeled.

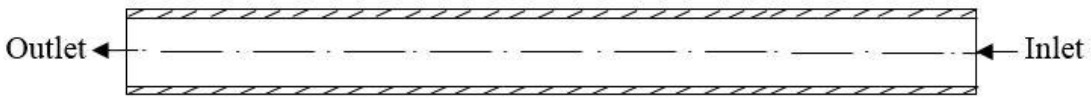

Figure 8.6 Transparent part of the pipe test section

A number of assumptions had been taken in order to be able to solve the governing equation, namely continuity, momentum, and energy equations. The assumptions used to derive the aforementioned equations are; steady flow, Newtonian fluid, incompressible fluid flow, and constant transport properties of fluid. The single-phase water flow was solved in FLUENT using Pressure based solver. Laminar and K-epsilon (2-equations) were selected for laminar and turbulent cases, respectively. The water properties have

been inserted in the FLUENT software according to Table 3.1. The solution methods selected to carry out the CFD calculation are the SIMPLE scheme for pressure-velocity coupling and second order upwind algorithm for momentum and turbulent equations.

Computations were performed assuming laminar flow even though the Re is in the turbulent regions. This assumption was made as an attempt to compare the flow with DRP to a turbulent flow free of turbulence. In Figures 8.7 up to 8.13, the agreement between the experimental data and the CFD prediction was found to be significant in most of the cases. The velocity profile comparisons for the turbulent flow shows that the velocities obtained from the simulation matched with the experimental data taken in the absence of DRP. However, the deviation between the computational and measured velocity profiles in the absence of DRP is shown in Table 8.1. In addition, these figures show the effect of existing DRP in the turbulent flow. It is clearly shown that, the existence of DRP helps in minimizing the chaotic behavior of the turbulent flow, which in turn rearrange the streamlines and boosting the average flow velocity. In fact, the new trend of the turbulent velocity profile in the presence of DRP urges us to compare it with the laminar-CFD predictions. An unmatched data obtained between experimental and simulation in the middle region of the pipe for all of the cases. But, in the region near the pipe wall, an agreement was found in some of the cases. The agreement in the results in this region can be attributed to the ability of DRP in increasing the laminar sub-layer near the pipe wall. As a result, the comparison between PIV and FLUENT software supports the revisited DRP mechanism.

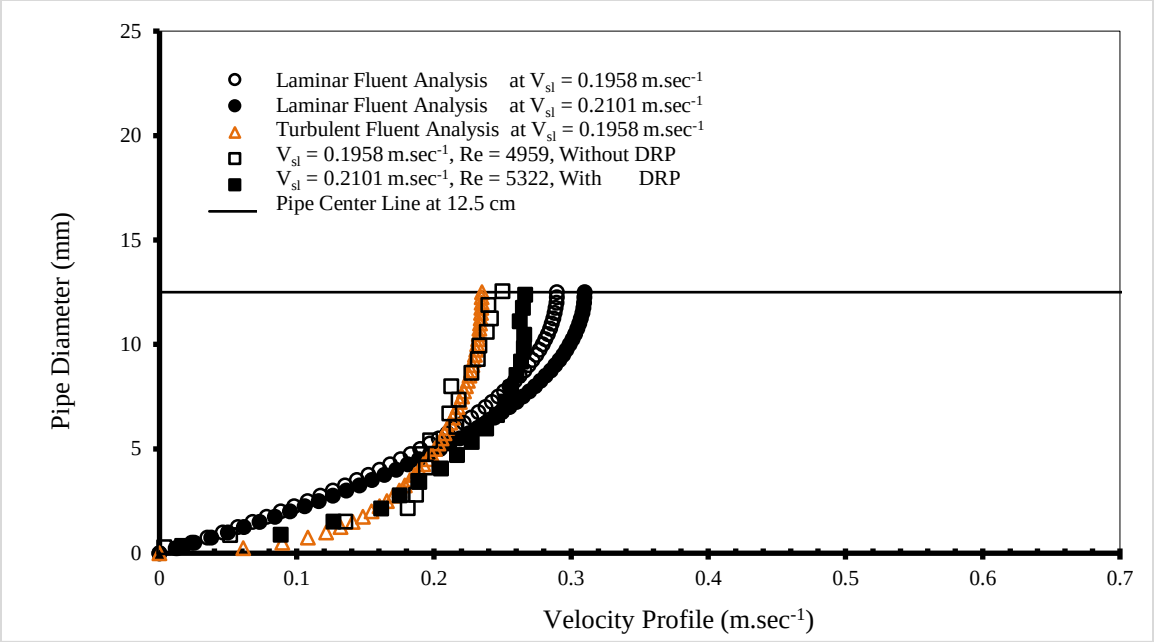

Figure 8.7 Comparison between Fluent Software and PIV results for single-phase water flow (PIV results show the effect of adding 116-ppm of DRP).

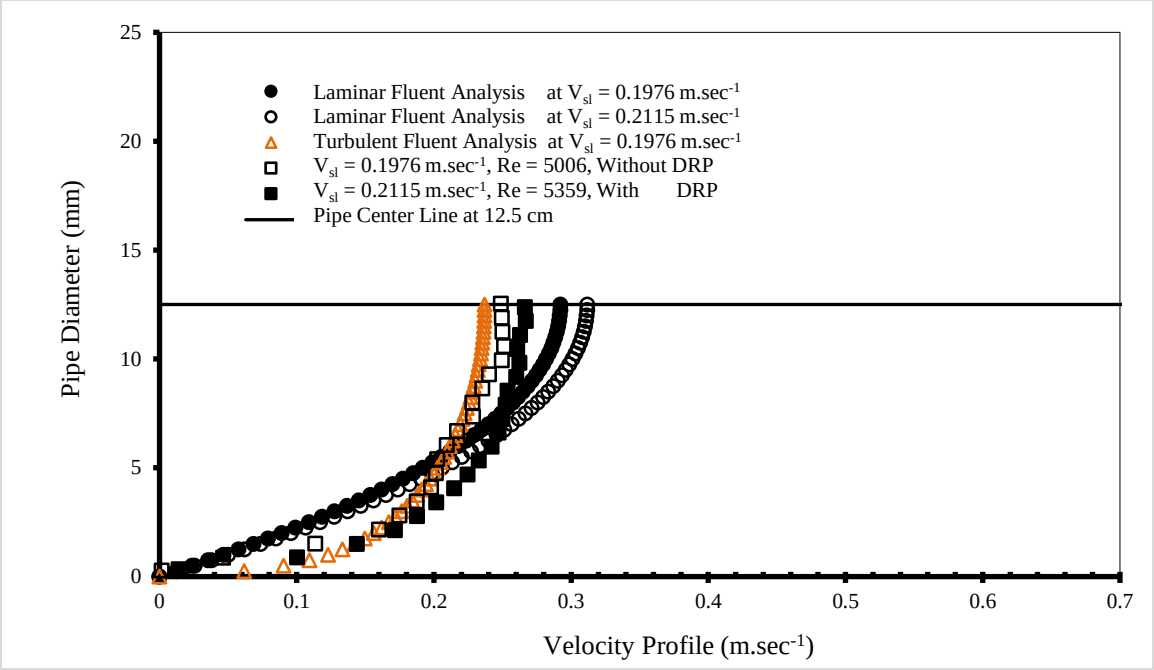

Figure 8.8 Comparison between Fluent Software and PIV results for single-phase water flow (PIV results show the effect of adding 115-ppm of DRP).

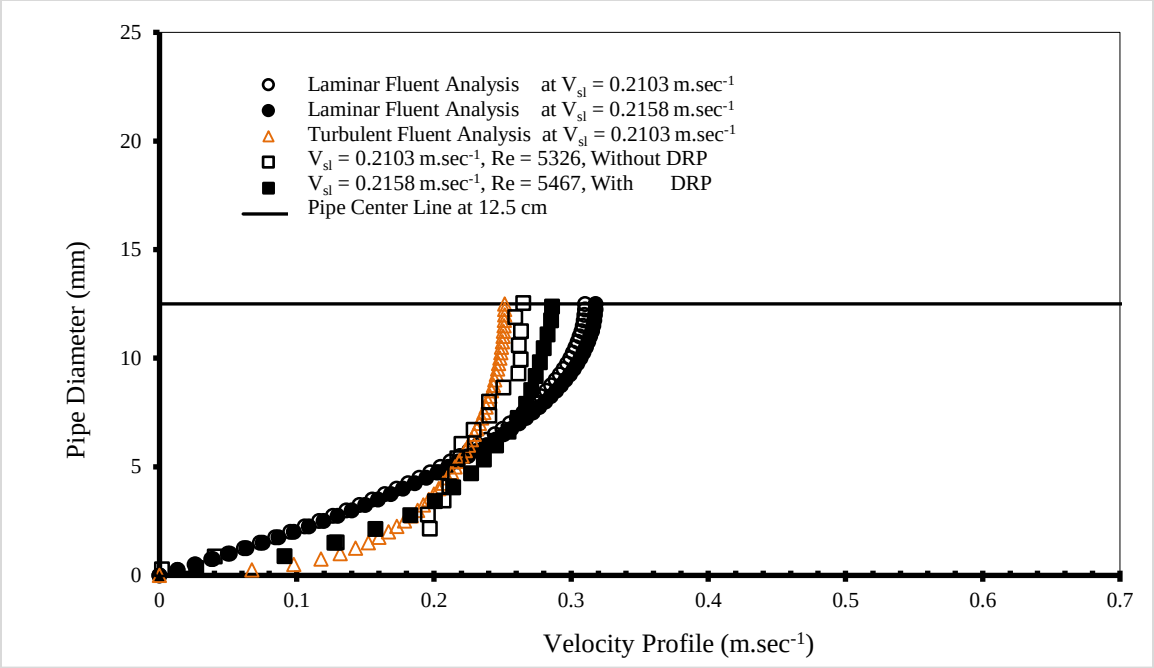

Figure 8.9 Comparison between Fluent Software and PIV results for single-phase water flow. (PIV results show the effect of adding 113-ppm of DRP).

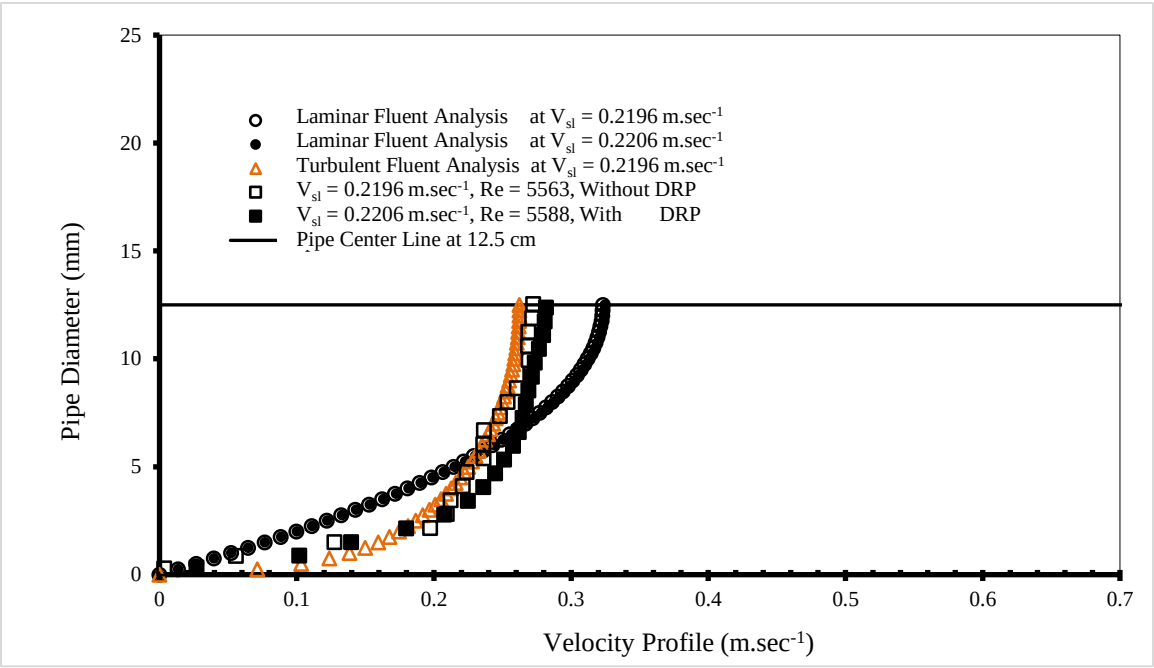

Figure 8.10 Comparison between Fluent Software and PIV results for single-phase water flow. (PIV results show the effect of adding 110-ppm of DRP).

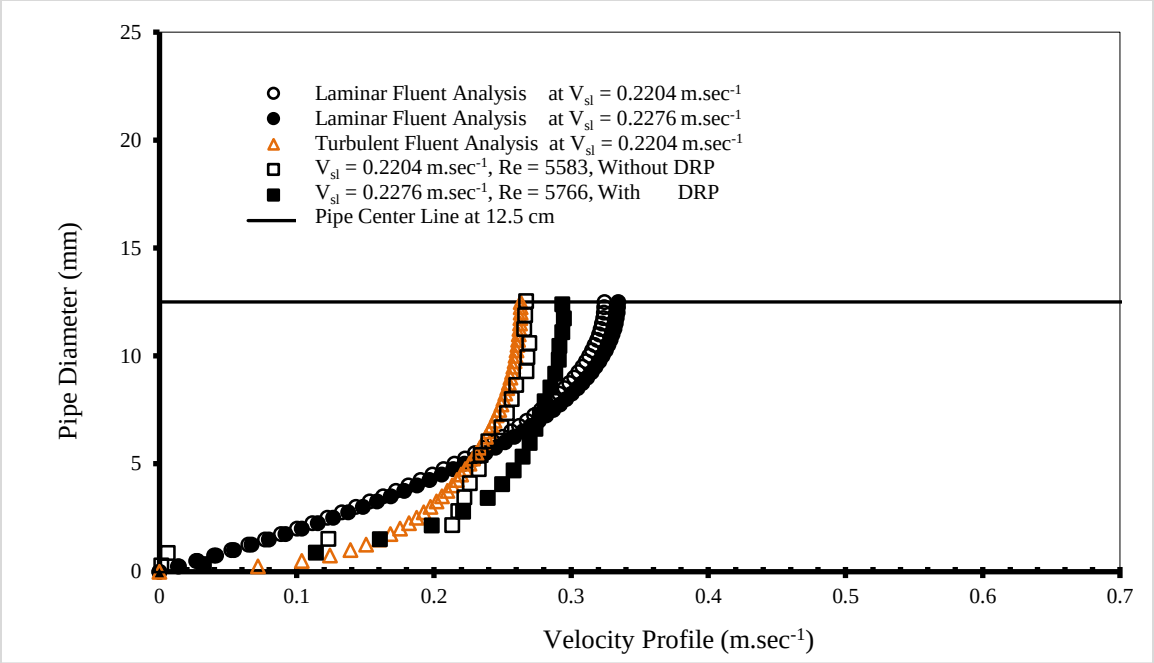

Figure 8.11 Comparison between Fluent Software and PIV results for single-phase water flow. (PIV results show the effect of adding 107-ppm of DRP).

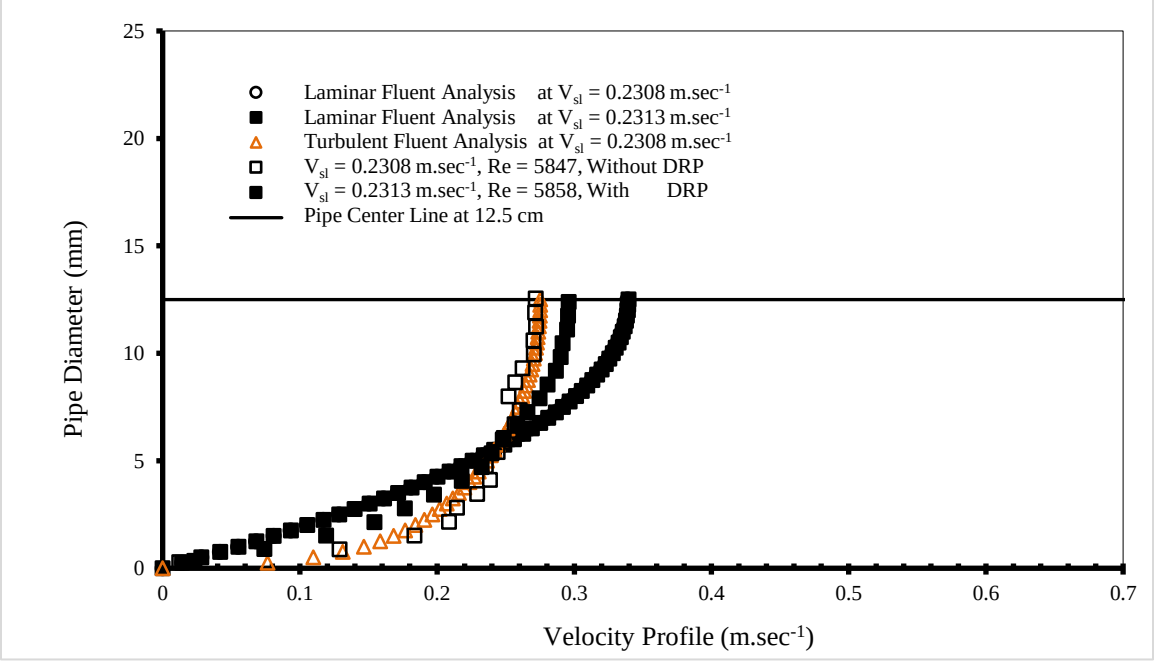

Figure 8.12 Comparison between Fluent Software and PIV results for single-phase water flow (PIV results show the effect of adding 86-ppm of DRP).

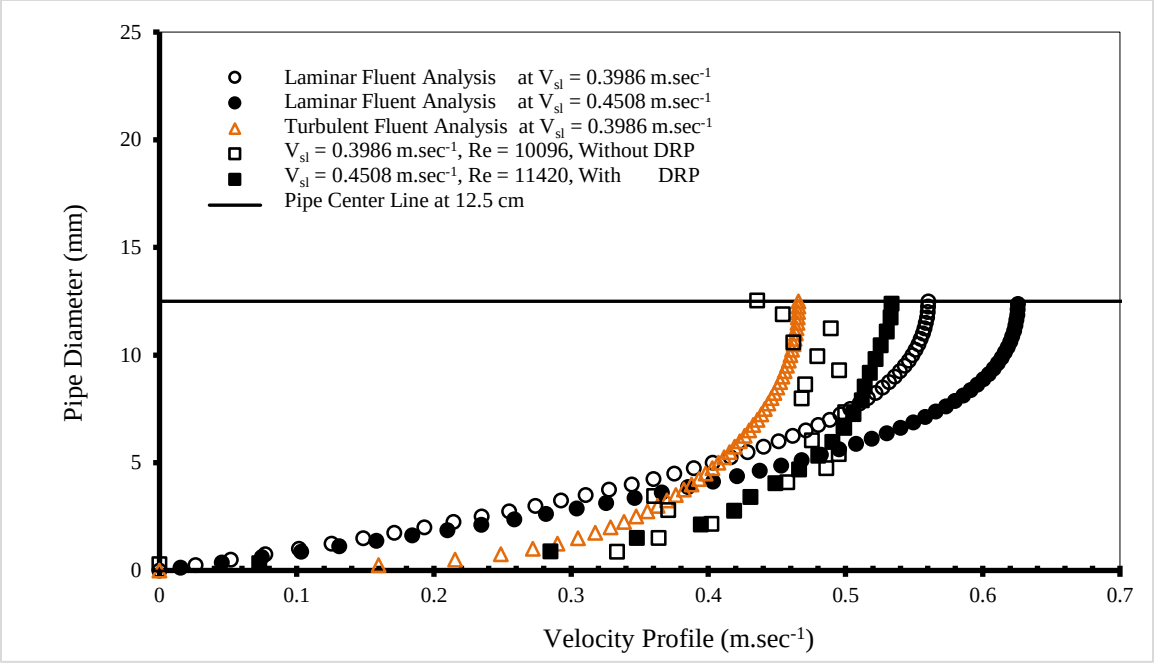

Figure 8.13 Comparison between Fluent Software and PIV results for single-phase water flow (PIV results show the effect of adding 54-ppm of DRP).

Table 8.1 Deviation between the computational and measured velocity profile in the absence of DRP

Figure No.	Mean absolute Percent Error (MAPE)
Figure 8.7	2.333
Figure 8.8	2.296
Figure 8.9	3.187
Figure 8.10	2.368
Figure 8.11	3.465
Figure 8.12	2.569
Figure 8.13	7.877
Over all	3.441

8.3.3 Experimental Investigation for Two-Phase Air-Water Flow by Using PIV Technique

For the case of two-phase air-water, the studied flow pattern was wavy stratified flow. As shown in Figure 8.14, almost half of the pipe was filled with water and the other half was occupied by air. The water phase was mixed gently with seeding particles to be able to capture the flow characteristics in the absence and presence of the DRP. Figures 8.14 and 8.15a revealed that the addition of (13, 45, 101, 127, 175) ppm of DRP to air-water wavy stratified flow had a spectacular effect on the region between water and the pipe wall, and on the interfacial region between air and water. In general, the average velocity close to the wall in the liquid region of the flow with DRP is larger than the average velocity for the flow without DRP. In contrary, the average velocity for the flow without DRP close to the gas-liquid interface is larger than that for the flow with DRP. The explanation of this phenomenon can be related to the ability of DRP to reduce the Reynolds shear stresses and wall-normal velocity fluctuations. In fact, turbulent bursts interact with the coiled DRP molecules in such a way that they are stretched, and absorb or dissipate the energy, which yield in reducing the momentum transfer. On the other hand, The air-water interface is smoothened by DRP (Figure 8.15b). DRP affects the flow patterns by damping the high amplitude waves and reducing the turbulence activities which control the waves and droplets formation mechanism. Thus, after injecting the DRP, the flow pattern was changed from stratified wavy to smooth stratified. As a result, adding DRP to the air-water flow changes the mean velocity profile. Figure 8.16 shows the effect of DRP on the percentage drag reduction. DRP molecules can change the flow structure in

turbulent flow which result in reduction the drag on the boundaries. The reduction of the drag about 42% was realized for DRP concentration of 175 ppm.

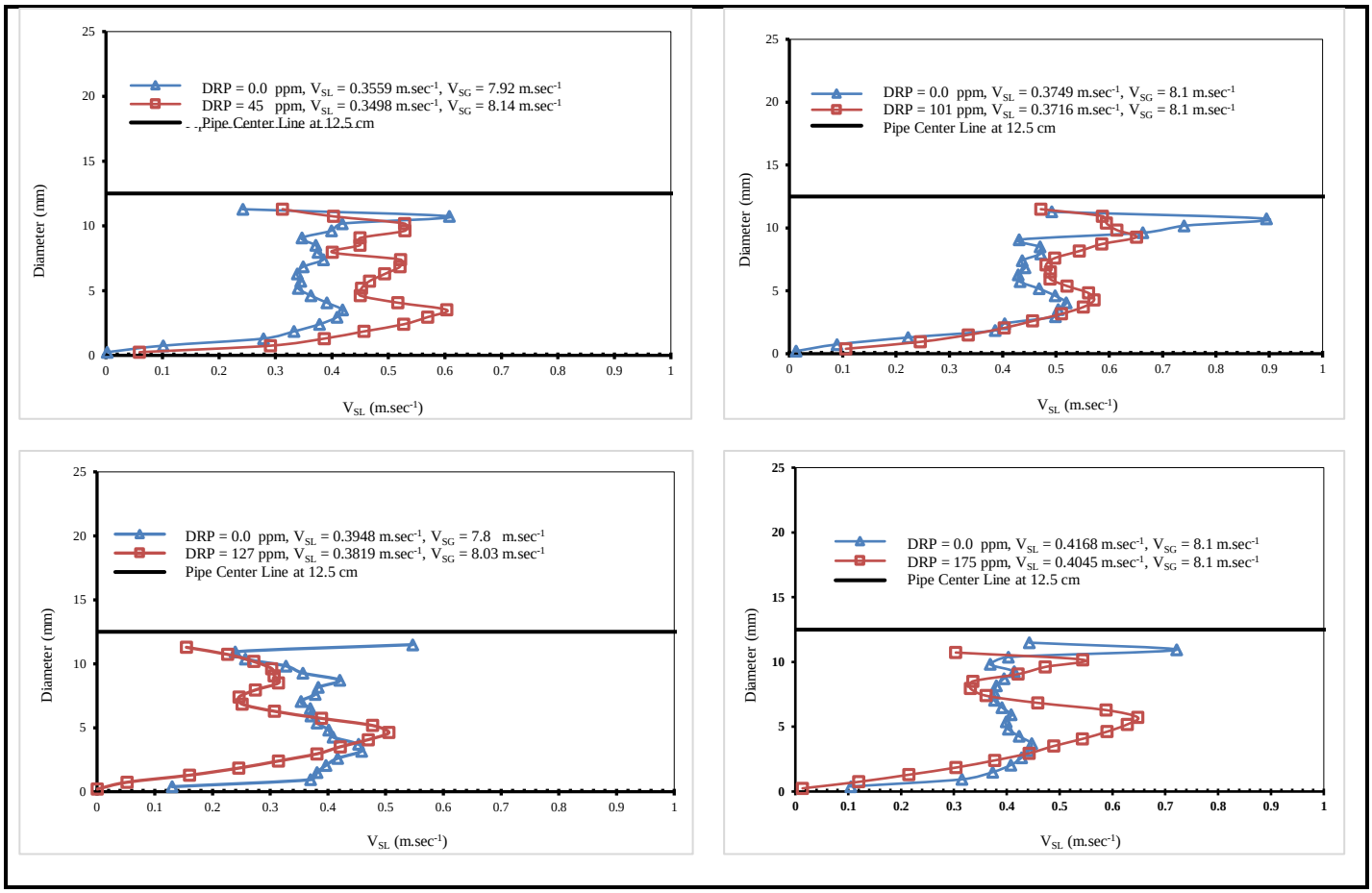

Figure 8.14 PIV results for two-phase water flow with and without DRP

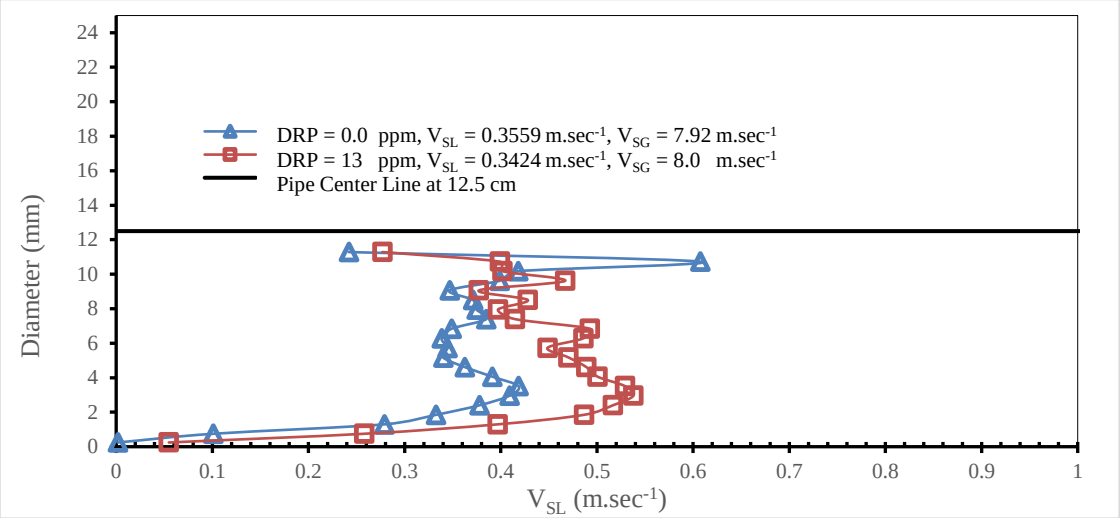

(a)

Streamlines

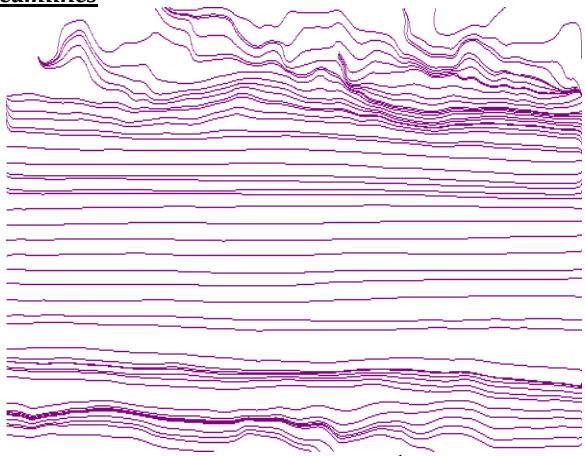

Pol.=0.0 ppm, V_{SL}= 0.3559 m.sec^{-1}, V_{SG}=7.92 m.sec^{-1}

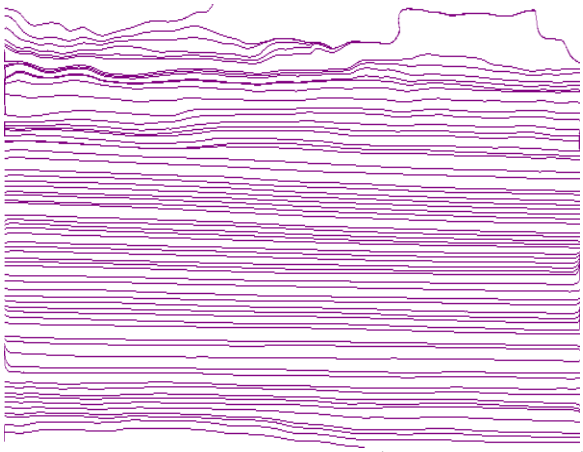

Pol.=13 ppm, V_{SL}= 0.3424 m.sec^{-1}, V_{SG}=8.00 m.sec^{-1}

(b)

Vorticity

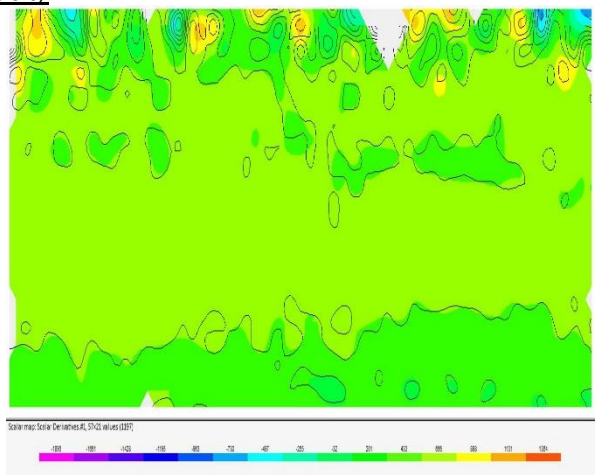

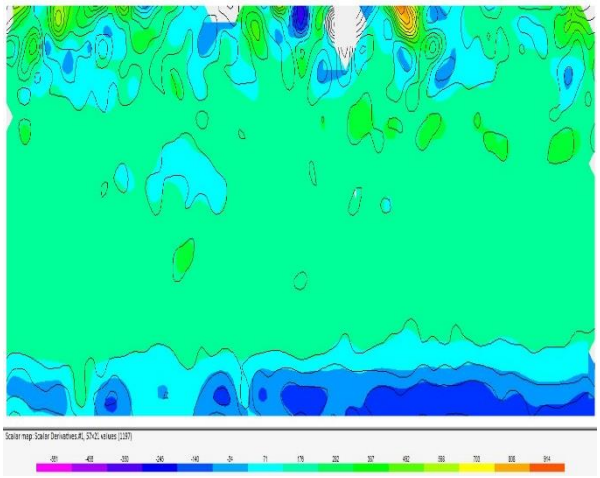

(c)

Turbulent Intensity in Streamwise (T.I.u)

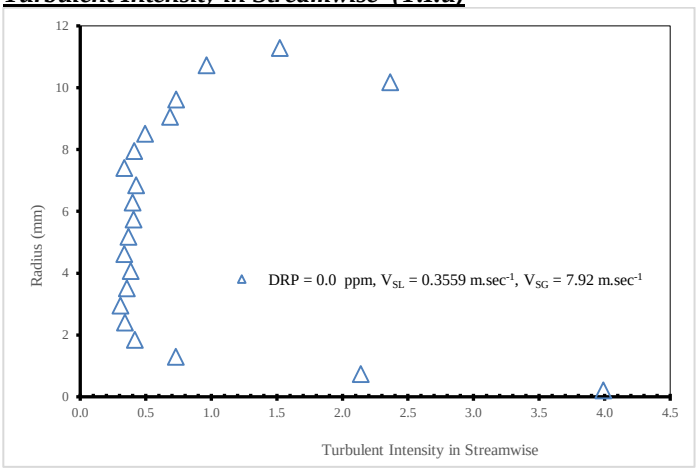

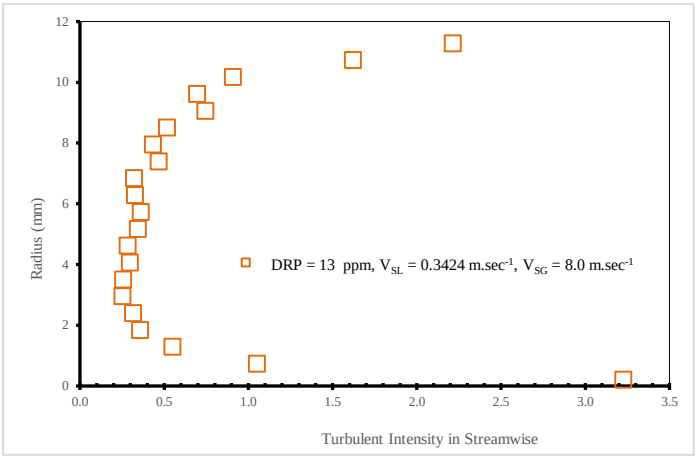

(d)

Turbulent Intensity in Spanwise (T.I.v)

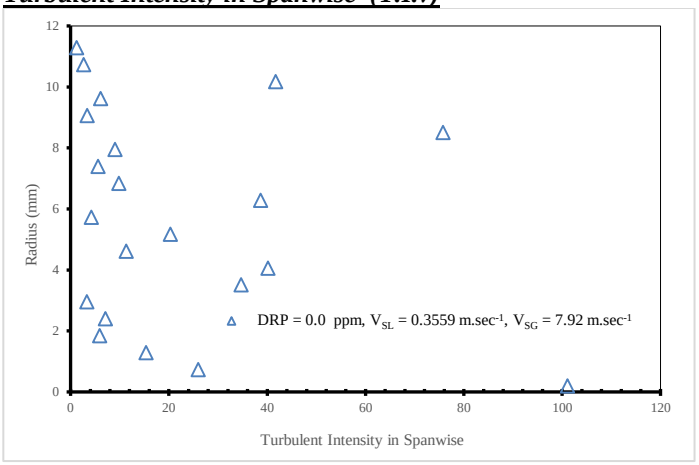

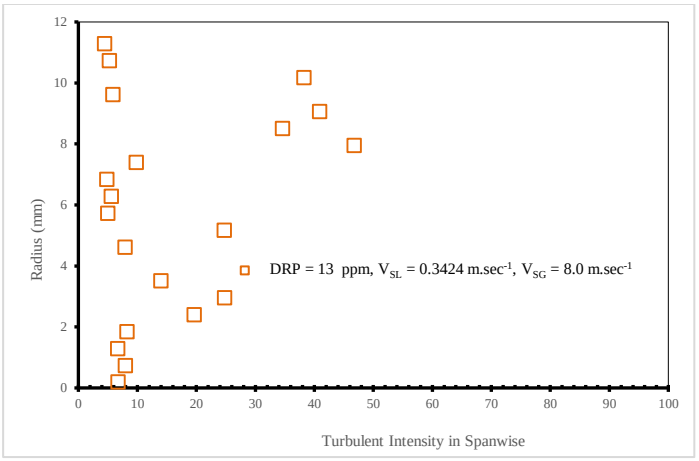

(e)

Figure 8.15 PIV results for two-phase water flow with and without DRP

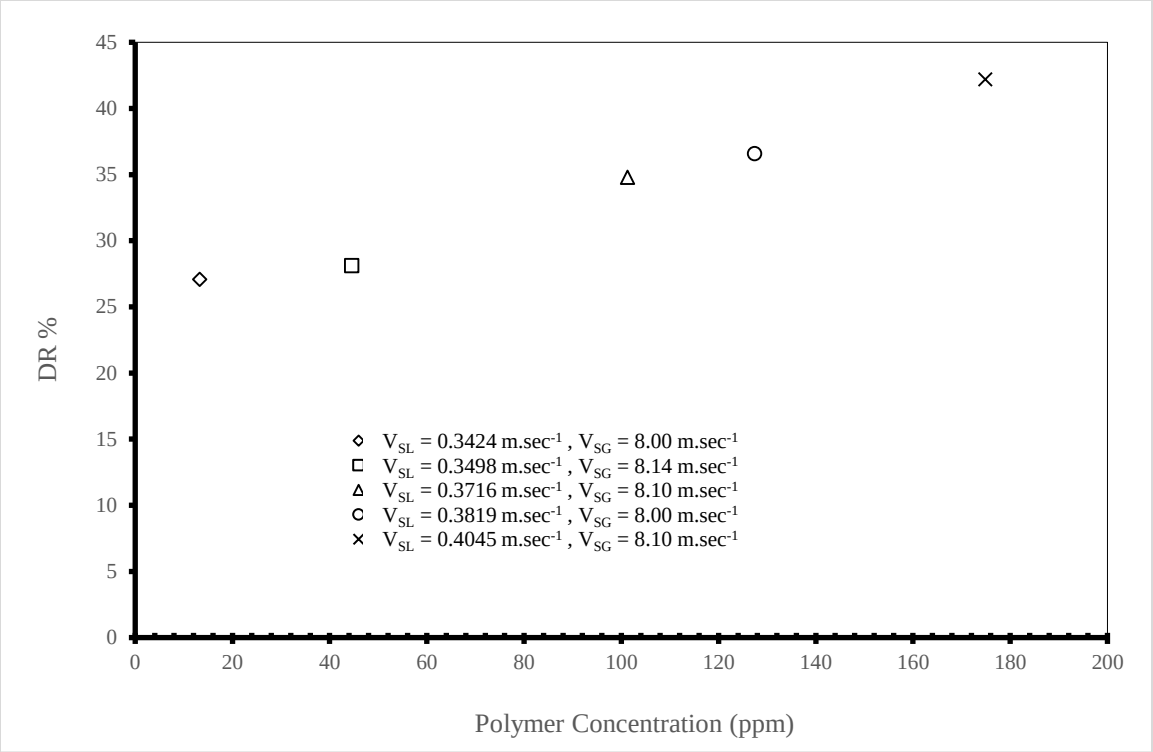

Figure 8.16 Percentage drag reduction versus polymer concentration (water-soluble DRP) for air-water flow. ◇ Re_{SL} = 7703, Re_{SG} = 11998; □ (Re_{SL} = 7973, Re_{SG} = 12213); △ (Re_{SL} = 8471, Re_{SG} = 12137); ○ (Re_{SL} = 8706, Re_{SG} = 11998); X (Re_{SL} = 9221, Re_{SG} = 12137).

8.4 Conclusion

This chapter showed that a sophisticated PIV set-up used to determine instantaneous flow velocities and streamline in the absence and presence of water-soluble DRP for single-phase and two-phase flow with the aid of PCC and Dantec Dynamic studios. Using PIV technique helped in understanding the mechanism of DRP specially when it compared with the FLUENT software.

One of noticeable phenomenological behavior of DRP is the ability to change the structure of single-phase turbulent water flow by eliminating the turbulent bursts and eddies which results in increasing the laminar layer near the pipe wall. This enhancement in the flow characteristics has an impact on the velocity profile as well.

A comparison between the PIV results and FLUENT software revealed that an agreement in the region near pipe wall was observed. Also, it was found that the DRP acts to destroy the turbulent disturbances waves which results in smoothing the air-water interface, and convert the flow pattern from wavy stratified to smoothed stratified flow. As a result, the comparison between PIV and FLUENT software support the revisited DRP mechanism.

Another deliverable results of this chapter indicates that an increase in DRP concentrations results in an increase in drag reduction up to 45% in single-phase water flow and up to 42% in air-water stratified flow.

CHAPTER 9

CONCLUSIONS AND RECOMMENDATIONS

The uniqueness of the present work is in the existing arrangement of using oil and water soluble DRPs in single, two and three-phase flow experiments in the same flow loop and similar conditions. The results of the present work shed the light on the challenging problem for selection the proper type of DRPs specially for three-phase flows, in addition to other valuable findings.

This chapter highlighted the precious findings based on the experimental outcomes and the analyzed data. Consequently, recommendations are outlined to cover more cases, enhance the quality of the data, and to extend the scope of the research.

9.1 Influence of DRPs on Frictional Pressure Drop

9.1.1 Single-Phase Oil and Water Flow

The influence of water-soluble and oil-soluble DRPs in single-phase water and oil flows have been presented for in a 22.5 mm ID and 8.33 m long PVC horizontal pipe.

For the case of water-soluble DRP, maximum drag reduction of 76% occurred at relatively high Reynolds number (35,522). It had been observed that the addition of water-soluble DRP clearly minimized the effect of turbulence activity, and decreased the pressure gradient and increased the %DR. Moreover, the increment in %DR with increasing DRP concentration was positive. However, no more reduction occurred above a critical concentration. Therefore, for the water-soluble DRP in single-phase water flow, the critical (effective) concentration obtained is 64 ppm.

For the case of oil-soluble DRP, at maximum oil-soluble DRP flow rate the percent drag reduction of 35 occurred at relatively high Reynolds number (13,934). But at relatively low Reynolds number (3,612), the drag reduction was 79%.

A comparison between single-phase water and oil flows, in the presence of ZETAG® 8165 (polar) and PIB (nonpolar) DRPs, respectively, based on the effect of Reynolds number on %DR was performed. Two different trends were observed. For the water flow, %DR initially increased with the increase in Re_{SL}; then it asymptotically flattened. On the contrary, for the oil flow, it sharply decreased in an approximately linear fashion.

9.1.2 Two-Phase Air-Oil and Air-Water Flow

The influence of water-soluble and oil-soluble DRPs in two-phase air-oil and air-water flows have been presented for in a 22.5 mm I.D. and 8.33 m long PVC horizontal pipe.

For the case of two-phase air-water flow, the %DR versus DRP dosage (ppm), with respect to constant values of Q_{liquid} and Q_{air}, varied showing a common trend. %DR initially increased rapidly up to a critical DRP concentration of 64 ppm. Beyond this value, it became asymptotic, showing insignificant influence of DRP dosage on %DR. This particular finding, exhibited in the presence of air, matches the single-phase %DR versus DRP dosage relation. Consequently, this means that the introduction of air did not transpose the fundamental relation between %DR and DRP dosage. Another two cases illustrate the %DR behavior for the two-phase air-water flow versus the Reynolds number based on superficial gas velocity Re_{SG}. The %DR, at maximum dosage of DRP of 190 ppm and at constant liquid flow rate (Q_{liquid} = 0.019 $m^3.min^{-1}$) was performed first. Same experiment was repeated again but with lower dosage of DRP of 4.2 ppm. At both cases, the %DR decreased with the increase of Re_{SG}. Therefore, the increase in the intensity of turbulence and the associated mixing decreased %DR in ZETAG® 8165-mediated air-water flow. The above DRP dosages showed to be unable to dampen the growth of eddy population with increasing Q_{air}. Nevertheless, at dosage of 4.2 ppm the effects are more pronounced, which, to the best of our knowledge, has not been reported in the literature. The comparison between the two dosages results shows that the drag reduction performance by water-soluble ZETAG®8165 at a low concentration (4.2 ppm) well exceeded that at a high concentration (190 ppm). This finding can be ascribed to the

change in DRP external environment, that is, flow pattern, polarity, and phase morphology that surrounded the DRP molecules. As demonstrated earlier in chapter 6, Figure 6.4. Water (a single-component fluid) and ZETAG® 8165 are both polar. Therefore, here air interacted with a continuum of polar fluid. Another important observation was illustrated in Figures 6.2B and 6.6. In these figures same dosages of water-soluble DRP of 190 ppm used. The only difference is the liquid flow rates Q_{liquid} = 0.019 $m^3.min^{-1}$ and Q_{liquid} = 0.009 $m^3.min^{-1}$ as demonstrated in Figures 6.2B and 6.6, respectively. It has been observed contrary trends of %DR versus Re_{SG}. This can be explained as follows. At lower liquid flow rate the 190 ppm DRP dosage showed to be able to dampen the growth of eddy population with increasing Re_{SG}. While, higher liquid flow rate affected the DRP capacity for damping the turbulent eddies. Accordingly, the %DR varied.

For the case of two-phase air-oil flow, the %DR behavior versus Reynolds number based on superficial gas velocity Re_{SG} was illustrated. See Figure 6.5B. The %DR, at constant dosage of DRP of 184 ppm and at constant liquid flow rate (Q_{liquid} = 0.0106 $m^3.min^{-1}$), decreased with the increase of Re_{SG}. These air-oil flow findings qualitatively match those of air-water flow. See Figures 6.2B and 6.3B, respectively. It can be concluded that the role played by the applied DRP (polar or nonpolar) and air on the continuum of fluid (polar or nonpolar) essentially remains the same.

9.1.3 Three-Phase Air-Oil-Water Flow

The influence of water-soluble and oil-soluble DRPs in three-phase air-oil-water flow have been presented for in a 22.5 mm I.D. and 8.33 m long PVC horizontal pipe.

For the case of injecting water-soluble DRP in three-phase air-oil-water flow, the investigation revealed that the water-soluble DRP ZETAG® 8165 even at a lower concentration showed much higher %DR at a higher mixture velocity Q_{liquid}. In fact, the main source of drag reduction was the existence of water-soluble DRP in the water layer, which was governed by wall shear stress reduction and interfacial shear reduction between phases. It can be concluded that DRP ZETAG® 8165 is able to absorb the turbulence activity at the phases interface and near the pipe wall.

For the case of injecting oil-soluble DRP in three-phase air-oil-water flow, the results show that the %DR fairly coincided with a common trend line and decreased with the increase of Re_{SG}. This is an interesting result; it is supported by the findings of the two-phase air-water and air-oil flows in Figures 6.2B, 6.3B, and 6.5B. In fact, the increments in Re_{SG} generated a larger amplitude of roll waves. These waves increased the air-oil interface, oil-water interface and wall stresses, which reduced the existing %DR.

The final result concluded from the comparisons in case of single-phase, two-phase, and three-phase, the water-soluble DRP ZETAG® 8165, because of structural difference, can dampen the turbulent eddies, decrease the interfaces roughness, and resist wall stresses much better than the oil-soluble DRP PIB.

9.2 Influence of DRPs in Flow Pattern

Slug and annular flow regimes were considered in case of two- and three-phase flow in a 22.5 mm I.D. and 8.33 m long PVC horizontal pipe. The DRPs injected into the two- and three-phase fluids changed the flow patterns except for flows at very high Reynolds number based on superficial gas velocity Re_{SG}. Visual observations revealed that both DRPs delayed the transition from low to high frequency slug flow and the appearance of annular flow.

The DRPs, depending on the slug flow frequency, altered the numbers of slugs SN that passed the transparent part of the test section. At a very high V_{SG} and in the presence of water-soluble DRP, an annular flow changed to a high frequency slug flow (SHF). However, for the oil-soluble DRP, the flow pattern did not change.

9.3 DRP Mechanism

A new insight into the conventional drag-reducing mechanism have been reported in this study. Drag reduction depends on the following factors. One is the DRP state that includes: the hydrodynamic size of the DRP molecules, dictated by the extent of uncoiling; and the chemical structure of the DRP (polar versus nonpolar, homo- versus copolymer, etc.), its molecular weight, and backbone stability. The other factor is DRP external environment that comprises: the fluid flow pattern, polarity, and phase morphology that surround the DRP molecules; and the intensity of turbulence and the associated mixing phenomena. The resultant interaction of the above two factors affect the capacity for dampening the turbulent eddies, streamlining the velocity field, and eventually increasing the thickness of viscous laminar sublayer.

9.4 Influence of DRPs in Flow Throughput

According to Appendix C, the effect of DRPs on flow throughput can be attained by examining the results obtained from performing energy analysis in terms of the head loss, and savings in energy consumption.

The influence of injecting water-soluble and oil-soluble DRPs in a 22.5 mm ID and 8.33 m long PVC horizontal pipe was tested. The results showed that there were drastic reductions in the head losses, and a huge savings in the energy consumptions. A comparison between single-phase water flow with water-soluble DRP and single-phase oil flow with oil-soluble DRP was performed. It was shown that the ability of water-soluble DRP is higher than the oil-soluble DRP in decreasing the head loss and increasing the percentage saving in energy consumption. Moreover, two-phase air-water and air-oil flows were investigated and confirm the previous result that the water-soluble DRP is much more effective than oil-soluble DRP in terms of decreasing the head loss and percentage saving in energy consumption. Also, significant reduction in the head loss and substantial saving in the energy consumption were obtained in the case of three-phase air-oil-water flow with water-soluble DRP.

9.5 Influence of Pipe Diameters and material on the performance of water-soluble DRP

According to Appendix C, results of two experiments have been presented for the case of two-phase air-water in presence of water-soluble DRP flow in two different pipe diameters and pipe materials. Energy analysis was chosen to compare between these two cases. The results shown that the reduction in savings in energy consumption were more effective in the pipe has smaller diameter and rougher surface. While, the reduction in head loss was more pronounced in larger pipe diameter which has smoother surface.

9.6 Recommendations

The following recommendations are suggested based on the results demonstrated in this dissertation. These suggestions would improve the variety of the obtained data and extend the scope of the research area:

a. It has been noticed while performing the experiments especially at high flow rates that the readings obtained from flow meter sensors and pressure sensor are fluctuating a little. This fluctuation due to pipe vibration. So, well mounted piping flow loop and enhancement the stability are required.
b. There is a need to Install higher power pumps in the flow loop to insure the coverage of all flow patterns. Then, all studied parameters in this dissertation can be revisited again.
c. A Modifications in PIV setup are needed as well. Time box and synchronizer may be added to get more accurate recordings.
d. Many other parameters can be studied to examine the DRPs performance such as; effect of temperature variation, effect of using different molecular weights, effect of heat transfer characteristics, effect of pipe inclination angle…etc.
e. Correlate the microstructures of DRPs such as tacticity, copolymer composition distribution, etc. to the corresponding %DR performance.
f. Study the %DR performance from the perspective of turbulent mixing models and theories.
g. Relate the DRP hydrodynamic radius to the scale of turbulence and DRP performance.

References

Abdulmouti, H. and Jassim, E., 2013. Visualization and Measurements of Bubbly Two-Phase Flow Structure Using Particle Imaging Velocimetry (PIV).European Scientific Journal, 9(21).

Açikgöz, M., Franca, F. and Lahey, R.T., 1992. An experimental study of three-phase flow regimes. International Journal of Multiphase Flow, 18(3), pp.327-336.

Ahmed, W.H. and Ismail, B.I., 2008. Innovative techniques for two-phase flow measurements. Recent Patents on Electrical & Electronic Engineering (Formerly Recent Patents on Electrical Engineering), 1(1), pp.1-13.

Abubakar, A., Al-Wahaibi, T., Al-Wahaibi, Y., Al-Hashmi, A.R. and Al-Ajmi, A., 2014. Roles of drag reducing polymers in single-and multi-phase flows. Chemical Engineering Research and Design, 92(11), pp.2153-2181.

Al-Sarkhi, A. and Soleimani, A., 2004. Effect of drag reducing polymers on two-phase gas–liquid flows in a horizontal pipe. Chemical Engineering Research and Design, 82(12), pp.1583-1588.

Al-Sarkhi, A. and Hanratty, T.J., 2001. Effect of drag-reducing polymers on annular gas–liquid flow in a horizontal pipe. International Journal of Multiphase Flow, 27(7), pp.1151-1162.

Al-Sarkhi, A. and Hanratty, T.J., 2001. Effect of pipe diameter on the performance of drag-reducing polymers in annular gas-liquid flows. Chemical Engineering Research and Design, 79(4), pp.402-408.

Al-Sarkhi, A. and Abu-Nada, E., 2005, May. Effect of drag reducing polymer on annular flow patterns of air and water in a small horizontal pipeline. In 12th international conference on multiphase production technology, Barcelona, Spain.

Al-Sarkhi, A., Abu-Nada, E. and Batayneh, M., 2006. Effect of drag reducing polymer on air–water annular flow in an inclined pipe. International journal of multiphase flow, 32(8), pp.926-934.

Al-Sarkhi, A., El Nakla, M. and Ahmed, W.H., 2011. Friction factor correlations for gas–liquid/liquid–liquid flows with drag-reducing polymers in horizontal pipes. International Journal of Multiphase Flow, 37(5), pp.501-506.

Al-Sarkhi, A., 2010. Drag reduction with polymers in gas-liquid/liquid-liquid flows in pipes: a literature review. Journal of Natural Gas Science and Engineering, 2(1), pp.41-48.

Al-Wahaibi, T., Smith, M. and Angeli, P., 2007. Effect of drag-reducing polymers on horizontal oil–water flows. Journal of Petroleum Science and Engineering, 57(3), pp.334-346.

Al-Yaari, M., Al-Sarkhi, A. and Abu-Sharkh, B., 2012. Effect of drag reducing polymers on water holdup in an oil–water horizontal flow. International Journal of Multiphase Flow, 44, pp.29-33.

Al-Yaari, M., Soleimani, A., Abu-Sharkh, B., Al-Mubaiyedh, U. and Al-Sarkhi, A., 2009. Effect of drag reducing polymers on oil–water flow in a horizontal pipe. International Journal of Multiphase Flow, 35(6), pp.516-524.

Angeli, P. and Hewitt, G.F., 2000. Flow structure in horizontal oil–water flow. International journal of multiphase flow, 26(7), pp.1117-1140.

Arirachakaran, S., Oglesby, K.D., Malinowsky, M.S., Shoham, O. and Brill, J.P., 1989, January. An analysis of oil/water flow phenomena in horizontal pipes. In SPE Production Operations Symposium. Society of Petroleum Engineers.

Aubin, J., Le Sauze, N., Bertrand, J., Fletcher, D.F. and Xuereb, C., 2004. PIV measurements of flow in an aerated tank stirred by a down-and an up-pumping axial flow impeller. Experimental Thermal and Fluid Science, 28(5), pp.447-456.

Baker, O., 1953. Design of Pipelines for the Simultaneous Flow of Oil and Gas. Oil and Gas Journal, v. 53, pp. 185.

Baik, S. and Hanratty, T.J., 2003. Effects of a drag reducing polymer on stratified gas–liquid flow in a large diameter horizontal pipe. International journal of multiphase flow, 29(11), pp.1749-1757.

Bannwart, A.C., Rodriguez, O.M., de Carvalho, C.H., Wang, I.S. and Vara, R.M., 2004. Flow patterns in heavy crude oil-water flow. Journal of energy resources technology, 126(3), pp.184-189.

Beggs, D.H. and Brill, J.P., 1973. A study of two-phase flow in inclined pipes. Journal of Petroleum technology, 25(05), pp.607-617.

Beretta, A., Ferrari, P., Galbiati, L. and Andreini, P.A., 1997. Horizontal oil-water flow in small diameter tubes. Flow patterns. International communications in heat and mass transfer, 24(2), pp.223-229.

Bonizzi, M. and Issa, R.I., 2003. On the simulation of three-phase slug flow in nearly horizontal pipes using the multi-fluid model. International journal of multiphase flow, 29(11), pp.1719-1747.

Buchhave, P., 1992. Particle image velocimetry—status and trends. Experimental Thermal and Fluid Science, 5(5), pp.586-604.

Burger, E.D., Munk, W.R. and Wahl, H.A., 1982. Flow increase in the Trans Alaska Pipeline through use of a polymeric drag-reducing additive. Journal of Petroleum Technology, 34(02), pp.377-386.

Charles, M.E., Govier, G.T. and Hodgson, G.W., 1961. The horizontal pipeline flow of equal density oil-water mixtures. the Canadian Journal of Chemical engineering, 39(1), pp.27-36.

Chen, X. and Guo, L., 1999. Flow patterns and pressure drop in oil–air–water three-phase flow through helically coiled tubes. International Journal of Multiphase Flow, 25(6), pp.1053-1072.

Choi, H.J. and Jhon, M.S., 1996. Polymer-induced turbulent drag reduction. Industrial & engineering chemistry research, 35(9), pp.2993-2998.

Coupland, J.M., Garner, C.P., Alcock, R.D. and Halliwell, N.A., 2006. Holographic particle image velocimetry and its application in engine development. In Journal of Physics: Conference Series (Vol. 45, No. 1, p. 29). IOP Publishing.

Czapp, M., Muller, C., Fernández, P.A. and Sattelmayer, T., 2012, July. High-speed stereo and 2D PIV measurements of two-phase slug flow in a horizontal pipe. In 16th international symposium on applications of laser techniques to fluid mechanics, Lisbon, Portugal (pp. 9-12).

Daas, M. and Bleyle, D., 2006. Computational and experimental investigation of the drag reduction and the components of pressure drop in horizontal slug flow using liquids of different viscosities. Experimental thermal and fluid science, 30(4), pp.307-317.

Deen, N.G., 1999. Multiphase Particle Image Velocimetry Measurements in a Bubble Column. Aalborg University Esbjerg.

Dieck, R. H. 2002. “Measurement Uncertainty: Methods and Applications,” 3rd ed. Research Triangle Park, NC: The Instrumentation, Systems and Automation Society.

Dudderar, T.D. and Simpkins, P.G., 1977. Laser speckle photography in a fluid medium. Nature, 270, pp.45-47.

Erickson, D. and Twaite, D., 1996, January. Pipeline integrity monitoring system for leak detection, control, and optimization of wet gas pipelines. In SPE Annual Technical Conference and Exhibition. Society of Petroleum Engineers.

Fernandes, R.L.J., Fleck, B.A., Heidrick, T.R., Torres, L. and Rodriguez, M.G., 2009. Experimental study of DRA for vertical two-phase annular flow. Journal of Energy Resources Technology, 131(2), p.023002.

Fernandes, R.L.J., Jutte, B.M. and Rodriguez, M.G., 2004. Drag reduction in horizontal annular two-phase flow. International journal of multiphase flow, 30(9), pp.1051-1069.

Flory, P.J., 1953. Principles of polymer chemistry. Cornell University Press.

Gao, Z.K., Yang, Y.X., Fang, P.C., Jin, N.D., Xia, C.Y. and Hu, L.D., 2015. Multi-frequency complex network from time series for uncovering oil-water flow structure. Scientific reports, 5, p.8222.

Greskovich, E.J. and Shrier, A.L., 1971. Drag reduction in two-phase flows. Industrial & Engineering Chemistry Fundamentals, 10(4), pp.646-648.

Gyr, A. and Bewersdorff, H.W., 1995. Drag Reduction by Additives. Fluid Mechanics and its Aplications Series, vol, 32.

Hall, A.R.W., 1992. Multiphase flow of oil, water and gas in horizontal pipes (Doctoral dissertation, Imperial College London (University of London)).

Harpold, A. and Mostaghimi, S., 2004, October. Stream discharge measurement using a large-scale particle image velocimetry prototype. In Proceedings of Virginia Water Research Symposium (pp. 178-185).

Hassan, Y.A., Blanchat, T.K., Seeley, C.H. and Canaan, R.E., 1992. Simultaneous velocity measurements of both components of a two-phase flow using particle image velocimetry. International Journal of Multiphase Flow, 18(3), pp.371-395.

Hasson, D., Mann, V. and Nir, A., 1970. Annular flow of two immiscible liquids I. Mechanisms. The Canadian Journal of Chemical Engineering, 48(5), pp.514-520.

Hewitt, G.F., 1998. Gaseliquid Flow: Multiphase Fluid Flow and Pressure Drop, Heat Exchanger Design Handbook, 1998. Begell House, New York, pp. 2.3.2-13e12.13.12-15.

Hubbard, M.G. and Dukler, A.E., 1966. The characterization of flow regimes for horizontal two-phase flow. Proceedings of the 1996 Heat Transfer and Fluid, pp.100-121.

Jubran, B.A., Zurigat, Y.H. and Goosen, M.F.A., 2005. Drag reducing agents in multiphase flow pipelines: recent trends and future needs. Petroleum science and technology, 23(11-12), pp.1403-1424.

Kabiri-Samani, A.R., Borghei, S.M. and Saidi, M.H., 2007. Fluctuation of air-water two-phase flow in horizontal and inclined water pipelines. Journal of Fluids Engineering, 129(1), pp.1-14.

Kang, C., Vancko, R.M., Green, A.S., Kerr, H. and Jepson, W.P., 1998. Effect of drag-reducing agents in multiphase flow pipelines. Journal of energy resources technology, 120(1), pp.15-19.

Karami, H.R. and Mowla, D., 2012. Investigation of the effects of various parameters on pressure drop reduction in crude oil pipelines by drag reducing agents. Journal of Non-Newtonian Fluid Mechanics, 177, pp.37-45.

Khor, S.H., 1998. Three-phase liquid-liquid-gas stratified flow in pipelines (Doctoral dissertation, Imperial College London (University of London)).

Langsholt, M., 2012, June. An experimental study on polymeric type DRA used in single-and multiphase flow with emphasis on degradation, diameter scaling and the effects in three-phase oil-water-gas flow. In 8th North American Conference on Multiphase Technology. BHR Group.

Li, F.C. and Hishida, K., 2009. Particle image velocimetry techniques and its applications in multiphase systems. Advances in Chemical Engineering, 37, pp.87-147.

Lindken, R. and Merzkirch, W., 2002. A novel PIV technique for measurements in multiphase flows and its application to two-phase bubbly flows. Experiments in fluids, 33(6), pp.814-825.

Lockhart, R.W. and Martinelli, R.C., 1949. Proposed correlation of data for isothermal two-phase, two-component flow in pipes. Chem. Eng. Prog, 45(1), pp.39-48.

Lovick, J. and Angeli, P., 2004. Experimental studies on the dual continuous flow pattern in oil–water flows. International journal of multiphase flow, 30(2), pp.139-157.

Mandhane, J.M., Gregory, G.A. and Aziz, K., 1974. A flow pattern map for gas—liquid flow in horizontal pipes. International Journal of Multiphase Flow, 1(4), pp.537-553.

Manfield, P.D., Lawrence, C.J. and Hewitt, G.F., 1999. Drag reduction with additives in multiphase flow: a literature survey. multiphase Science and Technology, 11(3).

Moré, P.P., Kang, C. and Magalhães, A.A.O., 2008, January. The Performance of Drag Reducing Agents in Multiphase Flow Conditions at High Pressure: Positive and Negative Effects. In 2008 7th International Pipeline Conference (pp. 149-157). American Society of Mechanical Engineers.

Mowla, D. and Naderi, A., 2006. Experimental study of drag reduction by a polymeric additive in slug two-phase flow of crude oil and air in horizontal pipes. Chemical Engineering Science, 61(5), pp.1549-1554.

Ning, T., Guo, F., Chen, B. and Zhang, X., 2009. PIV measurement of turbulent bubbly mixing layer flow with polymer additives. In Journal of Physics: Conference Series (Vol. 147, No. 1, p. 012014). IOP Publishing.

Novotný, J., Nožička, J., Adamec, J. and Nováková, L., 2005. Measurement of Two Phase Flow. Acta Polytechnica, 45(3).

Oddie, G., Shi, H., Durlofsky, L.J., Aziz, K., Pfeffer, B. and Holmes, J.A., 2003. Experimental study of two and three phase flows in large diameter inclined pipes. International Journal of Multiphase Flow, 29(4), pp.527-558.

Oglesby, K.D., 1979. An experimental study on the effects of oil viscosity, mixture velocity and water fraction on horizontal oil-water flow. University of Tulsa, Fluid Flow Projects.

Oliver, D. and Young-Hoon, A., 1968. Two Phase Non-Newtonian Flow: Part 1 Pressure Drop and Holdup. Trans. Instn. Chem. Engrs, vol. 46, pp. 106-115.

Pan L., 1996. "High Pressure Three-Phase (Gas/Oil/Water) Flow," PhD Dissertation, Imperial College of Science, Technology and Medicine, U. London, UK.

Raffel, M., Willert, C., Wereley, S. and Kompenhans, J., 2007. Particle image velocimetry. Experimental fluid mechanics. Springer, Berlin. doi, 10(1007), pp.978-3.

Rodriguez, O.M.H. and Oliemans, R.V.A., 2006. Experimental study on oil–water flow in horizontal and slightly inclined pipes. International Journal of Multiphase Flow, 32(3), pp.323-343.

Rosehart, R.G., Scott, D.S. and Rhodes, E., 1972. Gas-liqud slug flow with drag-reducing polymer solutions. AIChE Journal, 18(4), pp.744-750.

Russell, T.W.F. and Charles, M.E., 1959. The effect of the less viscous liquid in the laminar flow of two immiscible liquids. The Canadian Journal of Chemical Engineering, 37(1), pp.18-24.

Soleimani, A., Al-Sarkhi, A. and Hanratty, T.J., 2002. Effect of drag-reducing polymers on pseudo-slugs—interfacial drag and transition to slug flow. International journal of multiphase flow, 28(12), pp.1911-1927.

Saarenrinne, P., Honkanen, M., Parssinen, T. and Eloranta, H., 2004. Digital imaging and PIV methods in multiphase flows. Institute of Energy and Process Engineering, Tempere.

Schlichting, H. and Gersten, K., 2003. "Boundary-layer theory," Springer Science & Business Media.

Sifferman, T.R. and Greenkorn, R.A., 1981. Drag reduction in three distinctly different fluid systems. Society of Petroleum Engineers Journal, 21(06), pp.663-669.

Soleimani, A., Lawrence, C.J. and Hewitt, G.F., 2000. Spatial distribution of oil and water in horizontal pipe flow. SPE Journal, 5(04), pp.394-401.

Spedding, P.L., Bénard, E. and Donnelly, G.F., 2006. Prediction of pressure drop in multiphase horizontal pipe flow. International communications in heat and mass transfer, 33(9), pp.1053-1062.

Sylvester, N.D. and Brill, J.P., 1976. Drag reduction in two-phase annular-mist flow of air and water. AIChE Journal, 22(3), pp.615-617.

Sylvester, N.D., Dowling, R.H. and Brill, J.P., 1980. Drag reduction in cocurrent horizontal natural gas-hexane pipe flow. Polymer Engineering & Science, 20(7), pp.485-492.

Taitel, Y. and Dukler, A.E., 1976. A theoretical approach to the Lockhart-Martinelli correlation for stratified flow. International Journal of Multiphase Flow, 2(5), pp.591-595.

Taitel, Y., Barnea, D. and Brill, J.P., 1995. Stratified three phase flow in pipes. International Journal of Multiphase Flow, 21(1), pp.53-60.

Tassin, A.L., Li, C.Y., Ceccio, S.L. and Bernal, L.P., 1995. Velocity field measurements of cavitating flows. Experiments in fluids, 20(2), pp.125-130.

Thwaites, G.R., Kulov, N.N. and Nedderman, R.M., 1976. Liquid film properties in two-phase annular flow. Chemical Engineering Science, 31(6), pp.481-486.

Toms, B.A., 1948, September. Some observations on the flow of linear polymer solutions through straight tubes at large Reynolds numbers. In Proceedings of the 1st International Congress on Rheology (Vol. 2, pp. 135-141).

Utvik, O.H., Rinde, T. and Valle, A., 2001. An experimental comparison between a recombined hydrocarbon-water fluid and a model fluid system in three-phase pipe flow. Journal of energy resources technology, 123(4), pp.253-259.

Valle, A. and Kvandal, H., 1995, October. Pressure drop and dispersion characteristics of separated oil/water flow. In Proceedings of the International Symposium Two-phase flow modeling and experimentation (Vol. 2, pp. 583-592).

Warholic, M.D., Massah, H. and Hanratty, T.J., 1999. Influence of drag-reducing polymers on turbulence: effects of Reynolds number, concentration and mixing. Experiments in fluids, 27(5), pp.461-472.

Wegmann, A., Melke, J. and von Rohr, P.R., 2007. Three phase liquid–liquid–gas flows in 5.6 mm and 7mm inner diameter pipes. International Journal of Multiphase Flow, 33(5), pp.484-497.

Weisbach, J., 1845. Lehrbuch der Ingenieur-und Maschinen-Mechanik [Textbook of engineering and machine mechanics]. Friedrich Vieweg, Braunschweig, Germany.

Wilkens, R.J. and Thomas, D.K., 2007. Multiphase drag reduction: Effect of eliminating slugs. International journal of multiphase flow, 33(2), pp.134-146.

Zhang, H.Q. and Sarica, C., 2006. Unified modeling of gas/oil/water pipe flow-Basic approaches and preliminary validation. SPE Projects, Facilities & Construction, 1(02), pp.1-7.

Zhang, H.Q., Wang, Q., Sarica, C. and Brill, J.P., 2003. Unified model for gas-liquid pipe flow via slug dynamics—part 1: model development. Journal of energy resources technology, 125(4), pp.266-273.

APPENDIX A: EXPERIMENTAL SETUP AND SPECIFICATIONS

Table A1 Tanks and Pumps specifications

	Properties	Description
Supply and Separation Tanks	Dimensions	Height: 1.6 m Inner Diameter: 1.25 m
	Capacity	518.5 gallons (1962.73 Liters)
	Material	Plastic
Centrifugal Pump	General specifications	- Manufacturer: Crompton Greaves LTD - Single stage, end suction, centrifugal monoset pump, IPM series. - TEFC motor with class `F` insulation.
	Range	2.0 kW (3.0 HP)
	Supply	440 V, 3 phase, 60 Hz, AC.
	Pipe size	50 x 50 mm
	Total head	14.0 – 34.0 meters
	Capacity	420/150 LPM.
	Liquid	Clear water.
	Rotation	3470 RPM
	Electric Motors	- Voltage : 415 V - Phase : 3 phase, 50 Hz, AC
	Liquid temperature	(65.0 – 110.0) ^{0}C

Table A2 Specifications of the sensors connected to data acquisition system

	Properties	**Description**
Wet/wet Differential pressure Transmitter	Voltage	24 V DC
	Current	4-20 mA
	Operating Temperature	(-40.0 – 120) ºC
	Accuracy	± 0.75 %
	Media compatibility	Gas and Liquid
	Model no.	**PX 157**
	Manufacturer	**OMEGA Co.**
Flow Transmitter Sensors	Installation	It can be mounted in any position, vertical or horizontal
	Mass flow rate	Up to 150 GPM
	Current	4.0 – 20.0 mA
	Voltage	0.0 – 5.0 Volt DC
	Accuracy	± 2.0 %
	Pressure	- For Water: up to 3500 psi - For Oil: up to 3500 psi - For Air: up to 1000 psi
	Operating Temperature	- (-29.0 – 116) ºC
	Model no.	FLR 7710 D
	Manufacturer	OMEGA Co.
Data acquisition system	Chassis	• Accepts 3U PXI Express, Compact PCI Express, and hybrid slot-compatible PXI-1/Compact PCI modules: - x4 PCI Express link directly connected to the system slot from each hybrid slot. - 32-bit, 33 MHz PCI connected to each hybrid slot. • Accepts 4-slot wide PXI Express embedded controller. • Rugged, compact chassis with universal AC input • Auto/high temperature-controlled fan speed based on air intake temperature to minimize audible noise.
	Operating Temperature	(0.0 – 50.0) ºC
	Relative humidity	20.0 – 80.0 %
	Dimensions	- Height: 6.97 in - Width: 10.12 in - Depth: 8.43 in
	Chassis Material	Stainless Steel, Extruded Aluminum, Cold Rolled Steel, and PC-ABS
	Power	230 Watt
	Model no.	NI PXIe-1071
	Manufacturer	National Instrument

Table A3 Specifications of the pipes, fittings, control valves, and union

	Properties	Description
PVC pipe	Standard	ASTM D 1785
	Schedule	80
	Manufacturer	SAPPCO-KSA
	Nominal Size	2.0 in
	Outside Diameter	60.32 mm
	Wall thickness	0.218 in
	Nominal weight	1.43 $kg.m^{-1}$
	Working Pressure	400.0 psi
	Max. Temperature	73.0 ^{0}F
PVC pipe	Standard	ASTM D 1785
	Schedule	80
	Manufacturer	SAPPCO-KSA
	Nominal Size	1.0 in
	Outside Diameter	33.40 mm
	Wall thickness	0.179 in
	Nominal weight	0.614 $kg.m^{-1}$
	Working Pressure	630.0 psi
	Max. Temperature	73.0 ^{0}F
Acrylic PVC Pipe	Standard	ASTM D 1785
	Schedule	80
	Manufacturer	SPEARS- USA
	Outside Diameter	1.0 in
	Working Pressure	360.0 psi
	Max. Temperature	73.0 ^{0}F
90^0 Elbow-CPVC	Standard	ASTM F 439
	Schedule	80
	Manufacturer	SPEARS- USA
	Outside Diameter	2.0 in
	Working Pressure	400.0 psi
	Max. Temperature	73.0 ^{0}F
Wye Fittings-PVC	Schedule	40
	Manufacturer	CHANAL- USA
	Outside Diameter	2.0 in
	Working Pressure	235.0 psi
	Max. Temperature	73.0 ^{0}F
Tee Fittings – PVC	Standard	ASTM F 439
	Schedule	80
	Manufacturer	SPEARS - USA
	Outside Diameter	2.0 in
	Working Pressure	400.0 psi
	Max. Temperature	73.0 ^{0}F
Union – PVC	Schedule	80
	Manufacturer	SPEARS - USA
	Outside Diameter	2.0 in
	Working Pressure	235.0 psi
	Max. Temperature	73.0 ^{0}F
Compact Ball Valve – PVC	Schedule	80
	Manufacturer	SPEARS - USA
	Outside Diameter	(1.0 - 2.0) in
	Working Pressure	(235 - 150.0) psi
	Max. Temperature	73.0 ^{0}F
	Style	Socket ends
Gate Valve	Standard	1065 Forged Brass Full Bore Gate Valve
	Schedule	80
	Manufacturer	PEGLER – England
	Outside Diameter	(1.0 – 2.0) in
	Working Pressure	17.5 bar
	Max. Temperature	95.0 ^{0}F
	Style	Threaded ends

APPENDIX B: EXPERIMENTAL PERCENTAGE DRAG REDUCTION AND FLOW PATTERN

Table B1 Experimental test matrix and observed flow pattern For Water-Soluble DRP (22.5 mm ID).

	Water-Soluble DRP										
Types	V_{SW} (m.sec^{-1})	V_{SO} (m.sec^{-1})	V_{SG} (m.sec^{-1})	$Q_{pol.}$ (**m^3.min^{-1}**)	Q_{Liquid} (**m^3.min^{-1}**)	F.P. without DRP	F.P. with DRP	Max. %DR	Re_{SW}	Re_{SO}	Re_{SG}
Single-phase	0.344	--	--	0.0017	0.00991	SP	SP	50.6	9,479	--	--
	0.408	--	--	0.0017	0.01145	SP	SP	52	10,951	--	--
	0.466	--	--	0.0017	0.01284	SP	SP	50	12,271	--	--
	0.557	--	--	0.0017	0.01500	SP	SP	56	14,343	--	--
	0.630	--	--	0.0017	0.01674	SP	SP	62	16,008	--	--
	0.730	--	--	0.0017	0.01911	SP	SP	67.4	18,274	--	--
	0.801	--	--	0.0017	0.02046	SP	SP	72.5	19,563	--	--
	0.858	--	--	0.0017	0.02313	SP	SP	71.3	22,112	--	--
	1.036	--	--	0.0017	0.02642	SP	SP	72	25,261	--	--
	0.885	--	--	0.0-0.0033	0.0211	SP	SP	74.9	20,175	--	--
	1.156	--	--	0.0-0.0033	0.0278	SP	SP	73.5	26,353	--	--
	1.56	--	--	0.0-0.0033	0.037	SP	SP	76	35,563	--	--
	1.74	--	--	0.0-0.0033	0.0414	SP	SP	75.4	39,666	--	--
Two-Phase	0.389	--	6.32	0.0017	0.009	SHF	S	38	8,889	--	9,490
	0.394	--	8.70	0.0017	0.009	SHF	S	51	8,976	--	13,056
	0.397	--	11.0	0.0017	0.009	SHF	S	57	9,051	--	16,502
	0.396	--	12.9	0.0017	0.009	SHF	S	57	9,042	--	19,399
	0.409	--	17.3	0.0017	0.009	A	SHF	63	9,330	--	26,008
	0.417	--	19.8	0.0017	0.009	A	A	66	9,505	--	29,744
	0.421	--	25.0	0.0017	0.009	A	A	65	9,598	--	37,607
	0.74	--	3.31	0.0–0.0035	0.019	S	SLF	46	16,869	--	4,965
	0.95	--	3.31	0.0–0.0035	0.0227	S	SLF	54	21,657	--	4,965
	1.10	--	3.85	0.0–0.0035	0.0265	S	SLF	52	25,076	--	5,775
	0.65	--	5.4	0.0036	0.019	SHF	S	15	14,818	--	8,039
	0.65	--	8.0	0.0036	0.019	SHF	S	23.3	14,818	--	11,993
	0.65	--	8.4	0.0036	0.019	SHF	S	18	14,818	--	12,617
	0.65	--	12.4	0.0036	0.019	SHF	S	14.7	14,818	--	18,662
	0.65	--	18.7	0.0036	0.019	A	SHF	14	14,818	--	28,103
	0.65	--	25.2	0.0036	0.019	A	A	5.12	14,818	--	37,868
	0.65	--	28.1	0.0036	0.019	A	A	3.37	14,818	--	42,181
	0.65	--	29.93	0.0036	0.019	A	A	4.43	14,818	--	44,899
	0.65	--	30.1	0.0036	0.019	A	A	4.76	14,818	--	45,043
	0.65	--	31.7	0.0036	0.019	A	A	7.05	14,818	--	47,623
	0.65	--	31.3	0.0036	0.019	A	A	4.66	14,818	--	46,998
	0.65	--	37.3	0.0036	0.019	A	A	4.74	14,818	--	55,920
	0.65	--	39.7	0.0036	0.019	A	A	5.63	14,818	--	59,565
	0.65	--	41.1	0.0036	0.019	A	A	2.46	14,818	--	61,765
	0.79	--	13.9	7.95E-05	0.019	SHF	S	65	18,010	--	20,811
	0.79	--	16.7	7.95E-05	0.019	A	SHF	63	18,010	--	25,104
	0.79	--	20.2	7.95E-05	0.019	A	SHF	64	18,010	--	30,291
	0.79	--	24.0	7.95E-05	0.019	A	SHF	50	18,010	--	36,016
	0.79	--	29.9	7.95E-05	0.019	A	A	38	18,010	--	44,802
	0.79	--	31.3	7.95E-05	0.019	A	A	35	18,010	--	46,995
	0.79	--	35.4	7.95E-05	0.019	A	A	20	18,010	--	53,037
	0.79	--	35.4	7.95E-05	0.019	A	A	22	18,010	--	53,157
	0.79	--	37.0	7.95E-05	0.019	A	A	32	18,010	--	55,537
	0.79	--	37.1	7.95E-05	0.019	A	A	23	18,010	--	55,706
Three-Phase	0.666	0.316	2.27	0.003	0.026	S	SLF	20	11,816	5,606	3,405
	0.666	0.316	5.5	0.003	0.026	SHF	SLF	23	11,816	5,606	8,250
	0.666	0.316	9.8	0.003	0.026	SHF	SLF	26	11,816	5,606	14,700
	0.666	0.316	12.0	0.003	0.026	SHF	SLF	35	11,816	5,606	18,000
	0.666	0.316	16.6	0.003	0.026	A	SHF	45	11,816	5,606	24,900
	0.339	0.796	2.5	0.003	0.029	S	SLF	35	6,014	14,123	3,750
	0.339	0.796	5.3	0.003	0.029	SHF	SLF	56	6,014	14,123	7,950
	0.339	0.796	8.5	0.003	0.029	SHF	SLF	66	6,014	14,123	12,750

SP: Single-phase flow; **S:** Slug flow; **SLF:** Slug low frequency flow; **SHF:** Slug high frequency flow; **A:** Annular flow

Table B2 Experimental test matrix and observed flow pattern For Oil-Soluble DRP (22.5 mm ID).

	Oil-Soluble DRP										
Types	V_{SW} ($m.sec^{-1}$)	V_{SO} ($m.sec^{-1}$)	V_{SG} ($m.sec^{-1}$)	$Q_{pol.}$ ($m^3.min^{-1}$)	Q_{Liquid} ($m^3.min^{-1}$)	F.P. without DRP	F.P. with DRP	Max. %DR	Re_{SW}	Re_{SO}	Re_{SG}
Single- Phase	--	1.58	--	0.0–0.0024	0.0388	SP	SP	35	--	16,308	--
	--	1.35	--	0.0024	0.035	SP	SP	41.4	--	13,934	--
	--	0.92	--	0.0024	0.0245	SP	SP	71.7	--	9,496	--
	--	0.54	--	0.0024	0.0153	SP	SP	77.9	--	5,574	--
	--	0.35	--	0.0024	0.0107	SP	SP	79.3	--	3,612	--
Two-Phase	--	0.38	3.07	0.0013	0.0106	S	SLF	55	--	3,929	4,605
	--	0.38	6.20	0.0013	0.0106	SHF	SLF	48	--	3,929	9,283
	--	0.38	8.53	0.0013	0.0106	SHF	SLF	42	--	3,929	12,799
	--	0.38	11.1	0.0013	0.0106	SHF	SLF	32	--	3,929	16,617
	--	0.38	12.6	0.0013	0.0106	SHF	SLF	30	--	3,929	18,910
	--	0.38	17.4	0.0013	0.0106	A	SHF	22	--	3,929	26,092
	--	0.38	20.1	0.0013	0.0106	A	SHF	20	--	3,929	30,101
	--	0.38	21.4	0.0013	0.0106	A	SHF	18	--	3,929	32,066
	--	0.38	24.3	0.0013	0.0106	A	A	16	--	3,929	36,438
`Three-Phase	0.44	0.78	3.2-10.5	0.0	0.0296	--	--	--	5980	10554	4800-15764
	1.21	0.698	2.95	0.0023	0.0295	SHF	SLF	36	17200	9820	4437
	1.21	0.698	4.58	0.0023	0.0295	SHF	SLF	36	17200	9820	6870
	1.21	0.698	8.98	0.0023	0.0295	A	SHF	18	17200	9820	13476
	0.78	0.356	2.94	0.0023	0.0296	S	SLF	40	13,749	6,243	4,404
	0.78	0.356	4.97	0.0023	0.0296	SHF	SLF	36	13,749	6,243	7,456
	0.78	0.356	10.78	0.0023	0.0296	SHF	SHF	14	13,749	6,243	16,166

SP: Single-phase flow; **S:** Slug flow; **SLF:** Slug low frequency flow; **SHF:** Slug high frequency flow; **A:** Annular flow

Table B3 Experimental test matrix and observed percentage drag reduction for two-phase air-water with water-Soluble DRP (10.16 mm ID).

	Water-Soluble DRP							
Type	V_{SW} ($m.sec^{-1}$)	V_{SG} ($m.sec^{-1}$)	Q_{air} ($m^3.min^{-1}$)	Q_{water} ($m^3.min^{-1}$)	ppm	DR%	Re_{SW}	Re_{SG}
Two-Phase	0.617	2.056	1.67E-04	0.003	200	65	7032	1445
	0.617	4.112	3.33E-04	0.003	200	72	7032	2890
	0.617	6.167	5.00E-04	0.003	200	75	7032	4335
	0.617	8.223	6.67E-04	0.003	200	79	7032	5780
	0.617	10.279	8.33E-04	0.003	200	73	7032	7226
	1.233	2.056	1.67E-04	0.006	100	58	14065	1445
	1.233	4.112	3.33E-04	0.006	100	60	14065	2890
	1.233	6.167	5.00E-04	0.006	100	71	14065	4335
	1.233	8.223	6.67E-04	0.006	100	70	14065	5780
	1.233	10.279	8.33E-04	0.006	100	69	14065	7226
	1.850	2.056	1.67E-04	0.009	67	52	21097	1445
	1.850	4.112	3.33E-04	0.009	67	58	21097	2890
	1.850	6.167	5.00E-04	0.009	67	57	21097	4335
	1.850	8.223	6.67E-04	0.009	67	62	21097	5780
	1.850	10.279	8.33E-04	0.009	67	65	21097	7226
	2.467	2.056	1.67E-04	0.012	50	54	28130	1445
	2.467	4.112	3.33E-04	0.012	50	53	28130	2890
	2.467	6.167	5.00E-04	0.012	50	54	28130	4335
	2.467	8.223	6.67E-04	0.012	50	54	28130	5780
	2.467	10.279	8.33E-04	0.012	50	51	28130	7226
	3.084	2.056	1.67E-04	0.015	40	54	35162	1445
	3.084	4.112	3.33E-04	0.015	40	48	35162	2890
	3.084	6.167	5.00E-04	0.015	40	46	35162	4335
	3.084	8.223	6.67E-04	0.015	40	45	35162	5780
	3.084	10.279	8.33E-04	0.015	40	43	35162	7226
	3.700	2.056	1.67E-04	0.018	33	48	42195	1445
	3.700	4.112	3.33E-04	0.018	33	42	42195	2890
	3.700	6.167	5.00E-04	0.018	33	39	42195	4335
	3.700	8.223	6.67E-04	0.018	33	36	42195	5780
	3.700	10.279	8.33E-04	0.018	33	34	42195	7226
	4.317	2.056	1.67E-04	0.021	29	41	49227	1445
	4.317	4.112	3.33E-04	0.021	29	40	49227	2890
	4.317	6.167	5.00E-04	0.021	29	36	49227	4335
	4.317	8.223	6.67E-04	0.021	29	33	49227	5780
	4.317	10.279	8.33E-04	0.021	29	20	49227	7226

APPENDIX C: ENERGY ANALYSIS OF SINGLE AND MULTIPHASE FLOWS WITH DRPS IN HORIZONTAL PIPES

C.1 Introduction

Drag reducing polymers (DRPs), which do not require additional infrastructure, is a much better option to increase energy efficiency in a series of important industrial applications. Therefore, this chapter evaluates the effects of two DRPs—water-soluble polar ZETAG®8165 and nonpolar oil-soluble polyisobutylene—on energy efficiency for single-phase water and oil flows, two-phase air-water and air-oil flows, and three-phase air-oil-water flow.

The energy analysis is performed by investigating head loss and percentage saving in energy consumption (both per unit pipe length). Irrespective of flow types, and variation in liquid and air flow rates, both DRPs decrease head loss and increase saving in energy consumption. Based on single-phase flow experiments, ZETAG®8165 is found to be more energy-saving than polyisobutylene. Equivalent experiments, conducted using the ZETAG®8165 and the two-phase air-water flow in the 10.16 mm ID rough stainless steel pipe, show that the head loss drastically increases in the smaller pipe. However, here the percentage saving in power consumption significantly exceeds that found in the larger 22.5 mm ID smooth PVC pipe.

A comprehensive understanding of single and multiphase flows in pipes is highly desired to increase the energy efficiency in important industrial applications. Such applications include nuclear industry, high temperature heat exchangers, chemical reactors, oil and gas transportation, sustenance transformation, mining, pharmaceuticals, transportation of

pulverized coal in fuel pipes, etc. [Ahmed and Ismail, 2008]. Here, the common requirement is that these pipes transport a given fluid with smaller frictional pressure drop (drag), and hence save energy. The use of drag reducing polymers (which are also called drag reducing agents DRAs), instead of applying several pumps and/or looping, is a much better option to increase the efficiency.

It can be concluded from the literature introduced in chapter 2 that most of the studies focused on the amount of drag reduction and attempted to explain the DRAs mechanism/applications. Accordingly, none of these studies tackled a detailed energy analysis of this phenomena or presented the energy aspect of their findings.

On the other hand, a few number of researchers focused on the benefit of using the DRPs as flow improver. Burger et al. [1982] studied the effect of adding DRP on crude oil transportation in the trans-Alaska pipeline system (TAPS), having diameters of about 1220 mm and 356 mm. The main finding was the improvement in flow rate by adding 10 ppm polymer to 1,300 km pipelines. Gyr and Bewersdorff [1995] reported that the DRPs could be used as a flow improver in pipelines. They classified the flow improvement into two categories. The first category considers that the energy level remains the same and DRPs increase the flow. As a result, the throughput increases. The second one conceives that the flow rate remains the same and DRPs minimize the pumping energy. Therefore, they concluded that DRPs can help increase the system capacity and save power.

Karami and Mowla [2012] performed partial energy analysis. They investigated the effect of adding DRP in single-phase crude oil pipelines on the pressure drop and performed energy analysis by calculating only the head losses. They remarked that the use of DRP help decrease head loss of the flow.

The above review of the literature shows that none of the previous studies, despite industrial importance, conducted a detailed energy analysis for the single and multiphase flows with DRP. The lack of studies in this essential research area was the main motivation to undertake the present chapter. Our objective is to perform a comprehensive energy analysis by conducting experiments under various operational conditions. We shall consider the following:

- Two structurally different DRPs—one polar and the other nonpolar—with varying concentrations; and
- Two different diameter pipes.

We shall experiment single-phase, two-phase, and three-phase flows, consisting of (as appropriate) air, oil, and water with and without DRPs. Our detailed energy analysis will include head loss and percentage saving in power consumption (both per unit pipe length).

C.2 Experimental Set-up and Procedure

Two experimental facilities, capable of studying the influence of different pipe diameters and operational conditions on energy analysis, were used to achieve the objectives of this study.

The larger diameter multiphase flow facility was earlier explained in details in Chapter 3 (Figure 3.2). To investigate the effects of pipe diameter and operational conditions, the facility shown in Figure C.1 was used. The major difference between this facility and the previous one is as follows. Here, the test section is made of 5 m long horizontal 10.16 mm (0.4 in) ID stainless steel pipe and the distance between the two pressure tabs is 1.5 m. This facility was designed to investigate the effect of DRP on the flow behavior of the two-phase air-water mixture. A 1,000 ppm master solution was prepared.

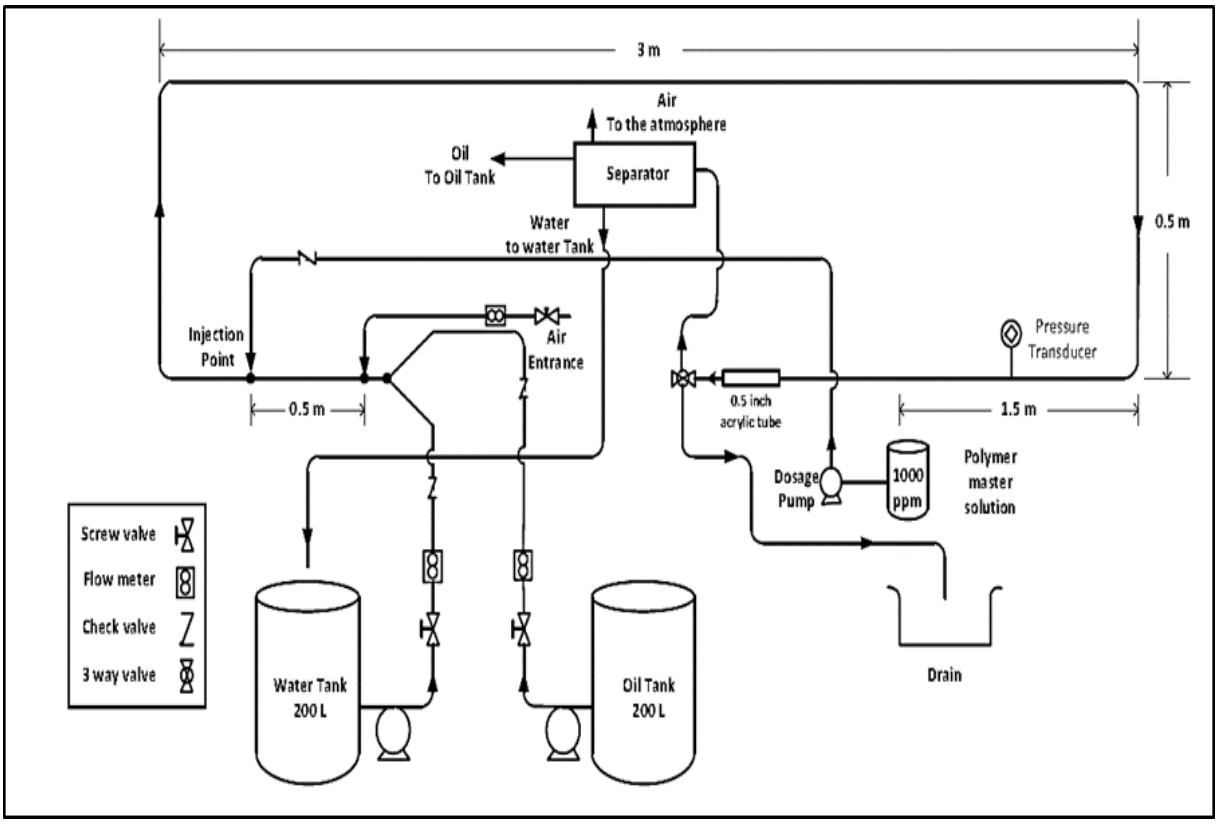

Figure C. 1 Schematics of the smaller diameter multiphase flow facility.

C.3 Results and Discussion

In this section, the effects of flow combinations was addressed; such as single-phase water flow, single-phase oil flow, two-phase air-water flow, two-phase air-oil flow, and three-phase air-oil-water flow on energy analysis. The outcomes of using different types and concentrations of DRPs were discussed, and the two varying pipe diameter results were compared.

C.3.1 Effect of Flow Combination and DRP Types

Figures C.2 to C.8 investigate the effects of the experimental DRPs (water-soluble ZETAG®8165 and oil-soluble polyisobutylene) on head loss per unit pipe length $\Delta h_L/\Delta L$ in single-phase water flow, single-phase oil flow, two-phase air-water flow, two-phase air-oil flow, and three-phase air-oil-water flow. The conduit comprises a horizontal pipe of 22.5 mm ID. The head losses were calculated using Equations 3.3, 3.4, and 3.10.

The results presented by these figures can be divided into two groups. Group I includes Figures C.2 to C.5, and Group II, Figures C.6 to C.8. Groups I and II show the variation of $\Delta h_L/\Delta L$ as the liquid flow rate Q_{liquid} and Q_{air} increase, respectively. Irrespective of single to multi-phase flows, and increase of Q_{liquid} and Q_{air}, the influence of applying a DRP qualitatively remains the same. Moreover, visual observations revealed that both

DRPs delayed the transition from low to high frequency slug flow, and the appearance of annular flow. They also reduced the pressure gradient dP/dL under all the experimental conditions. Consequently, DRP decreases $\Delta h_L/\Delta L$; hence, the amount of power consumption per volumetric flow rate. As a result, larger volume of fluid can be transported by using the same pump, or the same volume of fluid can be transported using a smaller pump. This means that either situation saves energy. Therefore, Figures C.2 to C.8 illustrate the energy-saving capability of both DRPs (ZETAG®8165 and polyisobutylene) in highly turbulent flow, which is also supported by the report of Karami and Mowla [2012]. This study specifically illustrates the varying effects of flow combinations on decreasing head loss per unit pipe length $\Delta h_L/\Delta L$.

After establishing the above common finding that DRP decreases $\Delta h_L/\Delta L$, the single-phase flow experiments were considered (Figures C.2 and C.3) to rate the energy-saving performance of water-soluble ZETAG®8165 and oil-soluble polyisobutylene (PIB). ZETAG®8165 shows more pronounced reduction in $\Delta h_L/\Delta L$ than polyisobutylene. Compare the performance of ZETAG®8165 (at concentration of 64 up to 172 ppm) over that of PIB (at concentration of 101 up to 329 ppm). Therefore, the former better suppresses the formation of turbulent bursts and the propagation of turbulent eddies. This performance differential can be attributed to the difference in their structures and hence, properties (polar versus nonpolar). See Figure 5.6A.

Figures C.9 to C.15 study the effects of the experimental DRPs on percentage saving in power consumption per unit pipe length $\%W_{PS}$ as a function of the flow combinations

listed above. $\%W_{PS}$ was calculated using Equation 3.12. Figures C.9 to C.12 relate to increasing Q_{liquid} whereas Figures C.13 to C.15 refer to increasing Q_{air}. The following general trend is noticed. $\%W_{PS}$ increased with the increase in Q_{liquid} and Q_{air} except for two cases in Figures C.11 and C.13. Here, the trend is the reverse; $\%W_{PS}$ decreased with the increase in Q_{air}. This finding can be explained considering that increasing air flow rate reduces the level of interaction between the water or oil-soluble DRP molecules and turbulent eddies of water or oil-phase, respectively. This study elaborates the varying effects of flow combinations on increasing power consumption per unit pipe length *W*.

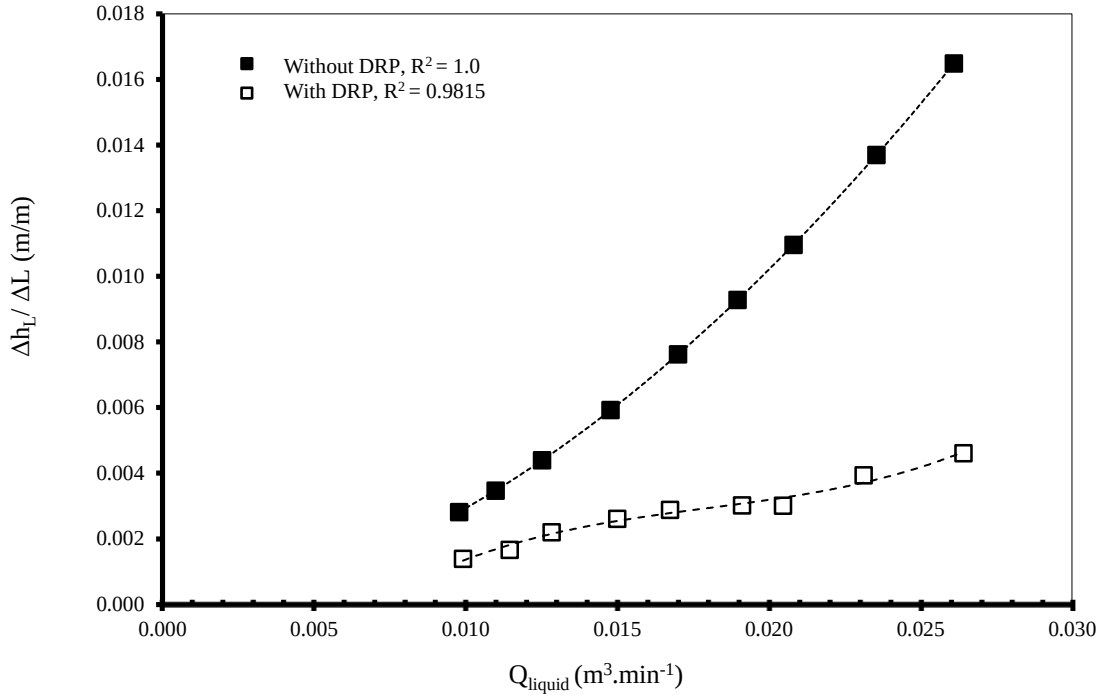

Figure C.2 Head loss per meter length versus liquid flow rate in single-phase water flow with and without water-soluble ZETAG®8165 DRP at concentrations of 64 ppm up to 172 ppm in horizontal pipe of 22.5 mm ID (dotted curve represents third order polynomial cure).

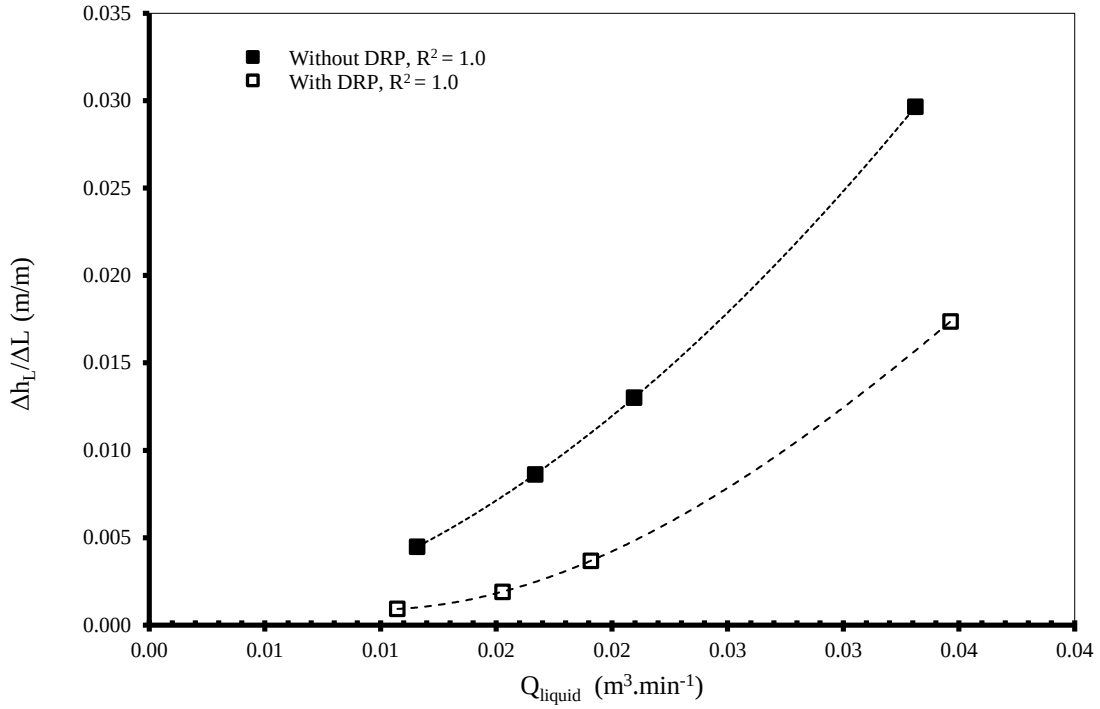

Figure C.3 Head loss per meter length versus liquid flow rate in single-phase oil flow with and without oil-soluble poly(isobutylene) DRP at concentrations of 101 ppm up to 329 ppm in horizontal pipe of 22.5 mm ID (dotted curve represents third order polynomial cure).

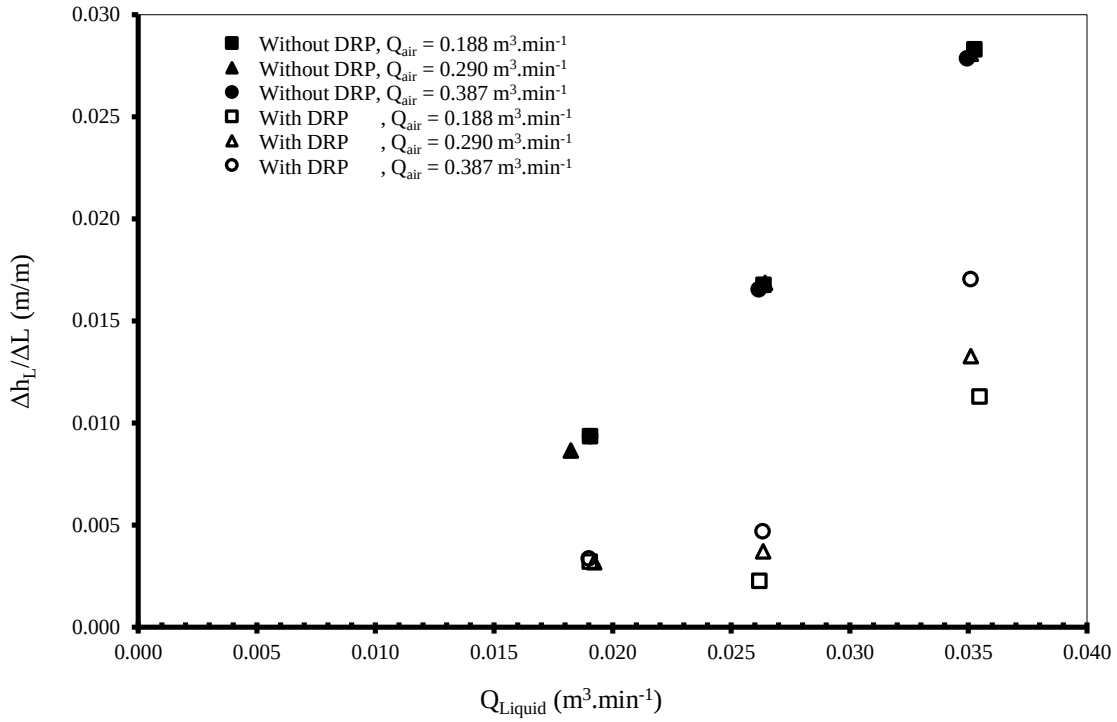

Figure C.4 Head loss per meter length versus liquid flow rate in two-phase air-water flow with and without water-soluble ZETAG®8165 DRP at concentrations of 2 ppm up to 4 ppm in horizontal pipe of 22.5 mm ID.

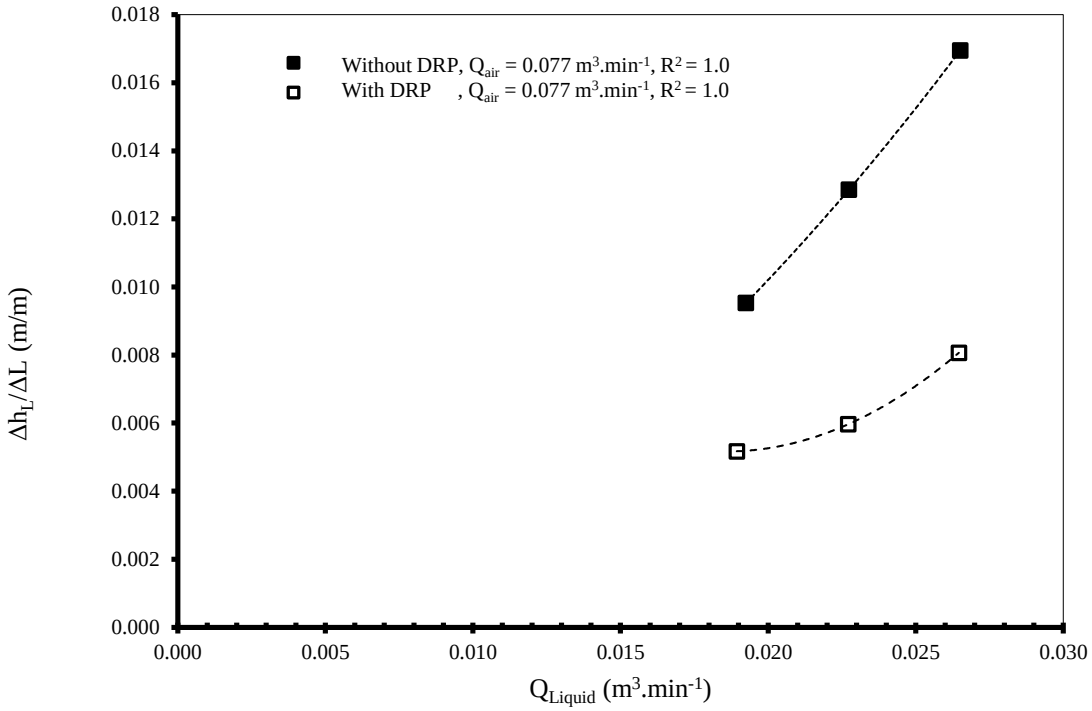

Figure C.5 Head loss per meter length versus liquid flow rate in two-phase air-water flow with and without water-soluble ZETAG®8165DRP at concentrations of 70 ppm up to 98 ppm in horizontal pipe of 22.5 mm ID (dotted curve represents third order polynomial cure).

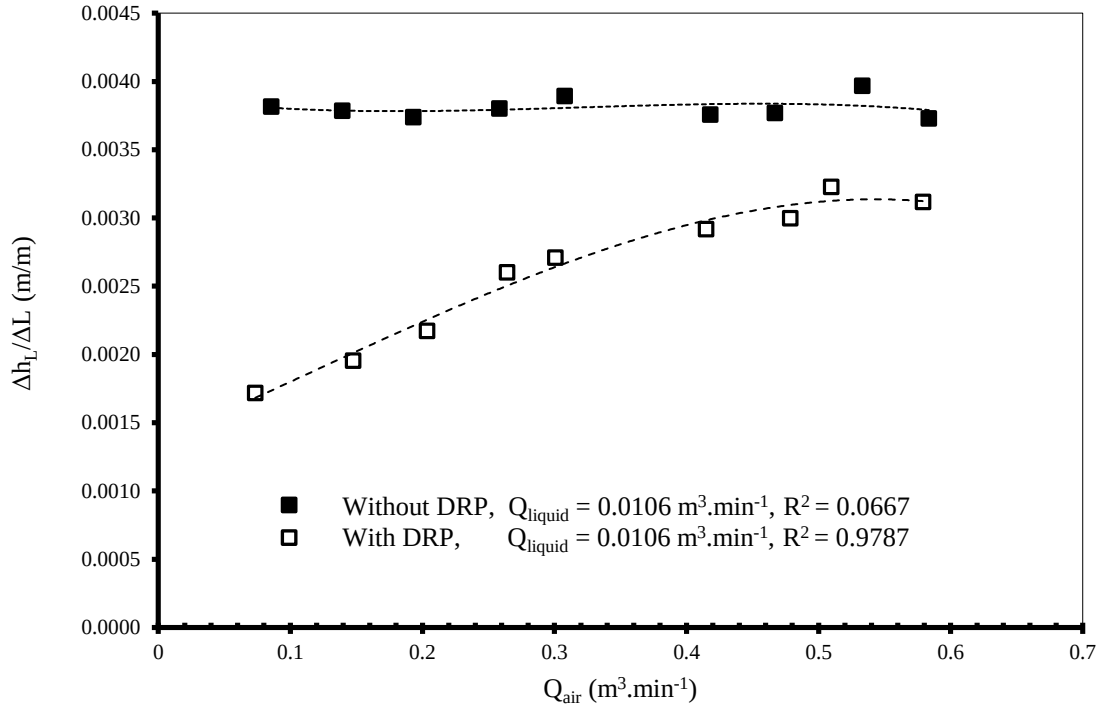

Figure C.6 Head loss per meter length versus liquid flow rate in two-phase air-oil flow with and without oil-soluble poly(isobutylene) DRP at concentration of 290 ppm in horizontal pipe of 22.5 mm ID (dotted curve represents third order polynomial cure).

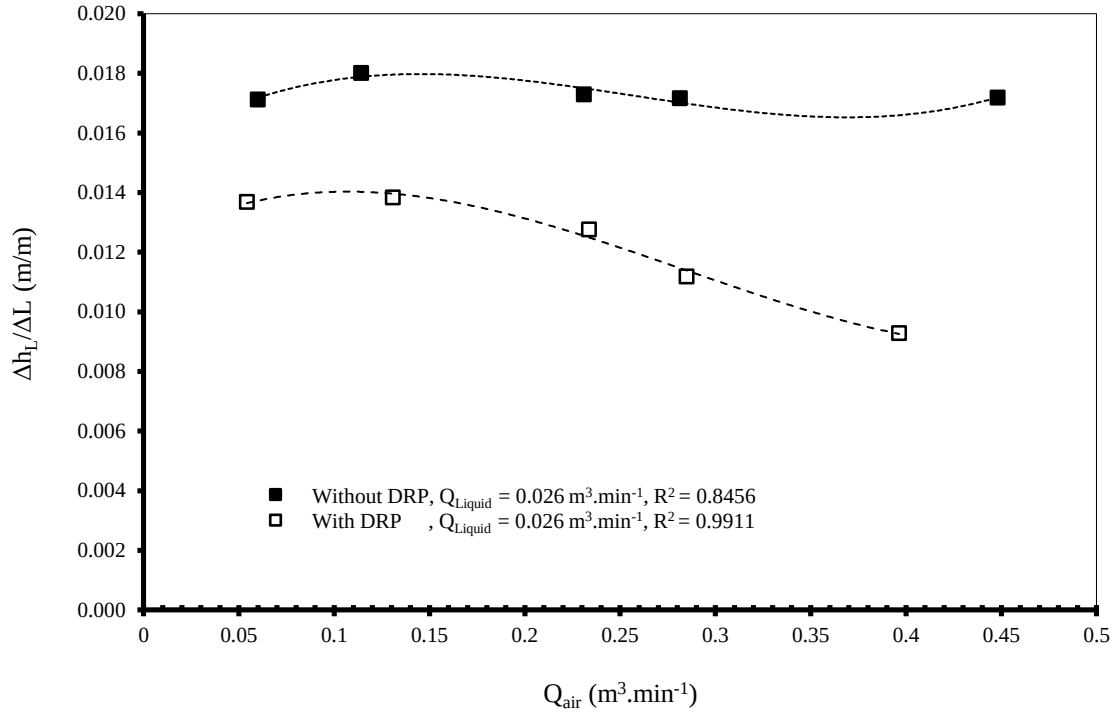

Figure C.7 Head loss per meter length versus liquid flow rate in three-phase air-oil-water flow with and without water-soluble ZETAG®8165 DRP at concentration of 113 ppm in horizontal pipe of 22.5 mm ID (dotted curve represents third order polynomial cure).

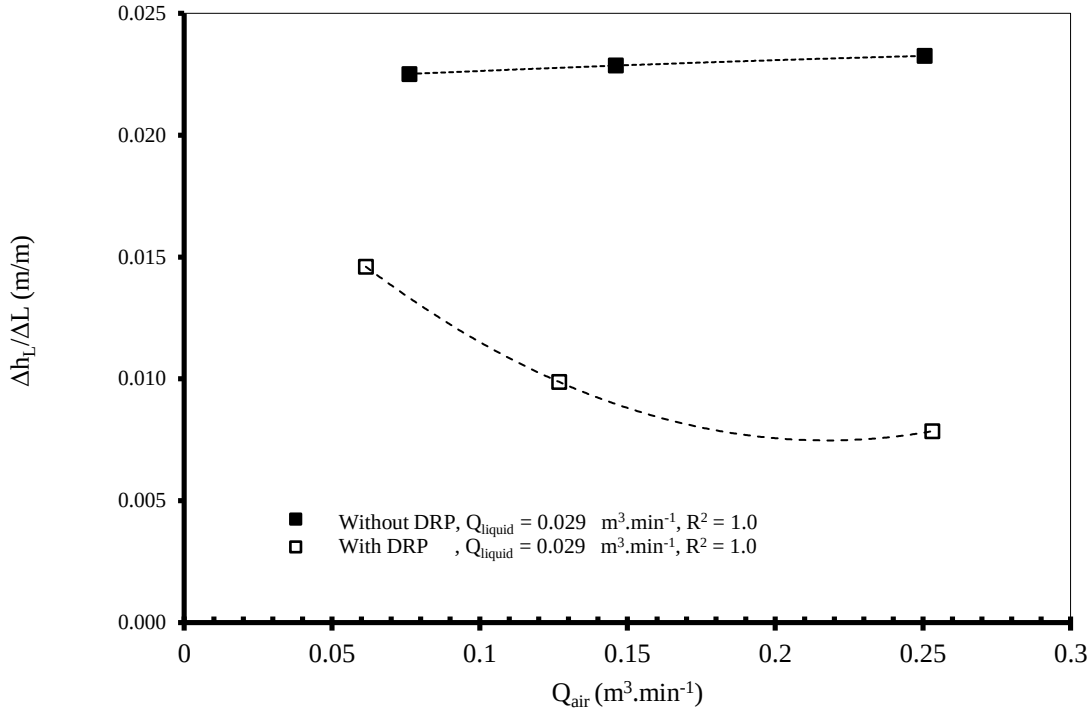

Figure C.8 Head loss per meter length versus liquid flow rate in three-phase air-oil-water flow with and without water-soluble ZETAG®8165 DRP at concentration of 100 ppm in horizontal pipe of 22.5 mm ID (dotted curve represents third order polynomial cure).

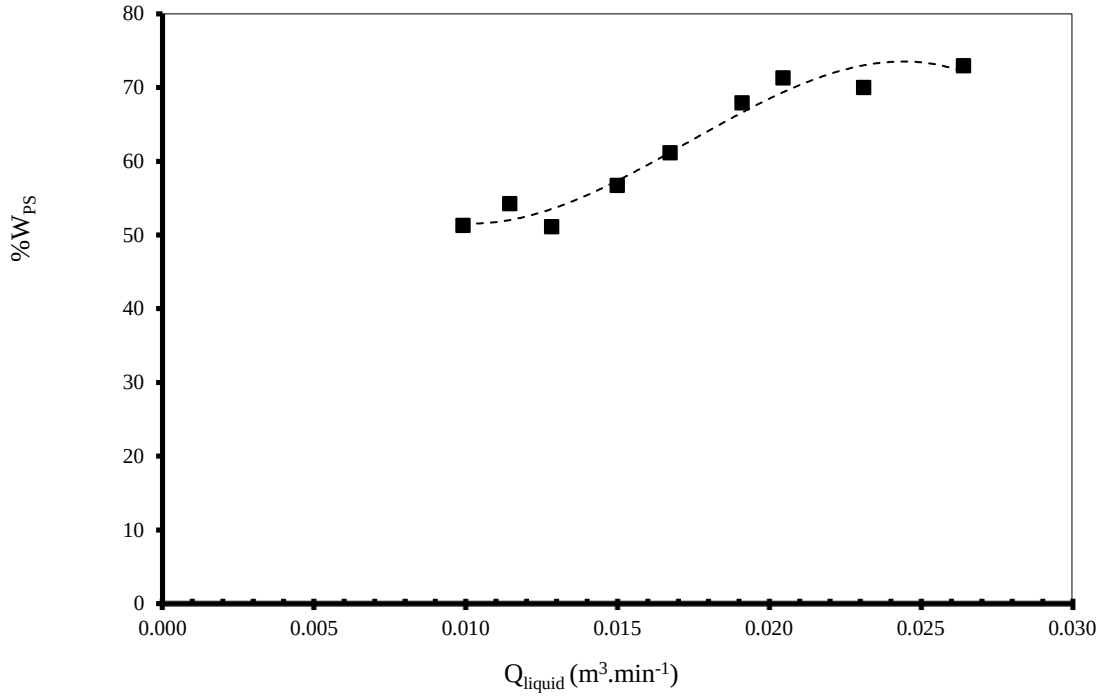

Figure C.9 Percentage saving in power consumptions per meter length by water-soluble ZETAG®8165 DRP (at concentrations of 64 ppm up to 172 ppm) versus liquid flow rate for single-phase water flow in horizontal pipe of 22.5 mm ID (dotted curve represents third order polynomial cure, $R^2 = 0.9577$).

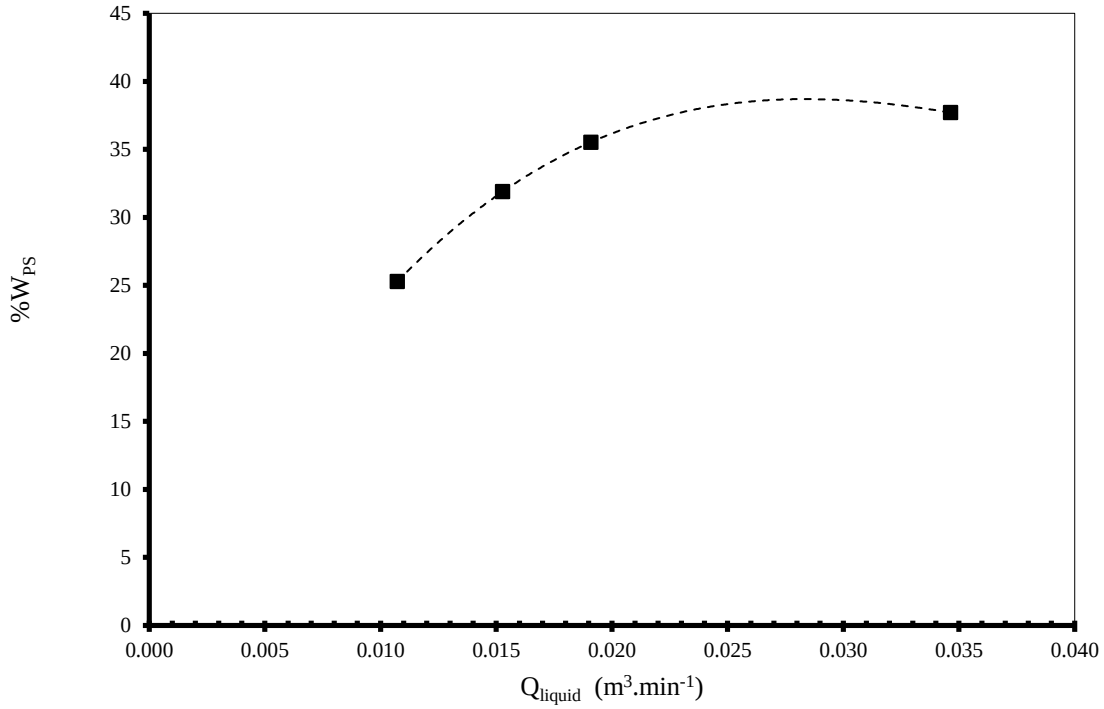

Figure C.10 Percentage saving in power consumptions per meter length by oil-soluble poly(isobutylene) DRP (at concentrations of 101 ppm up to 329 ppm) versus liquid flow rate for single-phase oil flow in horizontal pipe of 22.5 mm ID (dotted curve represents third order polynomial cure, $R^2 = 1.0$).

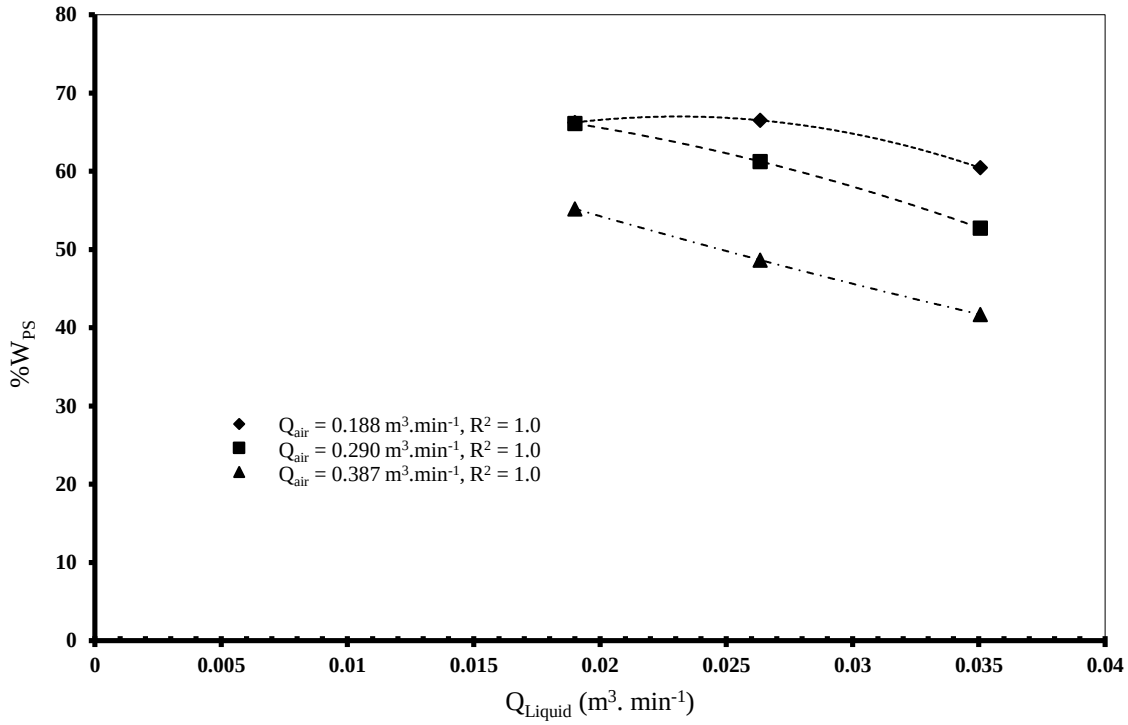

Figure C.11 Percentage saving in power consumptions per meter length by water-soluble ZETAG®8165 DRP (at concentrations of 2 ppm up to 4 ppm) versus liquid flow rate for two-phase air-water flow in horizontal pipe of 22.5 mm ID (dotted curve represents third order polynomial cure, $R^2 = 1.0$).

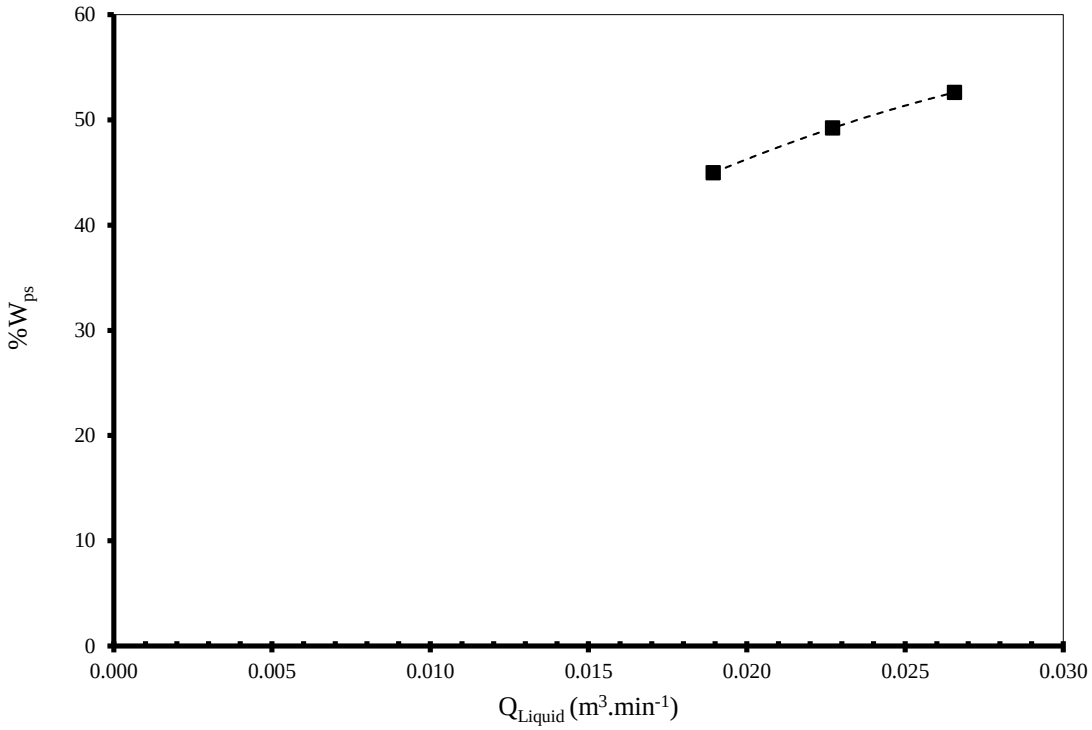

Figure C.12 Percentage saving in power consumptions per meter length by water-soluble ZETAG®8165 DRP (at concentrations of 70 ppm up to 98 ppm) versus liquid flow rate for two-phase air-water flow in horizontal pipe of 22.5 mm ID, at constant air flow rate of Q_{air} = 0.0770 m^3/min (dotted curve represents third order polynomial cure, R^2 = 1.0).

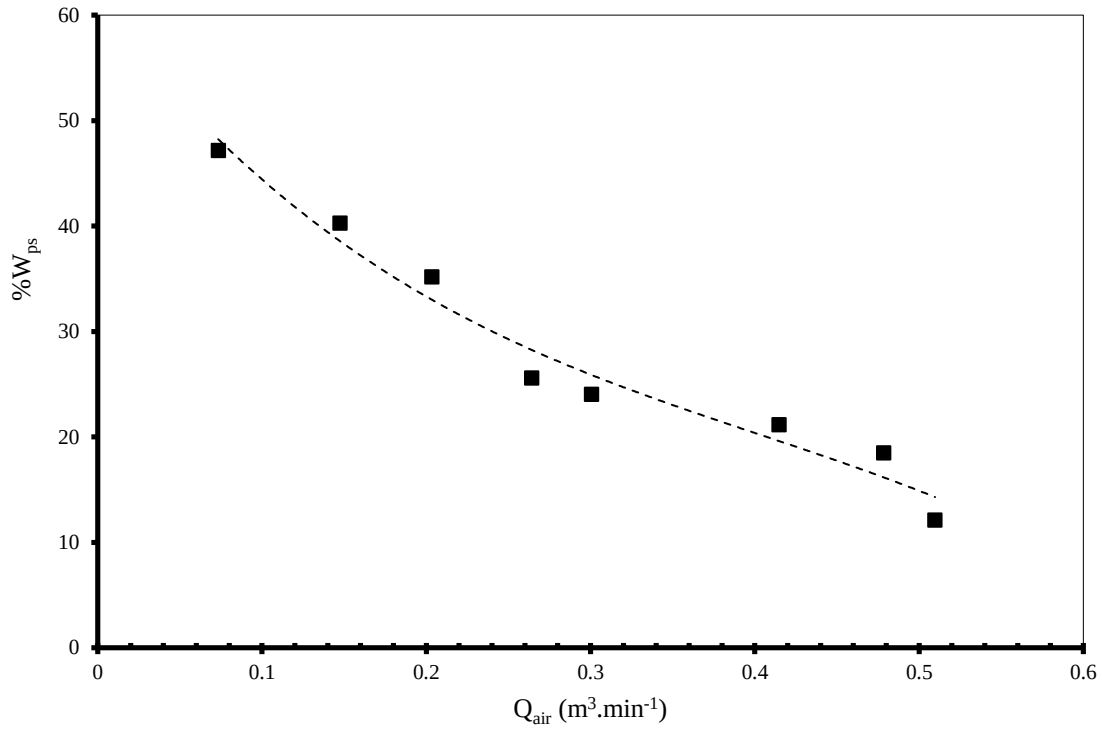

Figure C.13 Percentage saving in power consumptions per meter length by oil-soluble poly(isobutylene) DRP (at concentration of 290 ppm) versus air flow rate for two-phase air-oil flow in horizontal pipe of 22.5 mm ID, at constant liquid flow rate of Q_{Liquid} = 0.0106 m^3/min (dotted curve represents third order polynomial cure, R^2 = 0.9676).

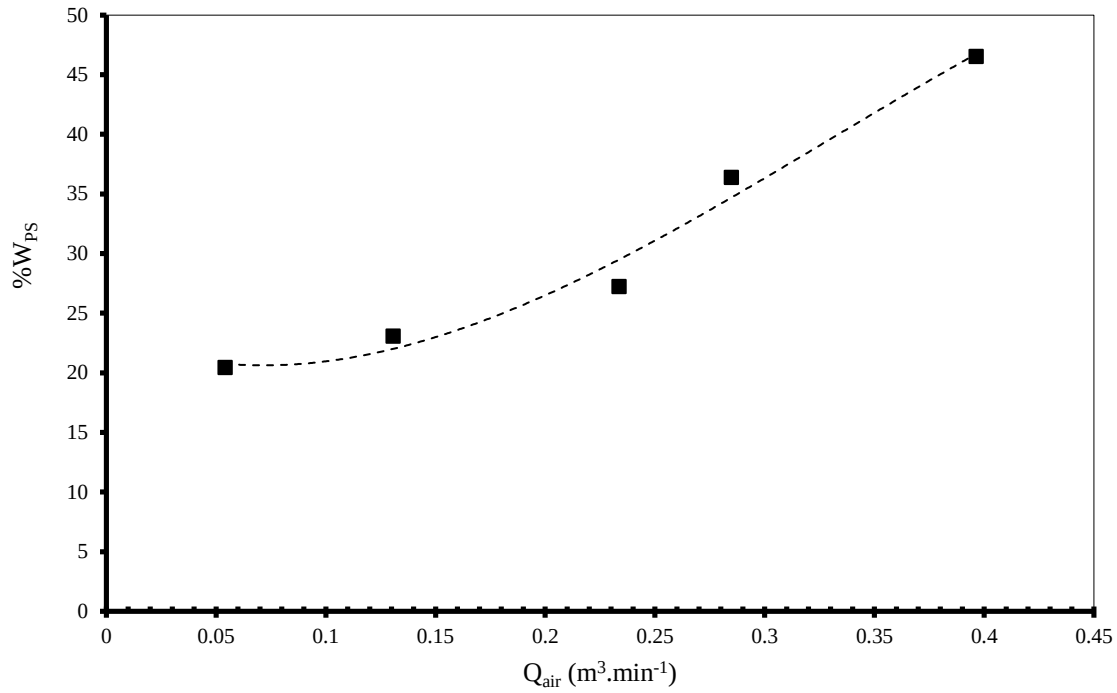

Figure C.14 Percentage saving in power consumptions per meter length by water-soluble ZETAG®8165 DRP (at concentration of 113 ppm) versus air flow rate for three-phase air-oil-water flow in horizontal pipe of 22.5mm ID, at constant liquid flow rate of Q_{Liquid} = 0.0260 m^3/min (dotted curve represents third order polynomial cure, R^2 = 0.9797).

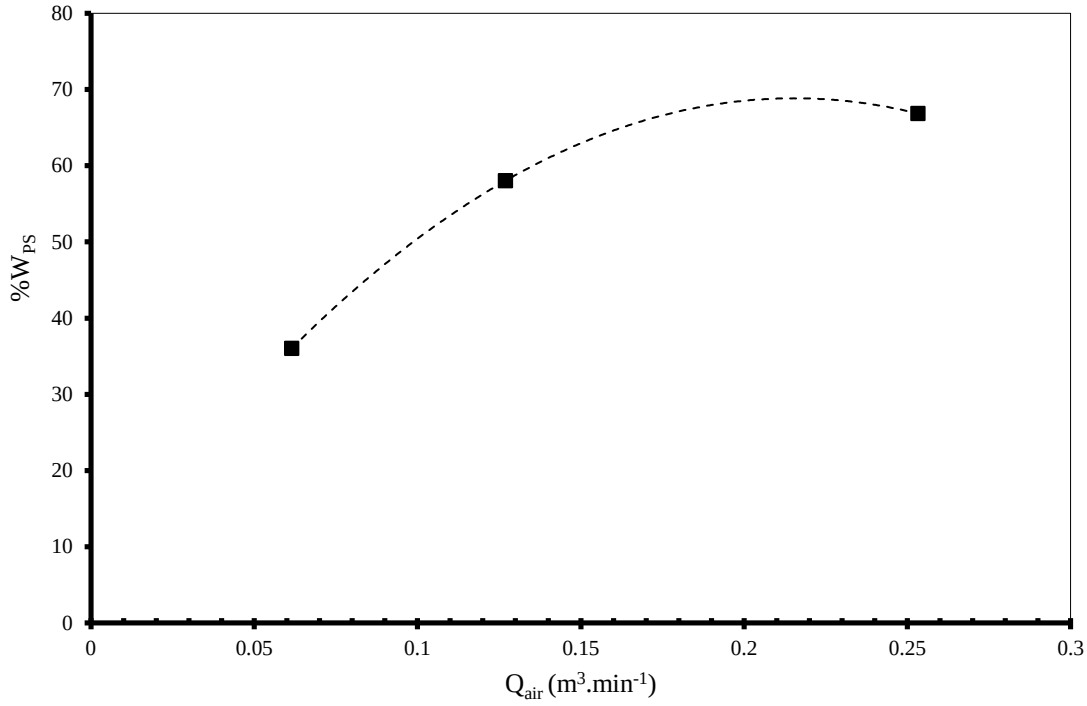

Figure C.15 Percentage saving per meter length in power consumptions by water-soluble ZETAG®8165 DRP (at concentration of 100 ppm) versus air flow rate for three-phase air-oil-water flow in horizontal pipe of 22.5mm ID, at constant liquid flow rate of Q_{Liquid} = 0.0290 m^3/min (dotted curve represents third order polynomial cure, R^2 = 1.0).

C.3.2 Effect of Pipe diameter

The effect of pipe diameter on head loss and percentage power saving were evaluated considering the following as a case study:

- Water-soluble ZETAG®8165 DRP;
- Two-phase air-water flow;
- 22.50 mm ID smooth PVC pipe (Figures C.4, C.5, C.11, and C.12); and
- 10.16 mm ID rough stainless steel pipe (Figures C.16 and C.17).

Figures C.4 and C.5 relate to the head loss per unit pipe length $\Delta h_L/\Delta L$ whereas Figures C.11 and C.12 concern the percentage saving in power consumption per unit pipe length $\%W_{PS}$ in the above 22.5 mm smooth PVC pipe. Figure C.16 corresponds to Figures C.4 and C.5, however, in the 10.16 mm ID rough stainless steel pipe. Figure C.17 is the analogue of Figures C.11 and C.12.

The comparison of results represented by the above figures shows that the head loss $\Delta h_L/\Delta L$ drastically increased in the smaller pipe. The effect on the percentage saving in power consumption $\%W_{PS}$ is opposite. $\%W_{PS}$ in the smaller pipe diameter was found to be significantly comparable with that in the larger pipe diameter.

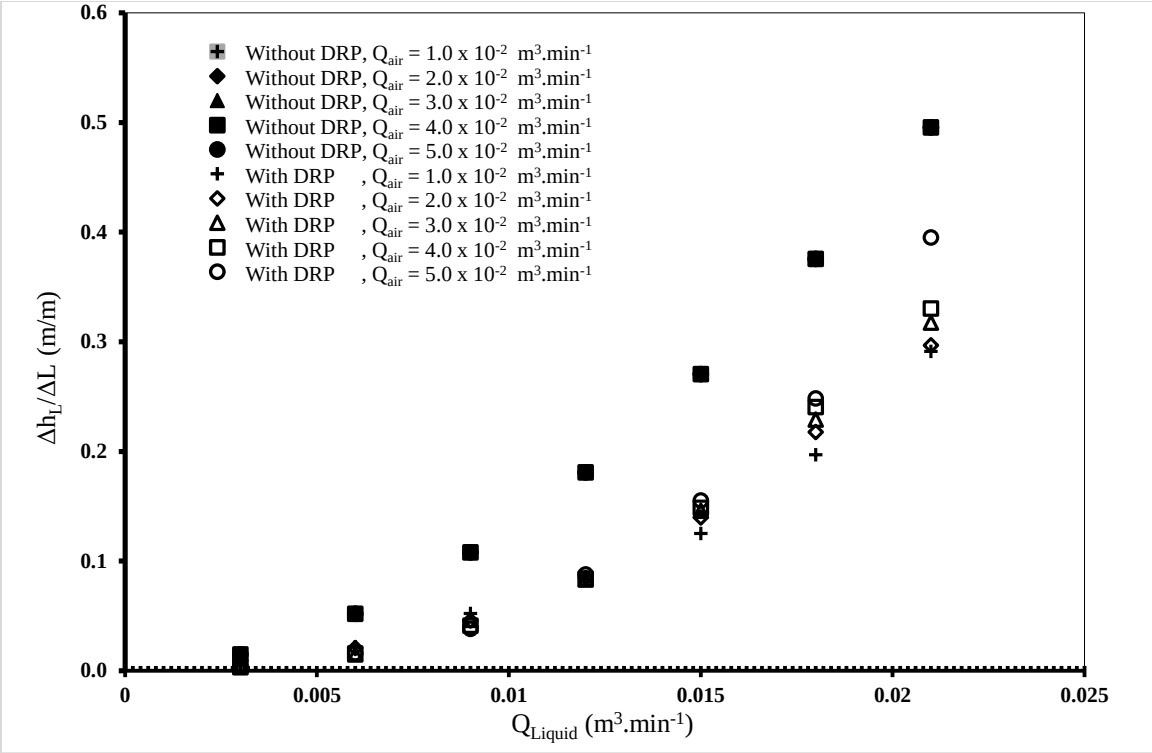

Figure C.16 Head loss per meter length versus liquid flow rate in two-phase air-water flow with and without water-soluble ZETAG®8165 DRP at concentrations of 28 ppm up to 200 ppm in horizontal pipe of 10.16 mm ID.

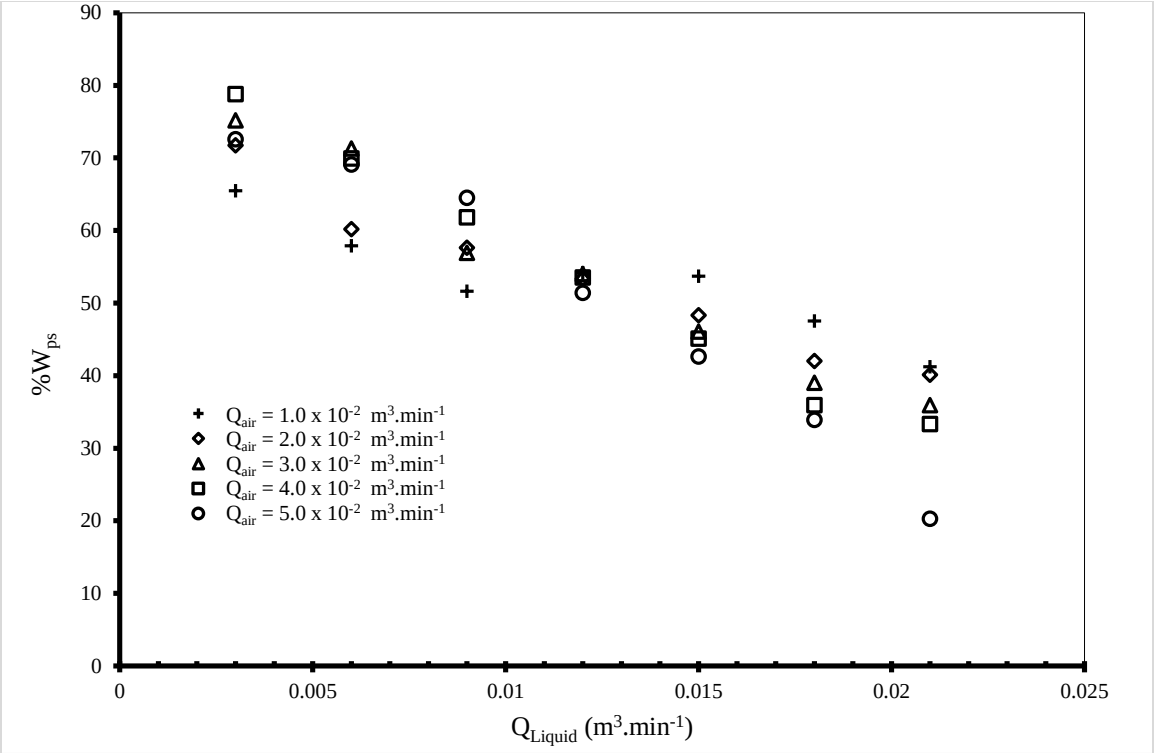

Figure C.17 Percentage saving in power consumptions per meter length by water-soluble ZETAG®8165 DRP (at concentrations of 28 ppm up to 200 ppm) versus liquid flow rate for two-phase air-water flow in horizontal pipe of 10.16 mm ID.

C.4 Conclusion

The use of drag reducing polymers (DRPs), which do not require additional infrastructure, is a much better option to increase energy efficiency in important industrial applications. Therefore, this study evaluates the effects of two DRPs—one water-soluble polar ZETAG®8165 and the other nonpolar oil-soluble polyisobutylene—on energy efficiency using single-phase water flow, single-phase oil flow, two-phase air-water flow, two-phase air-oil flow, and three-phase air-oil-water flow. The pipe comprises a horizontal pipe of 22.5 mm ID. The energy analysis is performed by investigating head loss and saving in energy consumption (both per unit pipe length).

Irrespective of single to multi-phase flows, and increase of liquid and air flow rates, the above DRPs decrease head loss and increase saving in energy consumption. As a result, larger volume of fluid can be transported by using the same pump, or the same volume of fluid can be transported using a smaller pump. This means that either situation saves energy. Based on single-phase flow experiments, ZETAG®8165 is found to be more energy-saving than polyisobutylene.

Equivalent experiments, conducted using the ZETAG®8165 and the two-phase air-water flow in the 10.16 mm ID rough stainless steel pipe, show that the head loss drastically increases in the smaller pipe. However, here the percentage saving in power

consumption significantly comparable with that found in the larger 22.5 mm diameter pipe.

Vitae

Name	:Ihab Hisham Hefzi Alsurakji
Nationality	:Jordanian
Date of Birth	:8/14/1985
Email	:ehabsarkagy@gmail.com
Academic Background	: **Bachelor of Science in Mechanical Engineering** May 2008 An-Najah National University, Nablus, Palestine **Master of Science in Mechanical Engineering** May 2012 King Fahd University of Petroleum and Minerals, Dhahran, Saudi Arabia **Doctor of Philosophy in Mechanical Engineering** November 2016 King Fahd University of Petroleum and Minerals, Dhahran, Saudi Arabia